VILNIUS UNIVERSITY
CENTER FOR PHYSICAL SCIENCE AND TECHNOLOGY

Hamid Reza Hamedi

LINEAR AND NONLINEAR PHENOMENA FOR SLOW LIGHT

Doctoral dissertation

Physical sciences
Physics (02P)

Vilnius, 2017

Doctoral dissertation was prepared in 2013 – 2017 at the Institute of Theoretical Physics and Astronomy of Vilnius University.

Scientific supervisor:

Prof. Habil. Dr. Gediminas Juzeliūnas (Institute of Theoretical Physics and Astronomy of Vilnius University)

Scientific consultant:

Prof. Julius Ruseckas (Institute of Theoretical Physics and Astronomy of Vilnius University)

Contents

List of Figures

Abbreviations

- EIT.....Electromagnetically induced transparency
- CPT.....Coherent population trapping
- 1D.....One dimensional
- 2D.....Two dimensional
- 3D.....Three dimensional
- KR5 model.....Kobrak and Rice five-level model
- SVEA.....Slowly varying envelope approximation
- RWA.....Rotating wave approximation
- NLSE.....Nonlinear Schrodinger equation

Chapter 1

Introduction

1.1 Motivation and background

What happens when light meets matter? This has always been one of the most important questions in quantum optics, especially in the field of spectroscopy which refers to study of the interaction of electromagnetic radiation and matter. Generally speaking, the term "spectroscopy" originates from the Latin word "spectron" for *spirit* or *ghost* and the Greek word "$\sigma\kappa o\pi\iota\varepsilon\nu$" for *to see*. These roots are used because when we shine light on a matter, we hardly see the matter, only its influence on the light. When light encounters matter, there is always an interaction. How light interplays with matter depends on the wavelength of the field of the light, its strength, and the matter itself. Light can be reflected, refracted, diffracted, scattered, transmitted, or absorbed.

There is a long, rich and precious history behind the interaction between light and matter. The invention of lasers in 1960 revolutionized the study of optics, leading to many interesting linear and nonlinear optical phenomena. Note that optical phenomena are linear (nonlinear) in the sense that the response of the system to an applied electromagnetic field depends on the strength of the optical field in a linear (nonlinear) manner.

With the recent development of quantum and nonlinear optics, a considerable attention has been drawn to new techniques [1, 2] which enable manipulation of linear and nonlinear propagation characteristics of probe electromagnetic waves using multi-level atomic configurations [3, 4, 5, 6, 7, 8]. A promising and flexible approach to manipulating linear and nonlinear pulse propagation characteristics

in atomic vapors involves the quantum interference and coherence [3, 9, 10, 11, 12, 13, 14, 15, 16, 17]. The quantum interference is similar to the destructive and constructive interference between classical waves. However, one should use the probability amplitudes in the quantum interference [18], whereas it is the field amplitudes that are interfering in the classical waves. The induced coherence between levels of a multi-level atomic system when interacting with a coherent electromagnetic field is known as the atomic coherence.

There are many motivations for us to understand propagation characteristics of pulse waves through atomic ensembles in linear and nonlinear regimes, most of which are related either to the underlying physics or to the applications. The propagation behavior of a light pulse inside various multi-level atomic structures is interesting by itself, and also represents a basis of many modern technologies. An understanding of how a light pulse is modified by different factors during its propagation can provide a perfect tool for us to explore optical characteristics that are unreachable by other means.

On the other hand, a perfect level structure with suitable quantum interference and coherence features will bring a great help in the implementation of various optical effects. The most popular three-level system is a so-called Λ configuration of atomic levels. It turns out that the quantum interference and coherence in the Λ level scheme can lead to the Electromagnetically induced transparency (EIT) [3, 7] and the slow light [10, 14, 19, 17]. In the EIT regime, a medium can be very dispersive leading to a slowly propagating beam of electromagnetic radiation. The slow light, forming due to the EIT can greatly enhance the interaction of atom and light and results in several interesting nonlinear optical phenomena [20, 21, 22, 23, 24]. More complex level schemes exhibiting additional interference and coherence features induced by extra atomic levels can generate more fascinating effects. For instance, the interaction of three laser fields with a four-level quantum system in a tripod configuration has been shown to exhibit a double electromagnetically induced transparency with a controlled group velocity [25]. A four-level N-type atomic system has been exploited to achieve an enhanced Kerr nonlinear index with a suppressed probe absorption [15, 20]. Tunable control of the group velocity from subluminal to superluminal was demonstrated for a weak probe pulse in an extended Λ-type four-level scheme with two extra control fields and an extra energy level [10]. This scheme was also employed to achieve a subwavelength atom localization via amplitude and phase control of the absorption spectrum [26]. Other multi-level atomic

configurations, such as a double-Λ [27], a double-tripod [28, 29], an inverted-Y [30] and an M- type [31, 32] level structures have been also explored. The fundamental and practical applications of these studies include a low-light-level nonlinear optics [33, 20, 17] and quantum information manipulation [34, 35].

However, despite growing understanding and expanding field of possible applications, there still remain many open questions of importance related to the linear and nonlinear optical characteristics induced by quantum interference and coherence in novel multi-level atomic configurations. The present work addresses some of these open important issues regarding possible new mechanisms for the EIT and slow light, complete physical understanding of the atom localization in two and three dimensions, formation and propagation of slow light optical solitons, and Kerr nonlinear characterization of multi-level atomic schemes.

1.2 The main goals of the thesis

The present work is aimed at modeling a theoretical framework for manipulating probe pulse propagation characteristics through multi-level atom-light coupling schemes, and providing a comprehensive study of important linear and nonlinear coherent phenomena that take place as a result of the interaction between the atoms and laser fields. To be more specific, a main objective of this thesis is to suggest novel atom-light coupling schemes which support a lossless propagation of slow light, a giant enhancement of Kerr nonlinearity, a perfect 2D and 3D atom localization, as well as a slow propagation of shape preserving optical solitons.

1.3 The main tasks of the thesis

- To utilize a semiclassical density matrix method in order to obtain equations of motion describing the evolution of atoms illuminated by the control and probe fields for various atom-light coupling schemes.

- To show a possibility of Kerr nonlinearity enhancement accompanied by a negligible absorption under a condition of slow light for multi-level atomic

structures.

- To investigate the signatures of the relative phase of applied fields stemming from closed-loop structure of the system on linear and nonlinear optical susceptibilities.

- To propose novel schemes of high-precision 2D and 3D atom localization using multi-level atom-light coupling configurations.

- To study a phase sensitive 2D and 3D atom localization in atomic media via measurement of the absorption of a weak probe field.

- To present new mechanisms for EIT and slow light using multi-level atom-light coupling configurations.

- To use the concept of slow light and EIT for generation of stable shape preserving optical solitons in multi-level atom-light coupling schemes.

1.4 Scientific novelty

- A novel five-level closed-loop phase sensitive atomic scheme is proposed in order to achieve the Kerr nonlinearity enhancement. It is demonstrated that by increasing a number of levels in such a way that they form a cyclic chain of four atomic states coupled to the ground state, it is possible to realize higher orders of nonlinearity compared to that for the three- and four-level schemes.

- An analytical model is proposed to elucidate the phase sensitive Kerr nonlinearity for five-level quantum systems. This phase sensitive property provides an extra degree of freedom for controlling the Kerr-nonlinear index, a feature that was absent in the previous analysis [15, 36].

- In addition to the steady-state nonlinear susceptibilities, the transient switching of the Kerr nonlinearity is investigated. The results obtained are helpful for realizing fast optical nonlinearities and optically controlled optical devices.

- It is found that the effect of the Doppler broadening can lead to a giant Kerr nonlinearity. This novel Kerr nonlinear enhancement is advantageous over the EIT technique ([15, 36, 16, 37]) because there is no need to use very strong coupling laser fields.

- The three dimensional (3D) atom localization gives a more specific information about the position of a moving atom compared to the 1D and 2D localization and has been previously investigated only in few proposals [38, 39, 40]. In this thesis, *the phase control of the 3D atom localization* is explored for the first time in the 3D space. It is found that the detection probability of finding the atom in a particular volume in the 3D space and within one period of standing waves can become 50% by properly adjusting the relative phase of the applied fields.

- We have considered propagation of a probe light in a novel atomic structure charactrized by a combined tripod and Lambda (Λ) atom-light coupling configuration. This provides a new mechanism for the electromagnetically induced transparency and slow light compared with the Λ [7, 8], tripod [14, 25, 41], or double tripod schemes [42, 29]. The scheme provides a possibility to control the EIT by changing the phase of the laser fields.

1.5 Statements to defend

1. For the first time, the use of the KR5 atomic system, which provides higher orders of optical nonlinearities for a giant Kerr effect is predicted theoretically.

2. The relative phase of applied fields stemming from the closed-loop structure of the subsystem can strongly affect the Kerr nonlinearity of the KR5 atomic configuration. It is theoretically predicted that under the effect of relative phase of applied fields, the Kerr nonlinearity of KR5 atom-light coupling scheme may be accompanied by four, three or even two linear and nonlinear absorption peaks.

3. It is predicted that in the five-level closed-loop KR5 atom-light coupling scheme, the relative phase plays an important role for achieving a perfect

detection probability of an atom in two dimensions and at a particular position within one period of standing-wave fields. In addition, the phase control of the 3D atom localization is explored for the first time in the 3D space for the KR5 system.

4. The transparency window for the probe field may appear under the influence of an external control field in a double-ladder system; simultaneously the subluminal light propagates inside the medium.

5. The existence of dark states, essential for the EIT, is theoretically predicted for a combined tripod and Lambda (Λ) atom-light coupling setup. In the limiting cases the scheme reduces to conventional Λ - or N -type atom-light couplings providing the EIT or absorption, respectively.

6. Generation of stable slow light optical solitons is expected in the combined tripod and Λ atomic system.

1.6 Author's contribution and approbation of the results

The author of the thesis has performed most of the analytical derivations of the equations as well as numerical calculations, and together with co-authors prepared the publications.

Scientific papers on the topic of the dissertation

1. **Hamid Reza Hamedi** and Gediminas Juzeliunas, *Phase-sensitive Kerr nonlinearity for closed-loop quantum systems*, Phys. Rev. A 91, 053823 (2015)

2. Ali Raheli, M. Sahrai, **Hamid Reza Hamedi**, *Atom position measurement in a four-level Lambda-shaped scheme with twofold lower-levels*, Opt. Quant Electronics 47, 3221-3236 (2015)

3. Ali Raheli, **Hamid Reza Hamedi** and M Sahrai, *Atom localization in two dimensions for five-level atomic schemes in X-configuration*, Laser Phys.

25, 095202 (2015)

4. **Hamid Reza Hamedi**, *Perfect Precision Detecting Probability Of An Atom Via SGC Mechanism*, Int. J. Theor. Phys. 54, 2012-2021 (2015)

5. **Hamid Reza Hamedi** and Gediminas Juzeliunas, *Phase-sensitive atom localization for closed-loop quantum systems*, Phys. Rev. A 94, 013842 (2016)

6. **Hamid Reza Hamedi**, Ali Hamrah Gharamaleki, M. Sahrai, *Colossal Kerr nonlinearity based on electromagnetically induced transparency in a five-level double-ladder atomic system*, Appl. Opt. 55, 5892-5899 (2016)

7. **Hamid Reza Hamedi**, M. R. Mehmannavaz, *Phase control of three-dimensional atom localization in a four-level atomic system in Lambda configuration*, J. Opt. Soc. Am. B 33, 41-45 (2016)

8. **Hamid Reza Hamedi**, *Optical switching, bistability and pulse propagation in five-level quantum schemes*, Laser Phys. 27, 066002 (2017)

9. **Hamid Reza Hamedi**, Julius Ruseckas and Gediminas Juzeliunas, *Electromagnetically induced transparency and nonlinear pulse propagation in a combined tripod and Λ atom-light coupling scheme*, accepted for publication in J. Phys. B (2017)

Some other scientific papers

1. **Hamid Reza Hamedi**, *Ultra-slow propagation of light located in ultra-narrow transparency windows through four quantum dot molecules*, Laser Phys. Lett. 11, 085201 (2014)

2. **Hamid Reza Hamedi**, Arash Radmehr, and M. Sahrai, *Manipulation of Goos-Hänchen shifts in the atomic configuration of mercury via interacting dark-state resonances*, Phys. Rev. A 90, 053836 (2014)

3. **Hamid Reza Hamedi,** *Optical bistability through the cavity effect in a four-level open atomic medium*, JETP Letters 100, 299-305 (2014)

4. **Hamid Reza Hamedi**, *Enormous enhancements of the Kerr nonlinearity at C-band telecommunication wavelength in an Er^{3+}-doped YAG crystal*, Physica B 442, 60–65 (2014)

5. **Hamid Reza Hamedi**, *Optical bistability and multistability via magnetic field intensities in a solid*, Appl. Opt. 53, 5391-5397 (2014)

6. **Hamid Reza Hamedi**, and S. H. Asadpour, *Realization of optical bistability and multistability in Landau-quantized graphene*, J. Appl. Phys. 117, 183101 (2015)

7. **Hamid Reza Hamedi**, Mohammad Reza Mehmannavaz, *Switching feature of EIT-based slow light giant phase-sensitive Kerr nonlinearity in a semiconductor quantum well*, Physica E 66, 309-316 (2015)

8. Seyyed Hossein Asadpour, **Hamid Reza Hamedi** and Hamid Rahimpour Soleimani, *Slow light propagation and bistable switching in a graphene under an external magnetic field*, Laser Phys. Lett. 12, 045202 (2015)

9. **Hamid Reza Hamedi**, *Storage and retrieval of light pulse propagating in quadruple quantum dot molecules*, J. Opt. Soc. Am. B 33, 151-157 (2016)

10. **Hamid Reza Hamedi**, *Pulse propagation and optically controllable switch in coupled semiconductor-double-quantum-dot nanostructures*, J. Appl. Phys. 119, 183104 (2016)

11. **Hamid Reza Hamedi** , Mostafa Sahrai, Habib Khoshsima and Gediminas Juzeliunas, Optical bistability forming due to a Rydberg state, J. Opt. Soc. Am. B 34 1923-1929 (2017)

Conference presentations

International conferences

1. **Hamid Reza Hamedi** and Gediminas Juzeliunas, *Transient switching of the Kerr nonlinearity and effect of Doppler broadening in a five-level*

Quantum system, 47th conference of the European Group on Atomic Systems (EGAS) July 14-17, Riga, Latvia (2015)

2. **Hamid Reza Hamedi** and Gediminas Juzeliunas, *Phase Sensitive 2D Atom Localization Via Probe Absorption measurement For Closed Loop Quantum Systems*, 12th European Conference on Atoms Molecules and Photons (ECAMP12) September 5-9, Frankfurt, Germany (2016)

3. **Hamid Reza Hamedi**, Julius Ruseckas and Gediminas Juzeliunas, *A new type of EIT in combined Tripod and Lambda atom-light coupling schemes*, 24th Central European Workshop on Quantum Optics (CEWQO) June 26-30, Copenhagen, Denmark (2017)

Local conferences

1. **Hamid Reza Hamedi** and G. Juzeliūnas, *Phase-Sensitive Kerr Nonlinearity for Closed Loop Quantum Systems*, 16th International Conference-School ADVANCED MATERIALS AND TECHNOLOGIES, August 27-31, Palanga, Lithuania (2014)

2. **Hamid Reza Hamedi** and G. Juzeliūnas, *Phase sensitive atom localization for Closed Loop Quantum Systems*, 17th International Conference-School ADVANCED MATERIALS AND TECHNOLOGIES, August 27-31, Palanga, Lithuania (2015)

3. **Hamid Reza Hamedi** and G. Juzeliūnas, *An enhanced Kerr nonlinearity for closed loop quantum systems*, Open readings, 59th International Conference for Students of Physics and Natural Sciences, March 15-18, Vilnius, Lithuania (2016)

4. **Hamid Reza Hamedi** and G. Juzeliūnas, *Dynamic Control of Pulse Propagation through Phase-Sensitive Five-Level Closed Loop Quantum Systems*, 18th International Conference-School, ADVANCED MATERIALS AND TECHNOLOGIES, August 27-31, Palanga, Lithuania (2016)

5. **Hamid Reza Hamedi** and G. Juzeliūnas, *Pulse propagation for closed loop quantum systems*, Open readings, 60th International Conference for

Students of Physics and Natural Sciences, March 14- 17, Vilnius, Lithuania (2017)

1.7 Acknowledgements

First and foremost, I wish to thank my supervisor, professor Gediminas Juzeliūnas, director of Institute of Theoretical Physics and Astronomy, Vilnius University. It has been always an honor of me to be his first non-Lithuanian Ph.D student. I appreciate all his patience, help, ideas, and contributions of time to advance my Ph.D pursuit. He has been supportive since the first day I arrived in Lithuania. The enthusiasm he has for the research was motivational for me, even during toughest times in my Ph.D studies. He has been an excellent example for me as a successful physicist and professor. Besides my supervisor, I would like to express my deepest gratitude to professor Julius Ruseckas not only for his invaluable comments, but also for being my excellent consultant for every scientific problem I have encountered during the period of my study.

I thank Tomas Andrijauskas, Algirdas Mekys and Viktor Novičenko for their inestimable help especially in Lithuanian language and culture. I would like to acknowledge honorary all members and staff of our group for their great support over the past years. The group has been a source of friendships as well as good advice and collaboration. A special acknowledgment must go to Artūras Acus and Viačeslav Kudriašov for their fruitful comments, which significantly improved my Ph.D dissertation. I also gratefully acknowledge the support of the Lithuanian Research Council (No. VP1-3.1-ŠMM-01-V-03-001).

I am thankful to professor Lorenzo Marrucci from University of Naples, Italy and professor Mostafa Sahrai from University of Tabriz, Iran, for offering me the internship opportunity in their group and leading me working on diverse exciting projects.

I finish with Iran, where the main source of my love, motivation and memoirs resides. I would like to thank my family because of all their encouragement and love. For my brothers who have taken care of my parents all these years in absence of me. For my mather and father who have been a source of my strength and inspiration. And for my supportive, encouraging, and loving wife

Neda who has been patient and faithful even during the difficult times. Thank you.

1.8 Thesis layout

The structure of this thesis is as follows.

Chapter 2: The necessary theoretical foundations related to our research are presented in this chapter. Following the semiclassical theory, a basic description of the interaction of electromagnetic radiation with two-state atoms is studied in Section 2.1. An understanding of this simple model of atom-light coupling is important in order to interrogate more complicated multi-level atomic schemes. In Section 2.2 we introduce the three-level Λ system, and obtain the equations of motion describing the evolution of the system. The main work presented in this thesis deals with the *Electromagnetically Induced Transparency (EIT)*. We provide a deeper inside into the concept of EIT (Section 2.3) and its associated phenomena i.e., *slow light* (Section 2.4) and *atom localization* (Section 2.5). Third-order nonlinear optical effects induced by the quantum interference and coherence are also reviewed in Section 2.6. In particular, the Kerr nonlinear index which is proportional to the refractive part of the third order nonlinear susceptibility is derived. Moreover, the basic equations describing the linear and nonlinear propagation of pulsed field are introduced.

The main results of this thesis are presented in Chapters (3)–(6).

Chapter 3: This chapter discusses the third-order nonlinear effects in a five-level atom-light coupling scheme. We first show that an enhanced Kerr nonlinearity can be obtained with a reduced absorption under the condition of slow light propagation. We then illustrate that the Kerr nonlinearity is very sensitive to the relative phase of the applied fields and study the influence of the relative phase on the linear and nonlinear optical properties of the medium. Analytical solutions are given to elucidate such phase dependence of the Kerr nonlinearity. We also make a comparison between the Kerr-nonlinear indices for this five-level system with that of the existing four and three-level atomic systems. The results of the work presented in this chapter have been published in [43].

Chapter 4: We employ two different atomic schemes to localize atoms in two and three dimensions (2D and 3D atom localization). First, in Section 4.1 we investigate the 2D and 3D localization of an atom in a five-level configuration in which the laser beams couple the ground level to a four-level closed-loop system. Second, in Section 4.2 we propose a four-level Λ-type atomic system with twofold lower levels to study the phase sensitive 3D atom localization. By employing different situations in which the atom could interact with the position-dependent standing-wave fields, we show that one can extract information about the position of the atom through measuring the absorption of the probe field. In particular, by appropriately choosing the amplitudes and phases of the driving fields, different localization patterns can be occurred in the probe absorption spectrum. The results of the work presented in this chapter have been published in [44, 45].

Chapter 5: The work presented in this chapter is concerned with linear and nonlinear optical phenomena in a five-level double-ladder atom light coupling scheme. We first investigate the effect of a control field on linear optical properties of a probe field, and explore the linear propagation dynamics of a weak probe Gaussian field through such a system. A dressed state analysis is presented which allows us to gain much physical insight. This chapter is also aimed at modeling the enhanced Kerr nonlinearity along with zero absorption for such an atom-light coupling scheme. The results of the work presented in this chapter have been published in [46, 47].

Chapter 6: This chapter describes the propagation of a probe pulse in an atomic medium characterized by a combined tripod and Lambda (Λ) atom-light coupling scheme. The existence of dark states, essential for the electromagnetically induced transparency (EIT) and slow light, is demonstrated analytically for such an atom-light coupling. Subsequently, a theoretical model is employed based on the coupled Maxwell-Bloch equations for the nonlinear pulse propagation. We demonstrate the formation of slow light stable optical solitons in such a highly resonant medium originating from the balance between dispersive and nonlinear effects. The results of the work presented in this chapter is submitted and is currently in review.

Chapter 7: The conclusions of this thesis and possible future works are presented in this chapter.

Chapter 2

Fundamentals and literature review

2.1 Atom-light interaction: the two-level atom

Since the interaction of atoms with the radiation field plays a role of pillar for this thesis, in this chapter we purpose to go through its fundamentals. We consider the simple case of interaction of a single mode of electromagnetic field, such as that produced by lasers, with the two-state atom. This simple frame can be generalized to more complicated problems. We utilize a semiclassical treatment. In this framework, the electromagnetic radiation is considered as a classically field, while the atomic matter with which the light interacts is treated quantum mechanically.

2.1.1 Schrödinger picture

Let us consider a two-level atomic system involving upper and lower atomic levels $|a\rangle$ and $|b\rangle$, which is illuminated by a laser field of frequency ν. A schematic of the two-level atom interacting with a single-mode field is shown in Fig. 2.1. The evolution of this system is governed by the Schrödinger equation

$$|\dot{\psi}(t)\rangle = \frac{-i}{\hbar} H|\psi(t)\rangle, \tag{2.1}$$

where H describes the total Hamlitonian of the system which can be expressed as

$$H = H_0 + H_I. \tag{2.2}$$

Here, H_0 denotes the free energy Hamiltonian (unperturbed Hamiltonian), while H_I describes the interaction of the atom and radiation field (interaction Hamiltonian). The atomic wavefunction reads

$$|\psi(t)\rangle = C_a(t)|a\rangle + C_b(t)|b\rangle, \tag{2.3}$$

where C_a and C_b represent the probability amplitudes of finding the atom in upper and lower states, respectively. The laser field of the frequency ν and the amplitude ϵ is given by

$$E(t) = \epsilon \cos(\nu t). \tag{2.4}$$

It should be pointed out that Eq. (2.4) is written in the *dipole approximation*, in which we only consider the field at the location of the atom by ignoring the spatial dependence or the propagation direction of the field. This approximation is valid when the size of the atom is much smaller than the optical wavelength.

The unperturbed Hamiltonian can be expressed as

$$H_0 = (|a\rangle\langle a| + |b\rangle\langle b|)H_0(|a\rangle\langle a| + |b\rangle\langle b|), \tag{2.5}$$

where in writing this equation we have used the completeness relation $|a\rangle\langle a| + |b\rangle\langle b| = 1$. Since $H_0|i\rangle = \hbar\omega_i|i\rangle$ $(i = a, b)$, Eq. (2.5) can be rewritten as

$$H_0 = \hbar\omega_a|a\rangle\langle a| + \hbar\omega_b|b\rangle\langle b|. \tag{2.6}$$

Furthermore, for the interaction Hamiltonian we have

$$\begin{aligned} H_I = -exE(t) &= -e(|a\rangle\langle a| + |b\rangle\langle b|)x(|a\rangle\langle a| + |b\rangle\langle b|)E(t) \\ &= -(\wp_{ab}|a\rangle\langle b| + \wp_{ba}|b\rangle\langle a|)E(t), \end{aligned} \tag{2.7}$$

where the electric field is assumed to be linearly polarized along the x-axis. Note that $\wp_{ab} = \wp_{ba}^* = e\langle a|x|b\rangle$ indicates the dipole matrix element of the atom

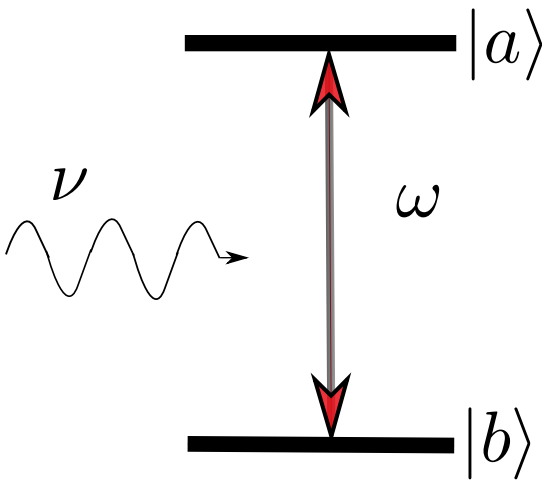

Figure 2.1: The two-level atom interacting with a single-mode field.

induced by the external field $E(t)$.

Substituting Eq. (2.4) into Eq. (2.7) leads to

$$H_I = -\hbar(\Omega_R|a\rangle\langle b| + \Omega_R^*|b\rangle\langle a|)\cos(\nu t), \tag{2.8}$$

where we have defined the Rabi-frequency $\Omega_R = \frac{|\wp_{ab}|\epsilon}{\hbar}$. Note that the Rabi-frequency Ω_R is different from the atomic transition frequency $\omega = \omega_a - \omega_b$. The resonance frequency ω is the frequency of light emitted or absorbed by the two-level system, while Ω_R characterizes the coupling strength between the atom and the field. Using Eqs. (2.2), (2.3), (2.6), and (2.8), the Schrödinger equation (2.1) yields

$$\begin{aligned} &i(\dot{C}_a(t)|a\rangle + \dot{C}_b(t)|b\rangle) \\ &= \omega_a C_a(t)|a\rangle + \omega_b C_b(t)|b\rangle - \left(\Omega_R e^{-i\phi} C_b(t)|a\rangle + \Omega_R e^{i\phi} C_a(t)|b\rangle\right)\cos(\nu t) \end{aligned} \tag{2.9}$$

which can result in the following equations of motion for the probability amplitudes C_a and C_b

$$\dot{C}_a = -i\omega_a C_a + i\Omega_R \cos(\nu t) e^{-i\phi} C_b, \tag{2.10}$$

$$\dot{C}_b = -i\omega_b C_b + i\Omega_R \cos(\nu t) e^{i\phi} C_a, \tag{2.11}$$

where the parameter ϕ corresponds to the phase of the dipole matrix element $\wp_{ab} = |\wp_{ab}|e^{i\phi}$. Transferring to a frame rotating with the eigenfrequencies of the atomic states (ω_a and ω_b)

$$C_a = c_a \mathrm{e}^{-i\omega_a t}, \tag{2.12}$$

$$C_b = c_b \mathrm{e}^{i\omega_a t}, \tag{2.13}$$

and using the exponential form of $\cos(\nu t)$ in both Eqs. (2.10) and (2.11), we arrive at the following coupled equations

$$\dot{c}_a = i\Omega_R c_b e^{-i\phi} \left(\frac{\mathrm{e}^{i(\omega+\nu)t} + \mathrm{e}^{i(\omega-\nu)t}}{2}\right), \tag{2.14}$$

$$\dot{c}_b = i\Omega_R c_a e^{i\phi} \left(\frac{\mathrm{e}^{-i(\omega+\nu)t} + \mathrm{e}^{-i(\omega-\nu)t}}{2}\right). \tag{2.15}$$

When the laser field frequency ν is near resonance with the atomic transition $|a\rangle \longleftrightarrow |b\rangle$, the difference $\omega - \nu$ is quite small, as a result, the exponential terms $\mathrm{e}^{\pm i(\omega-\nu)t}$ in Eqs. (2.14) and (2.15) oscillate slowly and must be kept. In contrast, the exponential terms $e^{\pm i(\omega+\nu)t}$ can be neglected from the coupled equations (2.14) and (2.15) since they oscillate rapidly. This is *Rotating wave approximation* (RWA) [18].

Defining the parameter $\Delta = \omega - \nu$ which describes the detuning of the laser field from the atomic resonance and under the Rotating wave approximation, the two coupled equations of the motion (2.14) and (2.15) reduce to

$$\dot{c}_a = \frac{i\Omega_R}{2} c_b \mathrm{e}^{-i\phi} \mathrm{e}^{i\Delta t}, \tag{2.16}$$

$$\dot{c}_b = \frac{i\Omega_R}{2} c_a \mathrm{e}^{i\phi} \mathrm{e}^{-i\Delta t}. \tag{2.17}$$

One way to solve the above equations is to differentiate them again with respect to t.

$$\ddot{c_a} = i\Delta\ \dot{c}_a - \frac{\Omega_R^2}{4}, \tag{2.18}$$

$$\ddot{c_b} = -i\Delta\ \dot{c}_b - \frac{\Omega_R^2}{4}. \tag{2.19}$$

The solutions for c_a and c_b are

$$c_a(t) = a_1 \mathrm{e}^{\frac{i(\Omega+\Delta)t}{2}} + a_2 \mathrm{e}^{\frac{-i(\Omega-\Delta)t}{2}}, \tag{2.20}$$

$$c_b(t) = b_1 \mathrm{e}^{\frac{i(\Omega-\Delta)t}{2}} + b_2 \mathrm{e}^{\frac{-i(\Omega+\Delta)t}{2}}, \tag{2.21}$$

where $\Omega = (\Omega_R^2 + \Delta^2)^{1/2}$ is the generalized Rabi frequency. In addition, the coefficients a_1, a_2, b_1,b_2 can be obtained from the initial conditions. After some algebraic calculations, one may find

$$a_1 = \frac{1}{2\Omega}\left(c_a(0)(\Omega - \Delta) + \Omega_R \mathrm{e}^{-i\phi} c_b(0)\right), \tag{2.22}$$

$$a_2 = \frac{1}{2\Omega}\left(c_a(0)(\Omega + \Delta) - \Omega_R \mathrm{e}^{-i\phi} c_b(0)\right), \tag{2.23}$$

$$b_1 = \frac{1}{2\Omega}\left(c_b(0)(\Omega + \Delta) + \Omega_R \mathrm{e}^{i\phi} c_a(0)\right), \tag{2.24}$$

$$b_2 = \frac{1}{2\Omega}\left(c_b(0)(\Omega - \Delta) - \Omega_R \mathrm{e}^{i\phi} c_a(0)\right). \tag{2.25}$$

The solutions for c_a and c_b featured in equations (2.20) and (2.21) imply that the application of the laser field causes the oscillation of the atom between the ground state $|b\rangle$ and the excited state $|a\rangle$.

Although the Schrödinger picture that we have used thus far can elucidate well the absorption and stimulated emission processes, it cannot explain the spontaneous emission. As demonstarted above, in this picture an atom prepared initially in the excited state cannot make a transition to the ground state, unless the external laser field is present to drive the atom. While in reality an atom in an excited state has finite lifetimes and will decay via spontaneous emission to a lower energy state. To describe atom-light interactions properly, we must include this process. In order to include the spontaneous emission process one may take the advantage of the density matrix formalism.

2.1.2 Density matrix formalism

We may alternatively describe the state of a quantum system through the density operator rather than the wavefunction. Imagine that we work with a quantum system which is in a pure state $|\psi\rangle$. All possible information about the system is stored in this pure quantum state. Extracting information about a part of system is then possible by calculating the expectation value of the corresponding operator (observable) A

$$\langle A\rangle_{QM} = \langle\psi|A|\psi\rangle, \tag{2.26}$$

where $\langle A\rangle_{QM}$ is the quantum mechanical average. However, in many physical problems we deal with mixed states prepared by statistically combining different pure states. This implies that we have imperfect information about the state of system. What we know in such a case is the probability P_ψ of being in the state $|\psi\rangle$. Thus, in addition to the quantum mechanical average, we need to take also an ensemble average in the expectation value calculations of an observable

$$\langle\langle A\rangle_{QM}\rangle_{ensemble} = \Sigma_\psi P_\psi\langle\psi|A|\psi\rangle. \tag{2.27}$$

Equation (2.27) can be rewritten by taking the advantage of the completeness $\Sigma_n|n\rangle\langle n| = 1$,

$$\begin{aligned}\langle\langle A\rangle_{QM}\rangle_{ensemble} &= \Sigma_n\Sigma_\psi P_\psi\langle\psi|A|n\rangle\langle n|\psi\rangle = \Sigma_n\Sigma_\psi P_\psi\langle n|\psi\rangle\langle\psi|A|n\rangle \\ &= \Sigma_n\langle n|\rho A|n\rangle = \mathrm{Tr}(A\rho),\end{aligned} \tag{2.28}$$

with the density operator defined by

$$\rho = \Sigma_\psi P_\psi|\psi\rangle\langle\psi|. \tag{2.29}$$

Note that for a pure state $|\psi_0\rangle$, the density operator becomes

$$\rho = |\psi_0\rangle\langle\psi_0|. \tag{2.30}$$

Differentiating Eq. (2.29) with respect to time, we have

$$\dot{\rho} = \Sigma_\psi P_\psi(|\dot{\psi}\rangle\langle\psi| + |\psi\rangle\langle\dot{\psi}|). \tag{2.31}$$

Recalling the Schrödinger equation (2.1) to substitute $|\ \dot{\psi}\rangle$ and $\langle\dot{\psi}\ |$ and with the help of Eq. (2.29), Eq. (2.31) reduces to

$$\dot{\rho} = -\frac{i}{\hbar}[H,\rho], \tag{2.32}$$

where the term in brackets is the commutator of the Hamiltonian and the density operator.

The density matrix approach presented above is equivalent to the Schrödinger picture. However this formalism enables us to include also the effect of spontaneous emission. If the atom is in its excited state, in the long run it will decay to the ground state by spontaneous emission. The origin of this phenomenon comes from the coupling of the atom to the electromagnetic vacuum field. In writing Eq. (2.32) the spontaneous emission decay rates are not incorporated. The density matrix equation of the motion including the decay rates is

$$\dot{\rho} = -\frac{i}{\hbar}[H,\rho] - \frac{1}{2}\{\Gamma,\rho\}, \tag{2.33}$$

where a relaxation matrix Γ is defined as

$$\langle i|\Gamma|j\rangle = \gamma_i \delta_{ij}, \tag{2.34}$$

with $\{\Gamma, \rho\} = \Gamma\rho + \rho\Gamma$. These decay rates can either add or remove population to the atomic states. Generally, the relaxation processes are more complicated and are out of the scope of this dissertation. Equation (2.33) is called the Liouville equation.

Equation (2.33) can be expanded, yielding

$$\dot{\rho}_{kl} = -\frac{i}{\hbar}\Sigma_m(H_{km}\rho_{ml} - \rho_{km}H_{ml}) - \frac{1}{2}\Sigma_m(\Gamma_{km}\rho_{ml} + \rho_{km}\Gamma_{ml}). \tag{2.35}$$

where ρ_{kl} is the klth element of the density matrix operator.

2.1.3 The density matrix equations for the two-level atom

Now we return to the two-level atom problem (Fig. 2.1), trying to analyze it using the density matrix approach. The density matrix operator of the system can be written by the dyadic product of the state of the system

$$\rho = |\psi\rangle\langle\psi| = |C_a|^2|a\rangle\langle a| + |C_b|^2|b\rangle\langle b| + C_aC_b^*|a\rangle\langle b| + C_bC_a^*|b\rangle\langle a|, \tag{2.36}$$

where $|\psi\rangle$ and $\langle\psi|$ are substituted from Eq. (2.3). It is more convenient to write the matrix form of the density operator. Considering the spin notation

$$|\psi\rangle = \begin{pmatrix} C_a \\ C_b \end{pmatrix}; \langle\psi| = \begin{pmatrix} C_a^* & C_b^* \end{pmatrix}, \tag{2.37}$$

we may write

$$\rho = \begin{pmatrix} C_a \\ C_b \end{pmatrix} \begin{pmatrix} C_a^* & C_b^* \end{pmatrix} = \begin{pmatrix} \rho_{aa} & \rho_{ab} \\ \rho_{ba} & \rho_{bb} \end{pmatrix}. \tag{2.38}$$

It is not then difficult to show

$$\rho_{aa} = \langle a|\rho|a\rangle = |C_a|^2, \tag{2.39}$$

$$\rho_{bb} = \langle b|\rho|b\rangle = |C_b|^2, \tag{2.40}$$

where $\rho_{aa} + \rho_{bb} = 1$ and $\rho_{ab} = \rho^*_{ba}$. The diagonal elements ρ_{aa} and ρ_{bb} are referred to as populations, and are related to the probabilities of being in states $|a\rangle$ and $|b\rangle$, respectively. The off-diagonal density matrix elements

$$\rho_{ab} = \langle a|\rho|b\rangle = C_a C^*_b = \rho^*_{ba}, \tag{2.41}$$

are termed as the coherences since they depend on the relative phases of different components of the system wavefunction.

Utilizing Eq. (2.35) one can write the coupled differential equations of the motion describing the evolution of two-level atomic system

$$\dot{\rho}_{ab} = -(i\omega + \gamma_{ab})\rho_{ab} - \frac{i}{\hbar}\wp_{ab}E(\rho_{aa} - \rho_{bb}), \tag{2.42}$$

$$\dot{\rho}_{aa} = -\gamma_a\rho_{aa} + \frac{i}{\hbar}(\wp_{ab}E\rho_{ba} - c.c), \tag{2.43}$$

$$\dot{\rho}_{bb} = -\gamma_b\rho_{bb} - \frac{i}{\hbar}(\wp_{ab}E\rho_{ba} - c.c), \tag{2.44}$$

where $E(t) = \epsilon\cos(\nu t)$ (Eq. (2.4)) and $\gamma_{ab} = (\gamma_a + \gamma_b)/2$ with γ_a and γ_b defined by Eq. (2.34). The above equations of motions are also called optical Bloch equations. When applying the rotating wave approximation, instead of $\cos(\nu t)$ we must use $e^{-i\nu t/2}$.

2.2 Three-level Λ atomic scheme

This section hints at the fact that three-level atomic systems can result in a wealth of novel optical phenomena, as compared to their two-level counterparts. Well-known examples include the effect of electromagnetically induced transparency, slow light, and their associated phenomena. By introducing the three-level Λ atomic scheme, in sections that follows, we present some theoretical foundations and formulations that are useful in understanding deeper these optical properties.

2.2.1 Hamiltonian of the atom-fields system and formulation

Having worked with the two-level atomic system, now we consider the so-called Λ configuration of atomic levels illustrated in Fig. 2.2. In the Λ atom-light coupling scheme, a probe field with amplitude ϵ_p and frequency ω_p connects the ground level $|1\rangle$ to the upper level $|3\rangle$. A control field of amplitude ϵ_c and frequency ω_c couples then the atomic transition $|3\rangle \longleftrightarrow |2\rangle$. The total Hamiltonian for this model is given by

$$H = H_0 + H_I, \tag{2.45}$$

where the free energy Hamiltonian H_0 characterizing the free atom without external fields is

$$H_0 = \hbar\omega_1|1\rangle\langle 1| + \hbar\omega_2|2\rangle\langle 2| + \hbar\omega_3|3\rangle\langle 3|, \tag{2.46}$$

while the interaction Hamiltonian of the system can be represented by

$$H_I = -\boldsymbol{\wp}.(\boldsymbol{E}_p(t) + \boldsymbol{E}_c(t)), \tag{2.47}$$

where $\boldsymbol{\wp}$ is the dipole moment operator. Using the two components $\mathbf{E}_j(t) = \hat{e_j}E_j(t)\,(j = p, c)$ of the total field with $E_j(t) = \frac{1}{2}\epsilon_j \mathrm{e}^{-i\omega_j t} + c.c.$ ($\hat{e_j}$ is the unit polarization vector while $c.c.$ denotes the complex conjugate of the first term), we get

$$H_I = -\frac{1}{2}\wp_{13}\epsilon_p \mathrm{e}^{-i\omega_p t} - \frac{1}{2}\wp_{23}\epsilon_c \mathrm{e}^{-i\omega_c t} + H.c., \tag{2.48}$$

where $H.c.$ represents the hermitian conjugate of the first two terms, and $\wp_{mn} = \wp^*_{nm} = \langle m|\wp|n\rangle$ shows the dipole matrix elements for the corresponding atomic transitions. By means of the Schrödinger equation (**2.1**), the general form of the atomic wavefunction can be written as

$$|\psi(t)\rangle = C_1(t)|1\rangle + C_2(t)|2\rangle + C_3(t)|3\rangle. \tag{2.49}$$

Moving to an appropriate frame rotating with the frequencies of applied fields ω_p and ω_c,

$$C_1(t) = c_1(t)\mathrm{e}^{-i\omega_1 t}, \tag{2.50}$$

$$C_2(t) = c_2(t)\mathrm{e}^{-i(\omega_1+\omega_p)t}, \tag{2.51}$$

$$C_3(t) = c_3(t)\mathrm{e}^{-i(\omega_1+\omega_p-\omega_c)t}, \tag{2.52}$$

and applying the rotating wave approximation, the following equations of the motion are obtained

$$\dot{c}_1 = \frac{i}{2}\Omega_p c_3, \tag{2.53}$$

$$\dot{c}_2 = -i(\Delta_p - \Delta_c)c_2 + \frac{i}{2}\Omega_c c_3, \tag{2.54}$$

$$\dot{c}_3 = -i\Delta_p c_3 + \frac{i}{2}\Omega_p c_1 + \frac{i}{2}\Omega_c c_2, \tag{2.55}$$

where $\Omega_p = \frac{\epsilon_p \wp_{13}}{\hbar}$ and $\Omega_c = \frac{\epsilon_c \wp_{23}}{\hbar}$ stand for the Rabi-frequencies of the probe and control laser fields, while $\Delta_p = \omega_{31} - \omega_p$ and $\Delta_c = \omega_{32} - \omega_c$ represent the detunings of probe and control fields, respectively. Note that for reasons of con-

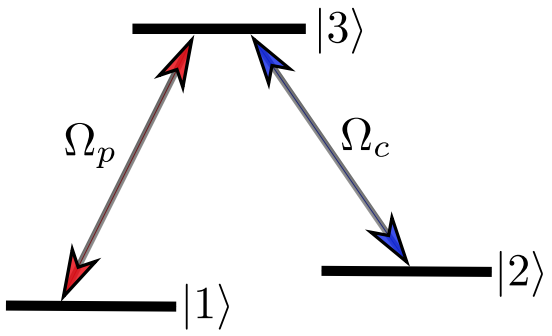

Figure 2.2: Three-level Λ atomic system.

venience we have used the transformation given in Eqs. (2.50)–(2.52) which is different from the transformation to the frame rotating with the eigenfrequencies of the atomic states (for example see Eqs. (2.12)–(2.13) for the two-level atom problem). However, in both frames the equation $c_1(t) = C_1(t)\mathrm{e}^{i\omega_1 t}$ is the same since it redefines the zero point energy to be the energy of level $|1\rangle$.

2.3 Electromagnetically induced transparency (EIT)

In this section, we discuss an important topic which is at the heart of this dissertation, termed as Electromagnetically Induced Transparency (EIT). EIT is an effect in which a probe light beam can suddenly go through the previously optically opaque medium just by applying a secondary coherent illumination beam on the other transition of the Λ scheme. The physical effect on which EIT is based is coherent population trapping (CPT). The crucial point for both CPT and EIT is the creation of a superposition state, through quantum interference, which cannot be excited by radiation. This superposition state is called *dark state*. To realize better how the atom-light interaction can create such a dark state we shall first consider CPT in Λ system.

Applying the rotating wave approximation, the Hamiltonian of the Λ system described by Eq. (2.45) in the frame rotating with the frequencies of applied fields can be represented, in matrix form by [3]

$$H = -\frac{\hbar}{2}\begin{pmatrix} 0 & 0 & \Omega_p \\ 0 & -2(\Delta_p - \Delta_c) & \Omega_c \\ \Omega_p & \Omega_c & -2\Delta_p \end{pmatrix}. \tag{2.56}$$

For the two photon resonance condition $\Delta_p - \Delta_c = 0$, the three eigenstates of the Hamiltonian H in terms of the bare states $|1\rangle$, $|2\rangle$, and $|3\rangle$ can be calculated to [3]

$$|b_1\rangle = \sin\theta \sin\phi|1\rangle + \cos\theta \sin\phi|2\rangle + \cos\phi|3\rangle, \tag{2.57}$$

$$|d\rangle = \cos\theta|1\rangle - \sin\theta|2\rangle, \tag{2.58}$$

$$|b_2\rangle = \sin\theta \cos\phi|1\rangle + \cos\theta \cos\phi|2\rangle - \sin\phi|3\rangle, \tag{2.59}$$

with their corresponding eigenvalues

$$\lambda_1 = \frac{\hbar}{2}(\Delta_p + \sqrt{\Delta_p^2 + \Omega^2}), \tag{2.60}$$

$$\lambda_d = 0, \tag{2.61}$$

$$\lambda_2 = \frac{\hbar}{2}(\Delta_p - \sqrt{\Delta_p^2 + \Omega^2}), \tag{2.62}$$

where the mixing angles θ and ϕ as well as the total Rabi-frequency Ω with

$$\tan\theta = \frac{\Omega_p}{\Omega_c}, \tag{2.63}$$

$$\tan\phi = \frac{\Omega}{\sqrt{\Delta_p^2 + \Omega^2} + \Delta_p}, \tag{2.64}$$

and

$$\Omega = \sqrt{\Omega_p^2 + \Omega_c^2}, \tag{2.65}$$

have been introduced. It becomes apparent from Eqs. (2.57)–(2.59) that both states $|b_{1,2}\rangle$ contain a contribution from all the bare atomic states, while state $|d\rangle$ has no component of the bare state $|3\rangle$. Since there is no transition from the superposition state $|d\rangle$ to the bare state state $|3\rangle$, it cannot interact with the light. As a result, an atomic system prepared in such a superposition becomes transparent to that field. This is why $|d\rangle$ is termed as a dark state.

Having introduced the essence of dark state, next we assume the specific situation in which the probe beam Ω_p is much weaker than the control beam Ω_c ($\Omega_p \ll \Omega_c$). In this case and under the resonance condition $\Delta_p = 0$ one has $\sin\theta \to 0$, $\cos\theta \to 1$ and $\tan\phi \to 1$ ($\phi = \pi/2$). It follows then from Eq. (2.58) that

$$|d\rangle \to |1\rangle, \tag{2.66}$$

which means that the bare state $|1\rangle$ is now a dark state. In this case $|1\rangle$ does not interact with the light, making the resonant medium transparent to the probe laser field.

The first experimental observation of EIT was carried out by Boller, İmamoğlu, and Harris at Stanford University in 1991 for Strontium vapour [48]. During recent years, there has been a vast amount of work investigating the EIT [14, 7, 48, 49, 50, 42], including a number of valuable review articles covering this important effect [3, 51, 52].

EIT can be employed to control and modify various optical properties in an atomic ensemble in a well controlled manner. Slow and stord light [53, 17], lasing without population inversion [24, 18], generation of ultraslow optical solitons [21, 54], an enhanced Kerr nonlinearity [15, 20], nonlinear Faraday effect [55], optical bistability [22, 56], and phase and intensity fluctuations correlation [57] are some of the fascinating applications of EIT.

It is also demonstrated that more complicated EIT structures can be constructed by adding additional energy levels and optical fields to the Λ system, such as the four-level tripod (Fig. 2.3(a)) [25, 41], the double-Λ (Fig. 2.3(b))

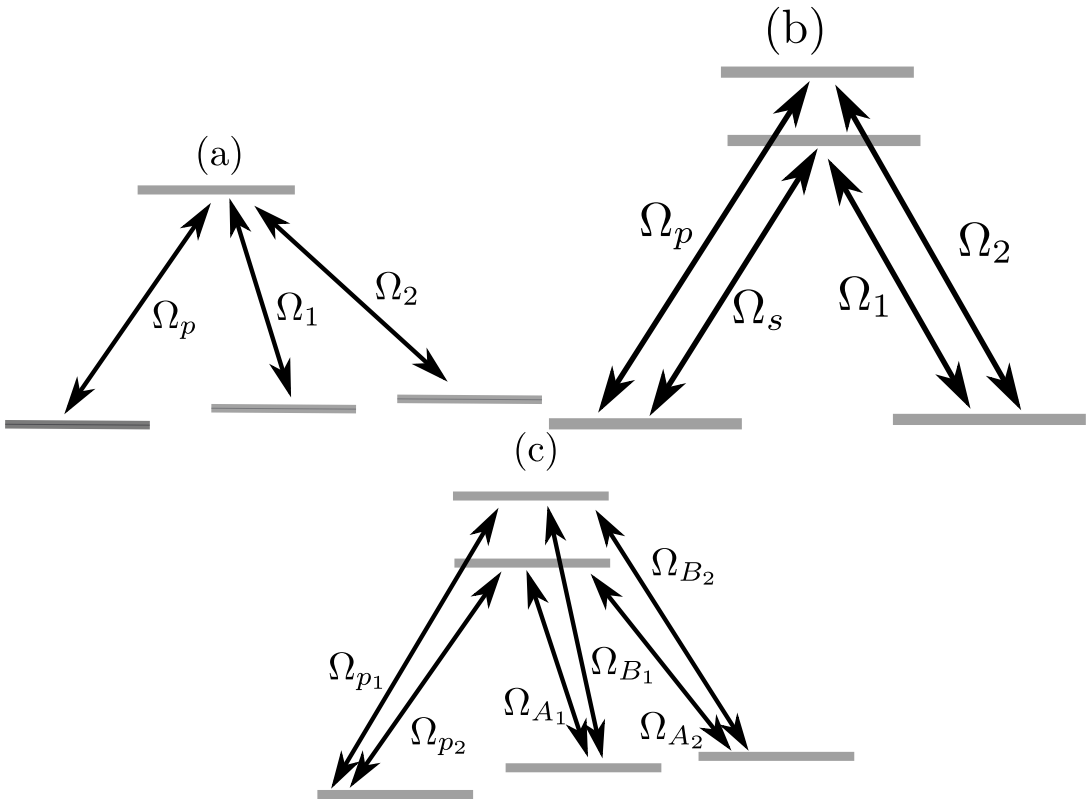

Figure 2.3: Level diagrams for various systems exhibiting EIT. (a) tripod scheme, (b) double Λ scheme, and (c) double tripod.

[27], and the double-tripod (Fig. 2.3(c)) [28, 29] atom light coupling schemes.

2.3.1 Optical Bloch equations for Λ scheme

The basic mechanism for the EIT phenomenon could be explained through the discussion given in previous section. However, this description has not taken into account the effect of decay rates due to spontaneous emission. Similar to the two-level problem, the density matrix approach is required to include the effect of decay rates. Substituting the Hamiltonian (2.56) into the Liouville equation (2.33) results in the following optical Bloch equations for the off-diagonal density matrix elements

$$\dot{\rho}_{31} = -(\gamma_1 + i\Delta_p)\rho_{31} + i\frac{\Omega_p}{2}(\rho_{11} - \rho_{33}) + i\frac{\Omega_c}{2}\rho_{21}, \tag{2.67}$$

$$\dot{\rho}_{21} = -(\gamma_3 + i(\Delta_p - \Delta_c))\rho_{21} + i\frac{\Omega_c}{2}\rho_{31} - i\frac{\Omega_p}{2}\rho_{23}, \tag{2.68}$$

$$\dot{\rho}_{32} = -(\gamma_2 + i\Delta_c)\rho_{32} + i\frac{\Omega_c}{2}(\rho_{22} - \rho_{33}) + i\frac{\Omega_p}{2}\rho_{12}, \tag{2.69}$$

where γ_1, γ_2 and γ_3 represent the the decay rates for the coherence terms ρ_{31}, ρ_{32} and ρ_{21}, respectively. In order to find the solutions for the above set of equations, we need to solve them in the steady state case. In doing so, we shall set the derivative of density matrix elements to zero as there will be no oscillation after the system reachs the steady state. In addition, we assume the weak probe field limit $\Omega_p \ll \Omega_c$ in which the probe field is too small to drive the transition from gound to excited level. This obligates $\rho_{11} \approx 1$ while ρ_{33}, $\rho_{22} \approx 0$. This is reasonable since in the steady state the population is trapped in the dark state $|d\rangle \equiv |1\rangle$. Under this approximation, one may arrive at a coupled pair of equations

$$-(\gamma_1 + i\Delta_p)\rho_{31} + i\frac{\Omega_c}{2}\rho_{21} + i\frac{\Omega_p}{2} = 0, \tag{2.70}$$

$$-(\gamma_3 + i(\Delta_p - \Delta_c))\rho_{21} + i\frac{\Omega_c}{2}\rho_{31} = 0. \tag{2.71}$$

The solution to the coupled equations (2.70) and (2.71) reads, in matrix form

$$R = M^{-1}A, \tag{2.72}$$

with

$$R = \begin{pmatrix} \rho_{31} \\ \rho_{21} \end{pmatrix} \tag{2.73}$$

$$M = \begin{pmatrix} (\gamma_1 + i\Delta_p) & -i\frac{\Omega_c}{2} \\ -i\frac{\Omega_c}{2} & (\gamma_3 + i(\Delta_p - \Delta_c)) \end{pmatrix}, \tag{2.74}$$

and

$$A = \begin{pmatrix} i\frac{\Omega_p}{2} \\ 0 \end{pmatrix}. \tag{2.75}$$

Using Eq. (2.72), the coherence terms ρ_{31} and ρ_{21} can be obtained as

$$\rho_{31} = \frac{i\Omega_p(\gamma_3 + i(\Delta_p - \Delta_c))}{2(\gamma_1 + i\Delta_p)(\gamma_3 + i(\Delta_p - \Delta_c)) + \Omega_c^2/2}, \tag{2.76}$$

$$\rho_{21} = \frac{\Omega_p\Omega_c/2}{2(\gamma_1 + i\Delta_p)(\gamma_3 + i(\Delta_p - \Delta_c)) + \Omega_c^2/2}. \tag{2.77}$$

2.3.2 Susceptibility of the Λ scheme

The impact of a medium on the light propagation is described by the susceptibility χ. The density matrix elements related to the coherence terms ρ_{31} and ρ_{21} have been derived in Eqs. (2.76) and (2.77). Now we demonstrate that the susceptibility of the medium as seen by the probe field is determined by the coherence term ρ_{31}.

Generally, the polarization density of a homogeneous, isotropic medium in presence of any external electric field E can be described by $\boldsymbol{P} = \epsilon_0\chi\boldsymbol{E}$, where ϵ_0 is the permittivity of free space, and χ characterizes the electric susceptibility of the medium [18]. Using this relation, the polarization density of the the Λ atomic system as a function of detunings becomes

$$\boldsymbol{P} = \epsilon_0\chi(\Delta_p)\boldsymbol{E}_p(t) + \epsilon_0\chi(\Delta_c)\boldsymbol{E}_c(t). \tag{2.78}$$

Next we substitute $\mathbf{E}_p(t) = \frac{1}{2}\hat{e_p}\epsilon_p e^{-i\omega_p t} + c.c.$ and $\mathbf{E}_c(t) = \frac{1}{2}\hat{e_c}\epsilon_c e^{-i\omega_p t} + c.c.$ into the above equation, yielding

$$\boldsymbol{P} = \frac{1}{2}\epsilon_0\chi(\Delta_p)\hat{e_p}\epsilon_p(e^{-i\omega_p t} + e^{i\omega_p t}) + \frac{1}{2}\epsilon_0\chi(\Delta_c)\hat{e_c}\epsilon_c(e^{-i\omega_c t} + e^{i\omega_c t}). \tag{2.79}$$

On the other hand, the polarization of a medium can be defined as the dipole moment per unit volume. In this case, the polarization can be expressed, by means of Eq. (2.28), in terms of expectation value of dipole moment of all the atoms

$$\boldsymbol{P} = N\langle\langle \wp \rangle\rangle_{ensemble} = N\,\mathrm{Tr}(\rho\wp), \tag{2.80}$$

where N is the number density of the ensemble of atoms. It is straightforward then to show

$$\boldsymbol{P} = N\,Tr\left(\begin{bmatrix} \rho_{11} & \rho_{12} & \rho_{13} \\ \rho_{21} & \rho_{22} & \rho_{23} \\ \rho_{31} & \rho_{32} & \rho_{33} \end{bmatrix} \begin{bmatrix} 0 & 0 & \hat{e}_p\wp_{13} \\ 0 & 0 & \hat{e}_c\wp_{23} \\ \hat{e}_p\wp_{31} & \hat{e}_c\wp_{32} & 0 \end{bmatrix}\right), \tag{2.81}$$

which results in

$$\boldsymbol{P} = N(\hat{e_p}\wp_{13}\rho_{31} + \hat{e_p}\wp_{31}\rho_{13} + \hat{e_c}\wp_{32}\rho_{23} + \hat{e_c}\wp_{23}\rho_{32}). \tag{2.82}$$

Moving to an appropriate rotating frame

$$\rho_{31} = \rho'_{31}\mathrm{e}^{-i\omega_p t}, \tag{2.83}$$

$$\rho_{32} = \rho'_{32}\mathrm{e}^{-i\omega_c t}, \tag{2.84}$$

$$\rho_{21} = \rho'_{21}\mathrm{e}^{i(\omega_c-\omega_p)t}, \tag{2.85}$$

we get from Eq. (2.82)

$$\boldsymbol{P} = N(\hat{e_p}\wp_{13}\rho'_{31}\mathrm{e}^{-i\omega_p t} + \hat{e_p}\wp_{31}\rho'_{13}\mathrm{e}^{i\omega_p t} + \hat{e_c}\wp_{32}\rho'_{23}\mathrm{e}^{i\omega_c t} + \hat{e_c}\wp_{23}\rho'_{32}\mathrm{e}^{-i\omega_c t}). \tag{2.86}$$

Comparing Eqs. (2.79) with (2.86) results in

$$\frac{1}{2}\epsilon_0\chi(\Delta_p)\epsilon_p = N\wp_{13}\rho_{31}^{'}. \tag{2.87}$$

Sovling Eq. (2.87) for $\chi(\Delta_p)$ gives

$$\chi(\Delta_p) = \frac{2N\wp_{13}}{\epsilon_0\epsilon_p}\rho_{31}, \tag{2.88}$$

where $\rho_{31}^{'}$ is replaced with ρ_{31} as in the steady state they are the same. One can rewrite this equation using the definition of Rabi-frequency of the probe field $\Omega_p = \frac{\epsilon_p\wp_{13}}{\hbar}$, yielding

$$\chi(\Delta_p) = \frac{2N|\wp_{13}|^2}{\hbar\epsilon_0\Omega_p}\rho_{31}. \tag{2.89}$$

It can be seen that the susceptibility of the atomic medium is characterized by the coherence term ρ_{31}. This equation can be generalized to obtain the susceptibility for any multi-level atomic system as

$$\chi(\Delta_p) = \frac{2N|\wp_{13}|^2}{\hbar\epsilon_0\Omega_p}\rho_{ij}. \tag{2.90}$$

where ρ_{ij} is the density matrix element for the probe transition $|i\rangle \longleftrightarrow |j\rangle$.

2.3.3 Description of EIT through Optical Bloch equations

As shown in Eq. (2.89), the linear response of the atomic medium to the applied fields is determined by the susceptibility χ. The susceptibility is generally a complex whose real and imaginary parts correspond to the dispersion and absorption of the probe field, respectively. Inserting the solution of coherence term ρ_{31} from Eq. (2.76) into Eq. (2.89), the explicit form of the linear susceptibility for the Λ system is given by

$$\chi(\Delta_p) = \frac{2N|\wp_{13}|^2}{\hbar\epsilon_0}\frac{i(\gamma_3 + i(\Delta_p - \Delta_c))}{2(\gamma_1 + i\Delta_p)(\gamma_3 + i(\Delta_p - \Delta_c)) + \Omega_c^2/2}. \tag{2.91}$$

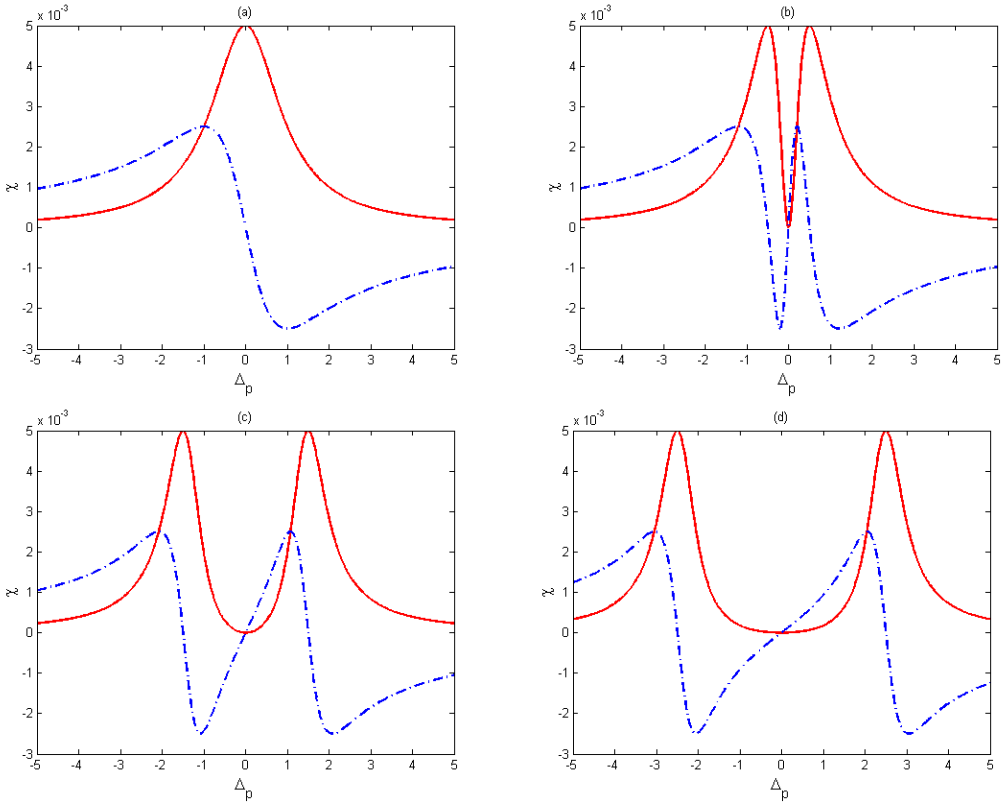

Figure 2.4: Imaginary (Im(χ)) and real(Re(χ)) components of susceptibility in equation (2.91) as a function of Δ_p for (a)$\Omega_c = 0$, (b) $\Omega_c = \gamma$, (c) $\Omega_c = 3\gamma$ and (d) $\Omega_c = 5\gamma$. The other parameters are $\gamma_3 = 0$,$\gamma_1 = \gamma$, $\Delta_c = 0$, and $\Omega_p = 0.01\gamma$.

A typical probe susceptibility profile of the Λ system is displayed in Fig. 2.4 in the ideal limit of $\gamma_3 = 0$. The imaginary part of susceptibility Im(χ) corresponding to absorption as a function of the probe detuning Δ_p is shown in Fig. 2.4 as solid lines. The simulations are in units of $\frac{2N|\wp_{13}|^2}{\hbar\epsilon_0}$ and all the parameters are scaled with dimensionless parameter γ. As illustrated in Fig. 2.4(a), for $\Omega_c = 0$ we observe a large probe absorption at resonance $\Delta_p = 0$. However, a transparency window appears immediately at zero probe detuning in the presence of the control field (see Figs. 2.4(b)–2.4(d)). In this case the absorption vanishes on resonance. Also, for larger values of control field Ω_c the width of transparency window increases. Since an opaque medium becomes transparent and since this induced transparency is due to applying a stronger laser field, this phenomenon is called electromagnetically induced transparency (EIT).

2.4 Slow light

We have observed in Figs. 2.4 that the application of a control laser field on the other transition of the Λ resonant scheme opens up a dip in absorption spectrum (which is related to the imaginary part of the susceptibility of the medium). Also illustrated in Fig. 2.4 is the real component of the susceptibility (blue dot-dash line), called dispersion, which determines how pulse propagates through the medium. As can be seen in Figs. 2.4(b)–2.4(d), in the presence of Ω_c the real part of the susceptibility, i.e., the index of refraction has a positive slope around zero probe detuning. A positive slope of the dispersion near the EIT window corresponds to the slow propagation of light pulse [17]. The steep slope of dispersion along with EIT has significant influence on pulse propagation. According to the definition of group velocity [17]

$$\nu_g = \frac{d\omega}{dk} = \frac{c}{n(\omega) + \omega dn/d\omega}, \tag{2.92}$$

the group velocity is inversely proportional to $dn/d\omega$. Note that here $k = \omega n/c$ shows the wave number and $n = n(\omega)$ denotes the refractive index. This relation implies that a very steep slope of dispersion leads to a large denominator in Eq. (2.92). Therefore, the propagating pulse can be extremely slowed down in the medium. It is apparent from Figs. 2.4(b)–2.4(d) that the steepness of dispersion curve depends strongly on the width of EIT window. The separation between absoption peaks reduces by turning down Ω_c which results in the steeper dispersion curve and hence the slower group velocity. The narrower the transparency window the steeper the slope of dispersion and the slower the light. This is the foundation for EIT-based slow light.

In order to figure out how the light propagating through the medium can be slowed down, one can visualize photons of light as a group of fast cars (Fig. 2.5). If such fast cars are suddenly attached to some heavy trailers, they get inevitably slowed down since their engine must pull also heavy trailers. Slow light has almost a similar scenario. Most of the fast photons are changed into some atomic excitations when traveling inside the medium. The atomic excitations produced in this way behave like heavy immobile trailers. The remaining photons which are not yet converted into atomic excitations have to pull the immobile excitations. As a result, the whole light pulse propagating inside the medium is

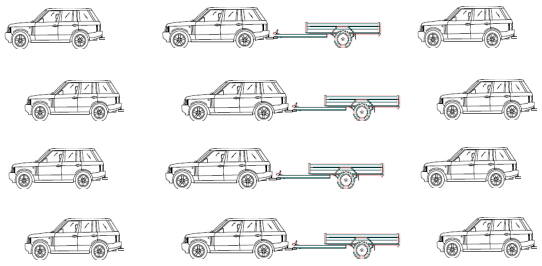

Figure 2.5: A simple scenario for slow light situation

slowed down significantly. In contrast, the atomic excitations change again into photons as the light reaches the tail of the atomic medium, so the light can move on with its full speed.

The subject of slow, or subluminal light has caused keen interest since 1999 when the group velocity of light was reduced to 17 $m\,s^{-1}$ in an experiment by Harris group [58]. The physical nature of slow light is electromagnetically induced transparency [7, 58]. Slow light has found potential applications in many areas of quantum optics and photonics [59], telecommunications and optical communications [60, 59], and optical switching [61]. Slow light is a scientific demonstration of the famous story of the rabbit and the tortoise: *the faster is not necessarily always better*. Having access to a considerable slow, but smart light rather than just a very fast light may provide new opportunities, for instance, in temporarily storing light with applications in all-optical memories [62].

2.5 Theory of atom localization

As the interaction of an atom with optical fields is concerned, in this section we discuss the concept of atom localization which is one of the important consequences of quantum coherence and interference [13, 63, 64, 65, 66]. It is known from the early days of quantum mechanics that the Heisenberg microscope [67] imposes limitation that the atomic position cannot be detected more precisely than the half-wavelength of radiation used for the detection. In the archetype of this measuring device, based on the uncertainty principle $\triangle p_x \triangle x \sim \hbar$, the largest momentum kick transferred from an optical photon to an atom $\triangle p_x = 2\hbar k$, indicates the precision in the measurement of the atomic

position in terms of the optical wavelength $\lambda = 2\pi/k$ as $\triangle x \sim \lambda/2$. Following these arguments the atom cannot be localized within distances beyond the optical half-wavelength. However, novel localization techniques based on quantum interference and coherence have made it possible to overcome this fundamental limit, and extremely high precision spatial resolutions have been achieved for measurement of the atomic position. For instance, Gorshkov et al. [68] suggested a method based on dark state of EIT to localize an atomic excitation with resolution that approaches a few nanometers. The Scully group reported experimentally the first proof of dark state-based localization in a *Rb* vapor cell [69]. Recently, Miles and co-workers have demonstrated an experiment in which the atomic excitation is confined to a spatial width of $100nm$, which is a factor of 8 smaller than the wavelength of the laser beams used in their experiment [70].

Precision position measurement of an atom is useful in neutral atom lithography with ultrahigh resolution [71], measurement of the center-of-mass wave function of moving atoms [72] and coherent patterning of matter waves [73].

Atom localization has been recently shown to be possible through detection of the spontaneously emitted photon during the interaction of an atom with the classical standing wave [13, 74, 75, 32]. For instance, Zubairy group [13] suggested a simple proposal for localization of a two-level atom based on resonance fluorescence from a standing wave. Closely related to this work, a three-level atomic configuration with two upper levels was employed by the same group [76]. It was shown that the measurement of spontaneously emitted photon from the upper level to lower level provides information about the atomic position.

It is, however, very tricky and difficult experimentally to observe the spontaneous emission spectrum. In this regard, Paspalakis and Knight considered another scheme for atom localization based on a three-level Λ-type EIT system illuminated by a weak probe laser field and a standing wave field [77]. It was demonstarted by them that when the probe field is much weaker than the control field, the population measurement in the upper level results in subwavelength localization of the atom during its motion in the standing wave. This is essentially the localization of atom based on absorption of the probe field. Based on this idea, i.e., atom localization using absorption of the probe field, Sahrai et al. described another method of atom localization based on electromagnetically induced transparency in a four-level system interacting with a weak probe field,

two driving fields and a standing wave field [26]. Along with theoretical studies, considerable progress has been made in realizing the atom localization from the experimental point of view [68, 70, 78, 79]. The key idea for all of these studies is to utilize the sensitivity of the dark state of EIT to the intensity of standing wave coupling laser.

Let us first consider again the three-level Λ system. We assume that the atomic system moves along the z direction and passes through a classical standing wave field which is aligned with the x axis. As a result of position dependent interaction between the atom and the standing wave, the Rabi-frequency of the standing wave is also position dependent and can be taken as $\Omega_c(x) = \Omega_c \sin(kx)$, where k is the wave vector of the standing wave ($k = \frac{2\pi}{\lambda}$). The center of mass position of the atom is assumed to be nearly constant along the direction of the standing wave. Thus, one can neglect the kinetic part of the atom from the Hamiltonian under the Roman-Nath approximation [80]. In this case and under the rotating wave approximation, one arrives at Eq. (2.56) for the Hamiltonian of the system. The probe susceptibility of the system given in Eq. (2.91) may be rewritten as

$$\chi = \frac{2N|\wp_{13}|^2}{\hbar\epsilon_0} \frac{i(\gamma_3 + i(\Delta_p - \Delta_c))}{2(\gamma_1 + i\Delta_p)(\gamma_3 + i(\Delta_p - \Delta_c)) + \Omega_c^2 \sin^2(kx)/2}. \tag{2.93}$$

Equation (2.93) determines an important feature of the system in presence of the position dependent standing wave field: it is possible to obtain information about the position of the atom via measuring the probe absorption which is related to imaginary part of Eq. (2.93). Equation (2.93) shows also that the probe absorption is not only dependent on position x, but also on the system parameters such as the amplitude of the standing wave Ω_c, the probe detuning Δ_p as well as the control detuning Δ_c. The maxima of probe absorption are obtained when the probe laser detuning fulfills the equation [77]

$$\Delta_p = \frac{\Delta_c}{2} \pm \frac{1}{2}\sqrt{\Delta_c^2 + (\gamma_1\gamma_3 + \Omega_c^2 \sin^2(kx)/4)}, \tag{2.94}$$

which indicates that the maxima are located at

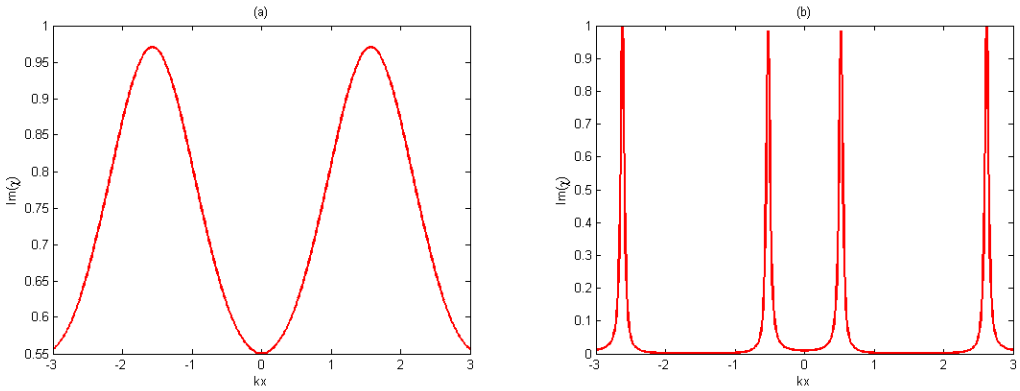

Figure 2.6: Imaginary ($\mathrm{Im}(\chi)$) component of susceptibility in equation (2.93) as a function of kx for (a) $\Omega_c = \gamma$ and (b) $\Omega_c = 4\gamma$. The other parameters are $\gamma_3 = 0, \gamma_1 = 0.1\gamma$,$\Delta_c = 0$, $\Delta_p = \gamma$, and $\Omega_p = 0.01\gamma$.

$$kx = \sin^{-1}\left(\frac{2\sqrt{\Delta_p^2 - \Delta_p\Delta_c - \gamma_1\gamma_3}}{\Omega_c}\right) + n\pi, \tag{2.95}$$

which n is an integer. Shown in Fig. 2.6(a), when the standing wave is on resonance $\Delta_c = 0$ and for $\Omega_c = \gamma$, localization appears in the system. In this case two peaks occur in absorption profile of the system, located at the antinodes of the standing wave field. However, the localization peaks are wide and the spatial resolution of the atom is not high. With increase of Ω_c to 4γ a strong localization of the atom appears around nodes of the standing wave (Fig. 2.6(b)). However, the detection probability of finding the atom in one period of standing wave is only 1/4.

2.6 Nonlinear optical phenomena

This section gives a brief introduction to the main characteristics of the third-order nonlinear optical effects. We shall consider how the polarization of a material depends on the strength of an external optical field in order to understand the physical meaning of the concept of optical nonlinearity. When laser light shines on the matter, it can reorient dipole moments of atoms, leading to a nonzero average dipole moment per unit volume or polarization of the material system. In the realm of linear optics where the applied field is not too large, the polarization is expressed as

$$\boldsymbol{P}(t) = \epsilon_0 \chi^{(1)} \boldsymbol{E}(t), \tag{2.96}$$

where ϵ_0 is known as the permittivity of free space and $\chi^{(1)}$ is the susceptibility of linear optics. Obviously, the induced polarization $\boldsymbol{P}(t)$ is linearly dependent on the electric field strength $\boldsymbol{E}(t)$. Such a linear polarization governs linear optical phenomena, such as electromagnetically induced transparency, slow light and so on. As the magnitude of the electric field increases, the linear relationship between $\boldsymbol{P}(t)$ and $\boldsymbol{E}(t)$ breaks down and we enter the realm of nonlinear optics. In this case, by generalizing the polarization $\boldsymbol{P}$(t) as a power series in the field strength $\boldsymbol{E}(t)$, one has

$$\begin{aligned} \boldsymbol{P}(t) &= \boldsymbol{P}^{(1)}(t) + \boldsymbol{P}^{(2)}(t) + \boldsymbol{P}^{(3)}(t) + ... \\ &= \epsilon_0 \left(\chi^{(1)} + \chi^{(2)} \boldsymbol{E}(t) + \chi^{(3)} \boldsymbol{E}(t) \boldsymbol{E}(t) + ... \right) \boldsymbol{E}(t), \end{aligned} \tag{2.97}$$

where $\boldsymbol{P}^{(1)}$, $\boldsymbol{P}^{(2)}$, and $\boldsymbol{P}^{(3)}$ are linear, second- and third-order nonlinear polarizations, respectively. In addition, $\chi^{(1)}$, $\chi^{(2)}$ and $\chi^{(3)}$ are referred to as first-, second- and third-order order susceptibilities. In writing Eqs. (2.96) and (2.97) we have considered for simplicity $\boldsymbol{E}(t)$ and $\boldsymbol{P}(t)$ to be scalar quantities.

2.6.1 Third-order nonlinear effects

Third-order optical nonlinearity is encountered in any material regardless of its spatial symmetry [81]. Since all even-order nonlinearities are identically equal to zero in central symmetric materials, the lowest-order nonvanishing nonlinear optical susceptibility is of third order. The polarization equation (2.97) in this case can be expressed as

$$\boldsymbol{P} = \boldsymbol{P}^{(1)} + \boldsymbol{P}^{(3)} = \epsilon_0 \left(\chi^{(1)} + \chi^{(3)} \boldsymbol{E}(t) \boldsymbol{E}(t) \right) \boldsymbol{E}(t). \tag{2.98}$$

Let us now consider a nonlinear medium with third-order nonlinear susceptibility $\chi^{(3)}$ and a monochromatic input field of the frequency ω with the form

$$\boldsymbol{E}(t) = E \mathrm{e}^{i\omega t} + c.c.\,. \tag{2.99}$$

The third-order response reads

$$\boldsymbol{P}^{(3)} = \epsilon_o \chi^{(3)} \boldsymbol{E}(t)\boldsymbol{E}(t)\boldsymbol{E}(t) = \epsilon_0 \chi^{(3)} E^3 \mathrm{e}^{i3\omega t} + 3\epsilon_0 \chi^{(3)} E^2 E^* \mathrm{e}^{i\omega t} + c.c.. \quad (2.100)$$

The first term in Eq. (2.100) describes a field which oscillates at the frequency 3ω which is created by the applied field of frequency ω. This term is related to the process of third-harmonic generation and is beyond the scope of this dissertation. The second term in this equation describes the nonlinear contribution to the polarization at the input frequency ω and is known as the AC or optical Kerr effect. Considering both linear and nonlinear contributions to the polarization, we get

$$\begin{aligned} \boldsymbol{P} &= \boldsymbol{P}^{(1)} + \boldsymbol{P}^{(3)}_{\omega} \\ &= \epsilon_0 \chi^{(1)} E \mathrm{e}^{i\omega t} + 3\epsilon_0 \chi^{(3)} E^2 E^* \mathrm{e}^{i\omega t} + c.c. \\ &= \epsilon_0 (\chi^{(1)} + 3\chi^{(3)} E E^*) E \mathrm{e}^{i\omega t} + c.c. \\ &= \epsilon_0 \chi E \mathrm{e}^{i\omega t} + c.c., \end{aligned} \quad (2.101)$$

where the total susceptibility is

$$\chi = \chi^{(1)} + 3|E|^2 \chi^{(3)}. \quad (2.102)$$

Before proceeding, it is clear from Eq. (2.102) that $\chi^{(3)} \propto (\chi - \chi^{(1)})$, which means that the nonlinear susceptibility $\chi^{(3)}$ has the opposite sign with the linear susceptibility $\chi^{(1)}$. As the linear absorption is related to the imaginary part of the linear susceptibility, the strong nonlinear effects can efficiently suppress the absorption of the field.

On the other hand, the second term in Eq. (2.100) can also lead to an intensity-dependent change of the refractive index of the medium. It is generally true that [81]

$$n^2 = 1 + \chi = 1 + \chi^{(1)} + 3|E|^2 \chi^{(3)}, \quad (2.103)$$

where n describes the total refractive index. Generally, the refractive index in the presence of the nonlinearity can be represented as

$$n = n_0 + n_2\langle \boldsymbol{E}(t)^2\rangle, \tag{2.104}$$

where the brackets surrounding the quantity $\boldsymbol{E}(t)^2$ correspond to a time average. Here, n_0 describes the linear weak-field refractive index, and n_2 represents the nonlinear refraction coefficient. For the field of the form given by Eq. (2.99), we have $\langle \boldsymbol{E}(t)^2\rangle = 2EE^* = 2|E|^2$, then Eq. (2.104) yields

$$n = n_0 + 2n_2|E|^2. \tag{2.105}$$

Similar to the electro-optical Kerr effect, the change in refractive index charactrized by Eq. (2.105) can be called as optical Kerr effect, because it is proporional to the squre of the applied field. Comparing Eqs. (2.103) and (2.105), and correcting to terms of order $|E|^2$ we find

$$n_0 = \sqrt{1 + \chi^{(1)}}, \tag{2.106}$$

which shows the linear refractive index, and

$$n_2 = \frac{3\chi^{(3)}}{4n_0}, \tag{2.107}$$

which represents the nonlinear refraction coefficient. Third-order nonlinearities can lead to several interesting nonlinear optical phenomena and many important applications which will be discussed in the next chapters.

2.6.2 Linear and nonlinear susceptibilities

We now obtain expressions representing the linear $\chi^{(1)}$ and nonlinear $\chi^{(3)}$ susceptibilities. As it is shown in Eq. (2.89) for the thee-level Λ system, the expression describing the total susceptibility for the probe transition $|i\rangle \rightarrow |j\rangle$ in terms of density matrix elements ρ_{ij} is

$$\chi = \frac{2N|\wp_{ji}|^2}{\hbar\epsilon_0\Omega_p}\rho_{ij}, \tag{2.108}$$

where $\wp_{ji}$ is the transition dipole moment between the levels $|i\rangle$ and $|j\rangle$. In order to obtain linear and nonlinear susceptibilities we shall expand the density matrix elements ρ_{ij} as

$$\rho_{ij} = \rho_{ij}^{(0)} + \rho_{ij}^{(1)} + \rho_{ij}^{(2)} + \rho_{ij}^{(3)} + ..., \tag{2.109}$$

where the constituting terms $\rho_{ij}^{(0)}$, $\rho_{ij}^{(1)}$, $\rho_{ij}^{(2)}$ and $\rho_{ij}^{(3)}$ are of the zeroth, first, second, and third- orders in the probe field Ω_p for the transition $|i\rangle \rightarrow |j\rangle$. Assuming that the level $|i\rangle$ is a ground level, the zeroth solution reads $\rho_{ii}^{(0)} = 1$, while other elements are zero ($\rho_{ij}^{(0)} = 0$). This is an obligation due to the weak probe field limit when the probe field is too small to drive the transition from gound to excited level. In this limit, the linear and nonlinear susceptibilities $\chi^{(1)}$ and $\chi^{(3)}$ can be obtained from substituting Eqs. (2.102) and (2.109) into Eq. (2.108), yielding

$$\chi^{(1)} = \frac{2N|\wp_{ji}|^2}{\hbar\epsilon_0\Omega_p}\rho_{ij}^{(1)}, \tag{2.110}$$

and

$$\chi^{(3)} = \frac{2N|\wp_{ji}|^4}{3\epsilon_0\hbar^3\Omega_p^3}\rho_{ij}^{(3)}. \tag{2.111}$$

Obviously, the linear and nonlinear susceptibilites are directly related to the off-diagonal density matrix elements $\rho_{ij}^{(1)}$ and $\rho_{ij}^{(3)}$. Having obtained the linear and nonlinear susceptibilities, one can explore the linear and nonlinear optical properties of an atomic system. It is well known that the Kerr nonlinearity (nonlinear dispersion) corresponds to the real part of the third order susceptibility $\chi^{(3)}$, while the imaginary part of $\chi^{(3)}$ determines the nonlinear absorption. The imaginary and real parts of linear susceptibility $\chi^{(1)}$ correspond to linear absorption and dispersion, respectively. That is the issue of next chapter to investigate the nonlinear optical properties of multi-level atomic structures in more details.

2.6.3 EIT enhanced Kerr nonlinearity

Apart from their intriguing linear optical properties, quantum interference and coherence in multi-level atomic structures can induce several nonlinear optical phenomena. These effects also hold great promise for applications in low-light-level nonlinear optics in terms of their ability to enhance the efficiencies of nonlinear optical processes. The absorption coefficient on resonance of a probe field can be efficiently eliminated through the effect of EIT, prompting the enhanced resonant nonlinear interaction strength in atomic configurations. Additionally, the slow light forming due to the EIT increases the effective interaction length of the probe field with the atomic ensemble, enabling nonlinear optical processes to be performed at very low light intensities [82, 33, 83, 84, 85, 86, 87, 88].

Over the last decades, several experiments were proposed in multi-level atomic schemes with the aim of enhancing nonlinear optical processes. Examples include optical harmonic generation [89], frequency conversion [90], EIT-induced beam focusing [91], and so on. A common problem with all of these nonlinear phenomena is yet the existence of a large linear absorption which makes it quite difficult to straightly measure the nonlinear coefficients intrinsic in these nonlinear processes. A giant Kerr nonlinearity is practically interesting since it can be accompanied with zero linear absorption in a multi-level atomic system.

The idea of EIT-based enhanced Kerr nonlinearity was first given by Schmidt and Imamoglu in 1996 [20]. They showed that a resonantly enhanced nonlinearity along with vanishing linear susceptibilities can be achieved in a four-level N-type atomic scheme. Thenceforward many proposals have been suggested both theoretically and experimentally for achieving enhanced Kerr nonlinearity accompanied by negligible absorption in multi-level atomic systems [37, 92, 93, 16, 15, 36, 20, 94, 95, 96]. Wang et al. [16] studied experimentally the enhanced Kerr nonlinear coefficient in a three-level Λ-type atomic system for various powers of the coupling beam. They showed that the Kerr nonlinear coefficient behaves very differently in the regions of strong- and weak-coupling power and changes its sign when the coupling or the probe frequency detuning changes a sign. It was found that the Kerr nonlinear index can be greatly enhanced (compared to that in a two-level atomic system) due to the atomic coherence in the three-level atomic system. A five-level M-type system was proposed by Matsko et al. to obtain a large EIT Kerr nonlinearity [95]. Niu

and Gong [93] investigated theoretically the effect of spontaneously generated coherence (SGC) on the Kerr nonlinearity of three-level systems of the Λ-, ladder-, and V-shape types. They found that with the SGC the Kerr nonlinearity can be clearly enhanced. In the Λ- and ladder- type systems, the maximum Kerr nonlinearity increases and at the same time enters the EIT window as the spontaneously generated coherence gets larger. As for the V-type system, the absorption property is significantly modified and thus an enhancement of the Kerr nonlinearity without absorption occurs for certain probe detuning.

In another study, Niu et al. [37] proposed a scheme for a giant enhancement of the Kerr nonlinearity in a four-level system with double dark resonances. They showed that the Kerr nonlinearity can be enhanced by several orders of magnitude (compared to the one generated in a single-dark-resonance system) accompanied by a vanishing linear absorption. This dramatic enhancement was attributed to the interaction of dark resonances [37]. By using an efficient state-preparation technique for the $^{87}Rb\,D_1$ line, Hun et al. demonstrated that an ideal four-level tripod-type atomic system can be formed that generates a large cross-Kerr-nonlinearity via interacting dark states in this system [92].

There are several potential applications that would benefit from giant Kerr nonlinearities. Examples are: four-wave mixing [97], formation of optical solitons [54], Quantum logic gates [20], and entangled states for quantum information processing [98].

2.6.4 Linear and nonlinear pulse propagation

2.6.4.1 Linear pulse propagation

It is known that the wave equation describing the propagation of light pulse through an optical medium is governed by Maxwell's equations (in SI units),

$$\nabla\cdot \boldsymbol{D} = \rho, \tag{2.112}$$

$$\nabla\cdot \boldsymbol{B} = 0, \tag{2.113}$$

$$\nabla\times \boldsymbol{E} = -\frac{\partial \boldsymbol{B}}{\partial t}, \tag{2.114}$$

$$\nabla\times \boldsymbol{H} = \frac{\partial \boldsymbol{D}}{\partial t} + \boldsymbol{J}, \tag{2.115}$$

where $\boldsymbol{E}$ and $\boldsymbol{H}$ represent electric and magnetic field vectors, respectively, while $\boldsymbol{D}$ and $\boldsymbol{B}$ are corresponding electric and magnetic flux densities. Also, the current density vector $\boldsymbol{J}$ and the charge density ρ are the electromagnetic field sources. In the absence of free charges in a medium, $\boldsymbol{J} = 0$ and $\rho = 0$. The response of the medium is given by

$$\boldsymbol{D} = \epsilon_0 \boldsymbol{E} + \boldsymbol{P}, \tag{2.116}$$

$$\boldsymbol{B} = \mu_0 \boldsymbol{H} + \boldsymbol{M}, \tag{2.117}$$

where $\boldsymbol{P}$ is the electric polarization and $\boldsymbol{M}$ shows the magnetization. The vacuum permittivity and the vacuum permeability are also denoted by ϵ_0 and μ_0, respectively. Assuming that the material is nonmagnetic, then we have $\boldsymbol{M} = 0$. In this case, by using Eqs. (2.112)-(2.117) we may obtain

$$\nabla \times (\nabla \times \boldsymbol{E}) + \frac{1}{c^2}\frac{\partial^2 \boldsymbol{E}}{\partial t^2} = -\frac{1}{\epsilon_0 c^2}\frac{\partial^2 \boldsymbol{P}}{\partial t^2}, \tag{2.118}$$

which describes the most general form of the wave propagation equation. Using

$$\nabla \times (\nabla \times \boldsymbol{E}) = \nabla(\nabla.\boldsymbol{E}) - \nabla^2 \boldsymbol{E} = -\nabla^2 \boldsymbol{E}, \tag{2.119}$$

we arrive at the equation

$$\nabla^2 \boldsymbol{E} - \frac{1}{c^2}\frac{\partial^2 \boldsymbol{E}}{\partial t^2} = \frac{1}{\epsilon_0 c^2}\frac{\partial^2 \boldsymbol{P}}{\partial t^2}, \tag{2.120}$$

where we have used $\nabla.\ \boldsymbol{D} = 0$ (Eq. (2.112)). Aassuming the field is traveling along the z direction, the electric field and the induced polarization vectors can

be written as

$$\boldsymbol{E}(r,t) = \hat{e}E(z,t);\ \boldsymbol{P}(r,t) = \hat{e}P(z,t), \tag{2.121}$$

where $\hat{e}$ is the unit polarization vector normal to the direction of propagation. The wave equation (2.120) then reduces to

$$\frac{\partial^2 E}{\partial z^2} - \frac{1}{c^2}\frac{\partial^2 E}{\partial t^2} = \frac{1}{\epsilon_0 c^2}\frac{\partial^2 P}{\partial t^2}. \tag{2.122}$$

Introducing a classical electric field of the carrier frequency ω and wavevector $k = \omega/c$,

$$E(z,t) = A(z,t)\mathrm{e}^{i(kz-\omega t)} + c.c., \tag{2.123}$$

where $A(z,t)$ represents a slowly varing in time and space envelope of the field, the induced polarization becomes

$$P(z,t) = p(z,t)\mathrm{e}^{i(kz-\omega t)} + c.c., \tag{2.124}$$

with $p(z,t)$ being a slowly varing in time and space function. Generally, both $A(z,t) = \overline{A}\mathrm{e}^{i\phi}$ and $p(z,t) = \overline{p}\mathrm{e}^{i\phi}$ are complex functions, with $\overline{A}$ and $\overline{p}$ representing real amplitudes, while ϕ is the phase. Next we adopt the *slowly varying envelope approximation* (SVEA)

$$\left|\frac{\partial \overline{A}}{\partial t}\right| \ll \omega\left|\overline{A}\right|,\ \left|\frac{\partial \overline{A}}{\partial z}\right| \ll k\left|\overline{A}\right|, \tag{2.125}$$

$$\left|\frac{\partial \phi}{\partial t}\right| \ll \omega,\ \left|\frac{\partial \phi}{\partial z}\right| \ll k, \tag{2.126}$$

$$\left|\frac{\partial \overline{p}}{\partial t}\right| \ll \omega\left|\overline{p}\right|,\ \left|\frac{\partial \overline{p}}{\partial z}\right| \ll k\left|\overline{p}\right|, \tag{2.127}$$

which means physically that we consider light waves whose amplitudes and phases vary little within an optical wavelength and optical period. Under the SVEA and by substituting Eqs. (2.123) and (2.124) into Eq. (2.122), we arrive at the following equation

$$\frac{\partial A}{\partial z} + \frac{1}{c}\frac{\partial A}{\partial t} = i\frac{k}{2\epsilon_0}p, \tag{2.128}$$

which is a starting point in many problems of quantum optics dealing with pulse propagation in atomic media.

2.6.4.2 Nonlinear Schrödinger equation

As stated before, strong laser pulses can induce a nonlinear polarization in matter. In this case the induced polarization $\boldsymbol{P}$ can be decomposed to its linear and nonlinear parts as

$$\boldsymbol{P} = \boldsymbol{P}^{(L)} + \boldsymbol{P}^{(NL)}, \tag{2.129}$$

where $\boldsymbol{P}^{(L)}$ and $\boldsymbol{P}^{(NL)}$ are the linear and nonlinear parts of $\boldsymbol{P}$. Then the wave equation (2.120) can be expressed as

$$\nabla^2\boldsymbol{E} - \frac{1}{c^2}\frac{\partial^2\boldsymbol{E}}{\partial t^2} = \frac{1}{\epsilon_0 c^2}\frac{\partial^2\boldsymbol{P}^{(L)}}{\partial t^2} + \frac{1}{\epsilon_0 c^2}\frac{\partial^2\boldsymbol{P}^{(NL)}}{\partial t^2}, \tag{2.130}$$

which presents the general form of nonlinear propagation of light pulse. Assuming that the polarization does not change during the propagation, then the scalars can be used instead of vectors. Using the slowly varying envelope approximation one can cast the Nonlinear Schrödinger equation (NLSE)

$$\frac{\partial A}{\partial z} = -i\beta\frac{\partial^2 A}{\partial \tau^2} + i\mathbb{k}|A|^2 A, \tag{2.131}$$

where the term with β is due to the group velocity dispersion, while the term with $\mathbb{k}$ represents the effect of third order Kerr nonlinearity which is responsible for soliton formation by inducing an index change directly proportional to the light intensity. Equation (2.131) describes intense optical pulse propagation

through nonlinear dispersive media which, depending on the sign of the group-velocity dispersion β, has two distinct types of solutions, bright or dark solitons. The full derivation of NLSE is extensively discussed in literature [81, 99].

2.6.4.3 Slow optical solitons

Laser-driven atomic media, as stated before, can be exploited to exhibit various nonlinear optical phenomena [15, 20, 54, 86, 96, 100, 101, 102, 103, 104]. A particular example is formation of optical solitons with applications for optical buffers, phase shifters [96], switches [105], routers, transmission lines [106], wavelength converters [107], optical gates [108] and others. Solitons represent a specific type of stable shape preserving waves propagating through nonlinear media. They can be formed due to a balance between dispersive and nonlinear effects leading to an undistorted propagation over long distance [100, 54, 108, 109, 110, 111, 99, 112]. Most of optical solitons are generated with highly intense electromagnetic fields. Also, far-off resonance excitation schemes are required to avoid any uncontrollable attenuation and distortion of optical waves propagation [16, 99]. As a result, optical solitons formed in this way popagate with the speed close the speed of light in vacuum. Fortunately, the EIT effect can result in significant reduction of the propagation velocity of an optical field [7, 17, 58]. The phenomenon of EIT leads also to the substantial enhancement of nonlinear effects such as a large enhancement of the Kerr nonlinearity in highly resonant media [15, 16, 20, 37, 95, 96]. The question of interest is if the coherent effect of EIT can also be utilized in generation and propagation of optical solitons with slow group velocity. Following a report of ultraslow optical solitons in a highly resonant atomic medium by Wu and Deng [100], these solitary waves have received a considerable attention [113, 114, 115, 116, 117, 118, 119, 120, 121, 122]. It was demonstrated that the significant probe field spreading and attenuation due to group velocity dispersion can be precisely balanced by the Kerr nonlinear effect in a highly resonant four-state atomic system [100]. Hang et al. showed that stable spatial optical solitons with extremely weak-light intensity can occur in a highly resonant three-state medium through the mechanism of EIT [115]. The formation and propagation of three-wave coupled vector optical solitons with ultraslow group velocities in a lifetime-broadened seven-state triple-Λ atomic system was also explored under Raman excitation [117]. Recently, the storage and retrieval of ultraslow optical solitons in an ultracold ladder-type three-level atomic gas was investigated by Chen and colleagues [120]. In our

work, we report a new atom-light coupling scheme to realize such slow optical solitons under the effect of EIT.

Chapter 3

An enhanced Kerr nonlinearity

Kerr nonlinearity, which is proportional to the refractive part of the third-order susceptibility, plays an important role in optical data processing because it can be used to control a signal of light by means of another light beam. The optical Kerr nonlinearity also allows propagation of ultrashort soliton-type pulses without spreading [54]. It is desirable to have large third-order nonlinear susceptibilities under conditions of low light power and high sensitivities [23, 123] since it can be used for realization of single-photon nonlinear devices. This requires that the linear susceptibilities should be as small as possible compared to the nonlinear ones. For many years, experimental research on quantum nonlinear optics has been limited because of a weak nonlinear response of even the best materials. Fortunately, EIT [7, 124] has opened a possibility to achieve large nonlinearities [4].

Recently, the self-Kerr-nonlinearity of a four-level N-type atomic system was investigated near atomic resonance by Sheng et al. [15]. They showed that the self-Kerr-nonlinear coefficient of the probe field can be greatly enhanced by properly adjusting the switching laser intensity. In addition, they compared both experimentally and theoretically the self Kerr-nonlinear coefficients for different atomic energy-level configurations of the two-, three-, and four-level cases. In particular, they found that the magnitude of the self-Kerr nonlinear index for the four-level N-type atomic has the same value as that for the three-level system. More recently, Khoa et al. [36] investigated theoretically the possibility of obtaining an enhanced self-Kerr-nonlinearity under the EIT condition for a five-level cascade system. They also made a comparison between the behavior of self-Kerr nonlinearity for such a five-level atomic system with that of four- and three-level cascade systems and observed the same magnitude

of the self-Kerr-nonlinear coefficient among the three systems.

Due to its possible application in all-optical switching, quantum information processing, and novel photonic devices, especially at the few-photon level [61, 125], it is expected that more experimental studies on this subject will be carried out. Thus, practical schemes are needed to achieve the Kerr nonlinearity enhancement.

In this chapter a five-level atomic system is proposed that was first introduced by Kobrak and Rice [126] to establish a complete population transfer [127, 128] to a single target of a degenerate pair of states. The Kobrak-Rice five-level (KR5) system was also employed to show advantages of the coherent control of atomic or molecular processes [129]. Moreover, by using intense laser fields, a new quantum measurement has been introduced in the KR5 system [130]. Dispersion and absorption and optical bistability of this configuration have also been investigated [131, 132]. However, the third-order nonlinear susceptibility for this medium has motivated our study.

We show that an enhanced Kerr nonlinearity with a reduced absorption can be obtained under the condition of slow light propagation for the KR5 atomic system. We find that the Kerr nonlinearity is very sensitive to the relative phase of the applied fields and explore the influence of the relative phase on the linear and nonlinear optical properties of the medium. In particular, it is shown that under the condition of the multiphoton resonance, one can enhance the Kerr nonlinearity of such a medium by properly adjusting the amplitudes and phases of the applied fields. In this case, the linear and nonlinear absorption are reduced remarkably in the region of the subluminal light propagation. Also, we make a comparison between the Kerr-nonlinear indices for this five-level system with that of the existing four and three-level atomic systems. We find that the magnitude of the Kerr nonlinearity of the KR5 system is larger than that of four- and three-level systems. The influence of the Doppler broadening on the Kerr nonlinearity is also studied. We find considerable changes in shape for the Kerr nonlinearity for a small Doppler width below the natural linewidth of the probe transition for which the linear susceptibility behaves very similarly in shape to the nonbroadened case. In addition, it is observed that the effect of the Doppler broadening can lead to a giant Kerr nonlinearity [43].

The main advantages of applying the considered five-level system over the

atomic schemes proposed in Refs. [15, 36] are as follows. First, different from the atomic schemes explored in those works, in the present study the higher orders of nonlinearity are achieved by increasing the number of atomic levels. This can be used for construction of nonclassical states of light as well as coherent processing of quantum information. Second, due to the closed-loop structure interacting with the ground level, this medium is phase sensitive. This phase sensitive property provides an extra degree of freedom for controlling the Kerr-nonlinear index, a feature that was absent in Refs. [15, 36]. This allows us to present an analytical model to elucidate the phase control of the Kerr nonlinearity. Third, in addition to the steady-state nonlinear susceptibilities, the transient switching of the Kerr nonlinearity is also investigated, which may provide results helpful for the realization of fast optical nonlinearities and optically controlled optical devices. Finally, the effect of the Doppler broadening effect on the Kerr nonlinearity is studied. In particular, it is found that the effect of the Doppler broadening can lead to a giant Kerr nonlinearity. This is an advantage of this type of Kerr nonlinearity enhancement over EIT technique (see, for instance, Refs. [15, 36, 16, 37]) because one does not need very strong coupling laser fields. A disadvantage of this method is that the linear and nonlinear absorption is not eliminated.

3.1 Model and equations

We shall consider the KR5 quantum system shown in Fig. 3.1(a). The system consists of an excited state $|1\rangle$, two non-degenerate metastable lower states $|3\rangle$ and $|5\rangle$, as well as two intermediate degenerate states $|4\rangle$ and $|2\rangle$. The Rabi frequencies Ω_{43}, Ω_{32}, Ω_{41}, and Ω_{21} couple a pair of atomic internal states $|1\rangle$ and $|3\rangle$ to another pair of states $|4\rangle$ and $|2\rangle$ in all possible ways to form a closed loop scheme of the atom-light interaction as depicted in Fig. 3.1(a). The transition between the states $|3\rangle$ and $|5\rangle$ is dipole-allowed. Such a configuration is equivalent to a cyclically coupled of four states $|1\rangle$, $|2\rangle$, $|3\rangle$ and $|4\rangle$, making a diamond-shape closed-loop system. By applying a weak coherent probe field with a Rabi frequency Ω_p, the diamond-shape system is coupled to a ground or metastable state $|5\rangle$. The spontaneous decay rates of the upper level $|i\rangle$ to the lower level $|j\rangle$ are denoted by $2\gamma_{ij}$. Furthermore, we did not include the spontaneous decay from the excited state $|1\rangle$ to the lower levels $|3\rangle$ and $|5\rangle$ assuming that the corresponding transitions are dipole forbidden.

The total Hamiltonian of the system is given by

$$H_{\text{5Levels}} = -\hbar(\Omega_p \left|3\right\rangle \left\langle 5\right| + \Omega_{41} \left|1\right\rangle e^{i\phi} \left\langle 4\right| + \Omega_{21} \left|2\right\rangle \left\langle 1\right| + \Omega_{32} \left|3\right\rangle \left\langle 2\right| + \Omega_{43} \left|4\right\rangle \left\langle 3\right|) + \text{H.c.}\,, \quad (3.1)$$

where $\phi = \phi_{41} + \phi_{43} - \phi_{32} - \phi_{21}$ is a relative phase accumulated after completing a cyclic loop and ϕ_{ij} represents the initial phase of the laser field which induces the transition $|i\rangle \longleftrightarrow |j\rangle$. The equation of the motion for the density operator of the atomic system is given by:

$$\dot{\rho} = -\frac{i}{\hbar}[H_{5Levels}, \rho] + L_\rho, \quad (3.2)$$

where the damping operator L_ρ represents the decay of the system and was defined in Eq. (2.33). Applying the rotating-wave approximation, the equation of motion (3.2) reduces to

$$\dot{\rho}_{11} = -2(\gamma_{14} + \gamma_{12})\rho_{11} + i\Omega_{41}(e^{i\phi}\rho_{41} - e^{-i\phi}\rho_{14}) - i\Omega_{21}(\rho_{12} - \rho_{21}), \quad (3.3)$$

$$\dot{\rho}_{22} = 2\gamma_{12}\rho_{11} - 2\gamma_{23}\rho_{22} + i\Omega_{32}(\rho_{32} - \rho_{23}) + i\Omega_{21}(\rho_{12} - \rho_{21}), \quad (3.4)$$

$$\dot{\rho}_{33} = 2\gamma_{43}\rho_{44} + 2\gamma_{23}\rho_{22} - 2\gamma_{35}\rho_{33} - i\Omega_p(\rho_{35} - \rho_{53}) + i\Omega_{32}(\rho_{23} - \rho_{32}) + i\Omega_{43}(\rho_{43} - \rho_{34}), \quad (3.5)$$

$$\dot{\rho}_{44} = 2\gamma_{14}\rho_{11} - 2\gamma_{43}\rho_{44} - i\Omega_{43}(\rho_{43} - \rho_{34}) - i\Omega_{41}(e^{i\phi}\rho_{41} - e^{-i\phi}\rho_{14}), \quad (3.6)$$

$$\dot{\rho}_{41} = \Im_1\rho_{41} + i\Omega_{43}\rho_{31} - i\Omega_{21}\rho_{42} + i\Omega_{41}e^{-i\phi}(\rho_{11} - \rho_{44}), \quad (3.7)$$

$$\dot{\rho}_{42} = \Im_2\rho_{42} - i\Omega_{21}\rho_{41} + i\Omega_{43}\rho_{32} - i\Omega_{32}\rho_{43} + i\Omega_{41}e^{-i\phi}\rho_{12}, \quad (3.8)$$

$$\dot{\rho}_{43} = \Im_3\rho_{43} + i\Omega_{41}e^{-i\phi}\rho_{13} - i\Omega_p\rho_{45} + i\Omega_{43}(\rho_{33} - \rho_{44}) - i\Omega_{32}\rho_{42}, \tag{3.9}$$

$$\dot{\rho}_{45} = \Im_4\rho_{45} + i\Omega_{41}e^{-i\phi}\rho_{15} - i\Omega_p\rho_{43} + i\Omega_{43}\rho_{35}, \tag{3.10}$$

$$\dot{\rho}_{21} = \Im_5\rho_{21} + i\Omega_{32}\rho_{31} - i\Omega_{41}e^{-i\phi}\rho_{24} + i\Omega_{21}(\rho_{11} - \rho_{22}), \tag{3.11}$$

$$\dot{\rho}_{23} = \Im_6\rho_{23} - i\Omega_p\rho_{25} + i\Omega_{21}\rho_{13} - i\Omega_{43}\rho_{24} + i\Omega_{32}(\rho_{33} - \rho_{22}), \tag{3.12}$$

$$\dot{\rho}_{25} = \Im_7\rho_{25} + i\Omega_{21}\rho_{15} + i\Omega_{32}\rho_{35} - i\Omega_p\rho_{23}, \tag{3.13}$$

$$\dot{\rho}_{31} = \Im_8\rho_{31} + i\Omega_{32}\rho_{21} - i\Omega_{21}\rho_{32} + i\Omega_p\rho_{51} - i\Omega_{41}e^{-i\phi}\rho_{34} + i\Omega_{43}\rho_{41}, \tag{3.14}$$

$$\dot{\rho}_{35} = \Im_9\rho_{35} + i\Omega_{43}\rho_{45} + i\Omega_{32}\rho_{25} + i\Omega_p(\rho_{55} - \rho_{33}), \tag{3.15}$$

$$\dot{\rho}_{15} = \Im_{10}\rho_{15} + i\Omega_{41}e^{i\phi}\rho_{45} - i\Omega_p\rho_{13} + i\Omega_{21}\rho_{25}, \tag{3.16}$$

$$\rho_{11} + \rho_{22} + \rho_{33} + \rho_{44} + \rho_{55} = 1, \tag{3.17}$$

where for simplicity we have defined $\Im_1 = -[i\triangle_{14} + (\gamma_{43} + \gamma_{14} + \gamma_{12})]$, $\Im_2 = [i(\triangle_{12} - \triangle_{14}) - (\gamma_{43} + \gamma_{23})]$, $\Im_3 = [i\triangle_{43} - \gamma_{43} - \gamma_{35}]$, $\Im_4 = -[i(\triangle_{43} + \triangle_p) - \gamma_{43}]$, $\Im_5 = -[i\triangle_{12} + (\gamma_{14} + \gamma_{12} + \gamma_{23})]$, $\Im_6 = [i(\triangle_{12} - \triangle) - \gamma_{23}]$, $\Im_7 = [i(\triangle_{23} - \triangle + \triangle_p) - \gamma_{23}]$, $\Im_8 = -[i(\triangle_{14} + \triangle_{43}) + (\gamma_{14} + \gamma_{12})]$, $\Im_9 = -(\gamma_{35} - i\triangle_p)$, and $\Im_{10} = [i(\triangle_{14} + \triangle_{43} + \triangle_p) - (\gamma_{14} + \gamma_{12})]$. Here, $\triangle_{43} = \omega_4 - \omega_{43}$, $\triangle_{23} = \omega_2 - \omega_{23}$, $\triangle_{14} = \omega_3 - \omega_{14}$, $\triangle_{12} = \omega_1 - \omega_{12}$ and $\triangle_p = \omega_p - \omega_{35}$ are the one-photon detuning for the transitions $|4\rangle \longleftrightarrow |3\rangle$, $|2\rangle \longleftrightarrow |3\rangle$, $|1\rangle \longleftrightarrow |4\rangle$, $|2\rangle \longleftrightarrow |1\rangle$ and $|3\rangle \longleftrightarrow |5\rangle$, respectively. The parameter $\triangle = \triangle_{12} - \triangle_{14} + \triangle_{23} - \triangle_{43}$ defines the frequency of multiphoton detuning and ω_i shows the central frequency of

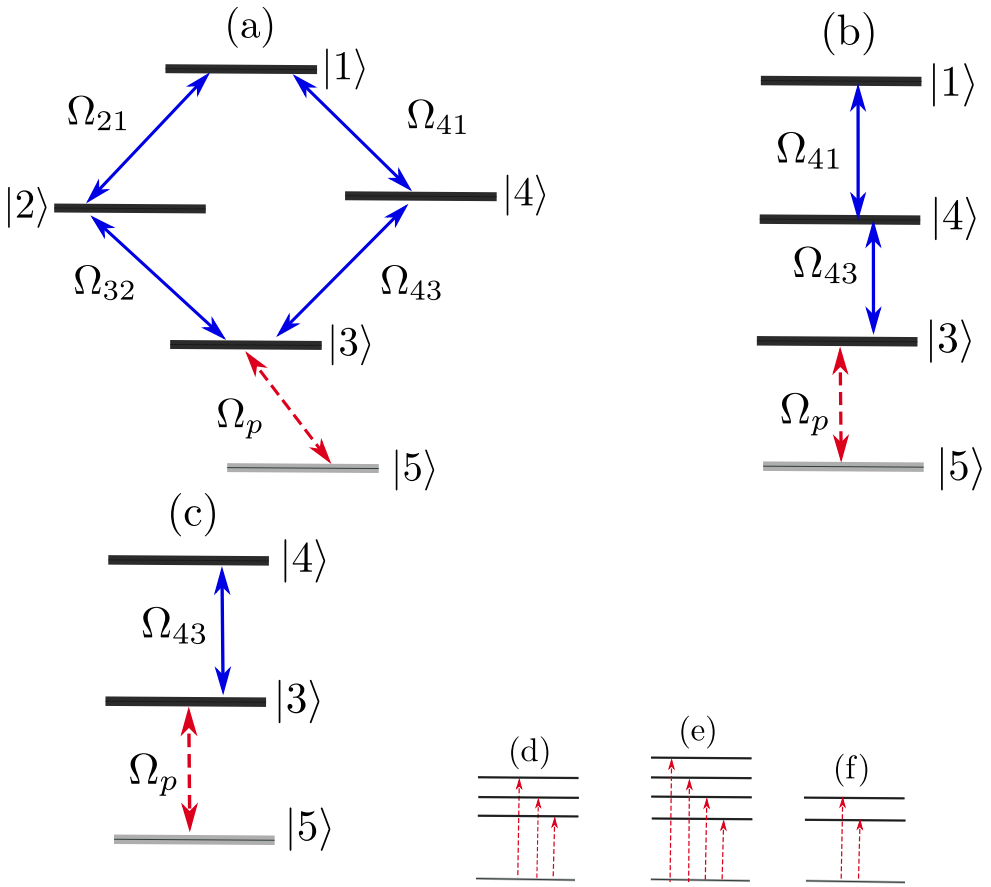

Figure 3.1: Schematic diagram of the (a) five-, (b) four-, and (c) three-level quantum systems. (d)–(f) General atom-field states in the new basis.

the laser fields.

In order to derive the linear and nonlinear susceptibilities, we need to solve the density-matrix equations for the steady state. Under the weak-field approximation one can apply the perturbation approach

$$\rho_{ij} = \rho_{ij}^{(0)} + \rho_{ij}^{(1)} + \rho_{ij}^{(2)} + \rho_{ij}^{(3)} + ..., \tag{3.18}$$

where $\rho_{ij}^{(0)}$, $\rho_{ij}^{(1)}$, $\rho_{ij}^{(2)}$, and $\rho_{ij}^{(3)}$ are the zeroth, first, second, and third orders in the probe field Ω_p. Due to the assumption $\Omega_p \ll \Omega_{43}, \Omega_{32}, \Omega_{41}, \Omega_{21}$, the zeroth-order solution is $\rho_{55}^{(0)} = 1$, while other elements being zero ($\rho_{ij}^{(0)} = 0$, where $i, j \neq 5$). Using this condition and substituting Eq. (3.18) into Eqs. (3.3)–(3.17), the equations of motion for the first-order density-matrix elements read

$$\dot{\rho}_{35}^{(1)} = \Im_9 \rho_{35}^{(1)} + i\Omega_{43}\rho_{45}^{(1)} + i\Omega_{32}\rho_{25}^{(1)} + i\Omega_p, \tag{3.19}$$

$$\dot{\rho}_{25}^{(1)} = \Im_7 \rho_{25}^{(1)} + i\Omega_{21}\rho_{15}^{(1)} + i\Omega_{32}\rho_{35}^{(1)}, \tag{3.20}$$

$$\dot{\rho}_{45}^{(1)} = \Im_4 \rho_{45}^{(1)} + i\Omega_{41}e^{-i\phi}\rho_{15}^{(1)} + i\Omega_{43}\rho_{35}^{(1)}, \tag{3.21}$$

$$\dot{\rho}_{15}^{(1)} = \Im_{10} \rho_{15}^{(1)} + i\Omega_{41}e^{i\phi}\rho_{45}^{(1)} + i\Omega_{21}\rho_{25}^{(1)}. \tag{3.22}$$

Similarly, the equations of motion for the third-order density-matrix element read

$$\dot{\rho}_{35}^{(3)} = \Im_9 \rho_{35}^{(3)} + i\Omega_{43}\rho_{45}^{(3)} + i\Omega_{32}\rho_{25}^{(3)} + i\Omega_p(\rho_{55}^{(2)} - \rho_{33}^{(2)}), \tag{3.23}$$

$$\dot{\rho}_{25}^{(3)} = \Im_7 \rho_{25}^{(3)} + i\Omega_{21}\rho_{15}^{(3)} + i\Omega_{32}\rho_{35}^{(3)} - i\Omega_p\rho_{23}^{(2)}, \tag{3.24}$$

$$\dot{\rho}_{45}^{(3)} = \Im_4 \rho_{45}^{(3)} + i\Omega_{41}e^{-i\phi}\rho_{15}^{(3)} + i\Omega_{43}\rho_{35}^{(3)} - i\Omega_p\rho_{43}^{(2)}, \tag{3.25}$$

$$\dot{\rho}_{15}^{(3)} = \Im_{10} \rho_{15}^{(3)} + i\Omega_{41}e^{i\phi}\rho_{45}^{(3)} + i\Omega_{21}\rho_{25}^{(3)} - i\Omega_p\rho_{13}^{(2)}. \tag{3.26}$$

After some algebraic calculations, we obtain the following off-diagonal density-matrix elements $\rho_{35}^{(1)}$ and $\rho_{35}^{(3)}$ corresponding to Ω_p:

$$\rho_{35}^{(1)} = i\Omega_p(\Omega_{21}^2\Im_4 - \Omega_{41}^2\Im_7 + \Im_4\Im_7\Im_{10})/\Re, \tag{3.27}$$

and

$$\begin{aligned}\rho_{35}^{(3)} = {} & \Omega_p\rho_{43}^{(2)}(\Omega_{41}\Omega_{21}\Omega_{32}e^{i\phi} - \Omega_{43}\Omega_{21}^2 - \Omega_{43}\Im_7\Im_{10})/\Re \\ & +\Omega_p\rho_{23}^{(2)}(i\Omega_{32}\Im_4\Im_{10} - \Omega_{32}\Omega_{41}^2 + \Omega_{41}\Omega_{21}\Omega_{43}e^{-i\phi})/\Re \\ & +i\Omega_p\rho_{55}^{(2)}(\Omega_{21}^2\Im_4 - \Omega_{41}^2\Im_7 + \Im_4\Im_7\Im_{10})/\Re \\ & -i\Omega_p\rho_{33}^{(2)}(\Omega_{21}^2\Im_4 - \Omega_{41}^2\Im_7 + \Im_4\Im_7\Im_{10})/\Re \\ & -i\Omega_p\rho_{13}^{(2)}(\Omega_{43}\Omega_{41}\Im_7e^{-i\phi} - \Omega_{21}\Omega_{23}\Im_4)/\Re,\end{aligned} \tag{3.28}$$

where

$$\begin{aligned}\Re = {} & \Im_4\Im_{10}\Omega_{32}^2 - \Omega_{41}^2\Omega_{32}^2 - \Omega_{43}^2\Omega_{21}^2 - \Im_7\Im_{10}\Omega_{43}^2 - \Im_4\Im_9\Omega_{21}^2 + \Im_7\Im_9\Omega_{41}^2 \\ & -\Im_4\Im_7\Im_9\Im_{10} + 2\Omega_{41}\Omega_{32}\Omega_{43}\Omega_{21}\cos\phi.\end{aligned} \tag{3.29}$$

Note that the second-order nonlinearity of Eq. (3.28) is solved to obtain $\rho_{ij}^{(2)}$, giving the steady-state results

$$\rho_{41}^{(2)} = [i\Omega_{41}e^{-i\phi}(\rho_{44}^{(2)} - \rho_{11}^{(2)}) - i\Omega_{43}\rho_{31}^{(2)} + i\Omega_{21}\rho_{12}^{(2)}]/\Im_1, \tag{3.30}$$

$$\rho_{42}^{(2)} = [-i\Omega_{43}\rho_{32}^{(2)} - i\Omega_{41}e^{-i\phi}\rho_{12}^{(2)} + i\Omega_{32}\rho_{43}^{(2)} + i\Omega_{21}\rho_{14}^{(2)}]/\Im_2, \tag{3.31}$$

$$\rho_{43}^{(2)} = [i\Omega_{43}(\rho_{44}^{(2)} - \rho_{33}^{(2)}) - i\Omega_{41}e^{-i\phi}\rho_{13}^{(2)} + i\Omega_{32}\rho_{42}^{(2)} + i\Omega_p\rho_{45}^{(1)}]/\Im_3, \tag{3.32}$$

$$\rho_{23}^{(2)} = [-i\Omega_{32}\rho_{33}^{(2)} + i\Omega_{32}\rho_{22}^{(2)} - i\Omega_{21}\rho_{13}^{(2)} + i\Omega_{43}\rho_{24}^{(2)} + i\Omega_p\rho_{25}^{(1)}]/\Im_6, \tag{3.33}$$

$$\rho_{21}^{(2)} = [-i\Omega_{32}\rho_{31}^{(2)} + i\Omega_{21}(\rho_{22}^{(2)} - \rho_{11}^{(2)}) + i\Omega_{41}e^{-i\phi}\rho_{24}^{(2)}]/\Im_5, \tag{3.34}$$

$$\rho_{31}^{(2)} = [i\Omega_{32}\rho_{21}^{(2)} - i\Omega_{13}\rho_{41}^{(2)} + i\Omega_{41}e^{-i\phi}\rho_{34}^{(2)} + i\Omega_{21}\rho_{32}^{(2)} - i\Omega_p\rho_{51}^{(1)}]/\Im_8, \tag{3.35}$$

$$\rho_{11}^{(2)} = [i\Omega_{41}e^{i\phi}\rho_{41}^{(2)} - i\Omega_{41}e^{-i\phi}\rho_{14}^{(2)} + i\Omega_{21}\rho_{12}^{(2)} + i\Omega_{21}\rho_{21}^{(2)}]/(2\gamma_{14} + 2\gamma_{12}), \tag{3.36}$$

$$\rho_{22}^{(2)} = [2\gamma_{12}\rho_{11}^{(2)} + i\Omega_{32}\rho_{32}^{(2)} - i\Omega_{32}\rho_{23}^{(2)} + i\Omega_{21}\rho_{12}^{(2)} - i\Omega_{21}\rho_{21}^{(2)}]/2\gamma_{23}, \tag{3.37}$$

$$\rho_{33}^{(2)} = [2\gamma_{43}\rho_{44}^{(2)} + 2\gamma_{23}\rho_{22}^{(2)} - i\Omega_{43}\rho_{34}^{(2)} + i\Omega_{43}\rho_{43}^{(2)} - i\Omega_{32}\rho_{32}^{(2)} + i\Omega_{32}\rho_{23}^{(2)} - i\Omega_{p}\rho_{35}^{(1)} + i\Omega_{p}\rho_{53}^{(1)}]/2\gamma_{35}, \tag{3.38}$$

$$\rho_{44}^{(2)} = [2\gamma_{14}\rho_{11}^{(2)} + i\Omega_{43}\rho_{34}^{(2)} - i\Omega_{43}\rho_{43}^{(2)} + i\Omega_{41}e^{-i\phi}\rho_{14}^{(2)} - i\Omega_{41}e^{i\phi}\rho_{41}^{(2)}]/2\gamma_{43}, \tag{3.39}$$

where

$$\rho_{15}^{(1)} = -i\Omega_{p}(\Omega_{32}\Omega_{21}\Im_{4} - \Omega_{43}\Omega_{41}\Im_{7}e^{i\phi})/\Re, \tag{3.40}$$

$$\rho_{25}^{(1)} = \Omega_{p}(-\Omega_{41}\Omega_{21}\Omega_{43}e^{i\phi} + \Omega_{41}^{2}\Omega_{32} - \Omega_{32}\Im_{4}\Im_{10})/\Re, \tag{3.41}$$

$$\rho_{45}^{(1)} = \Omega_{p}(-\Omega_{41}\Omega_{21}\Omega_{32}e^{-i\phi} + \Omega_{21}^{2}\Omega_{43} - \Omega_{43}\Im_{7}\Im_{10})/\Re. \tag{3.42}$$

Then, according to equations (2.110) and (2.111) the linear susceptibility $\chi^{(1)}$ and the third-order nonlinear susceptibility $\chi^{(3)}$ of the medium for the weak probe laser field are related to the atomic coherences as

$$\chi^{(1)} = \frac{2N\wp_{53}^{2}}{\epsilon_{0}\hbar\Omega_{p}}\rho_{35}^{(1)}, \tag{3.43}$$

$$\chi^{(3)} = \frac{2N\wp_{53}^{4}}{3\epsilon_{0}\hbar^{3}\Omega_{p}^{3}}\rho_{35}^{(3)}, \tag{3.44}$$

where N is the atomic number density matrix and $\wp_{53}$ denotes the transition dipole moment between the levels $|3\rangle$ and $|5\rangle$. The analytical expression for first- and third-order susceptibilities depends on the controllable parameters of the system such as the detunings and intensities of the driving fields as well as the relative phase of applied fields. It is well known that the Kerr nonlinearity corresponds to the refraction part of the third-order susceptibility $\chi^{(3)}$, while the imaginary part of $\chi^{(3)}$ determines the nonlinear absorption [81]. The real and imaginary partsof $\chi^{(1)}$ correspond to the linear dispersion and absorption, respectively. The slope of the linear dispersion with respect to the probe detuning represents the group velocity of a weak probe field.

3.2 An enhanced Kerr nonlinearity for the KR5 model

Now we focus on the third-order susceptibility behavior of the KR5 atomic system through numerical simulation. For linear and nonlinear susceptibilities we plot the curves in units of $\frac{2N\wp_{53}^2}{\epsilon_0\hbar\Omega_p}$ and $\frac{2N\wp_{53}^4}{3\epsilon_0\hbar^3\Omega_p^3}$, respectively. Here we are interested in the linear and nonlinear properties of the KR5 medium. The linear and nonlinear susceptibilities can be modified by the controlling parameters such as intensity and frequency detuning of coupling fields, i.e., Rabi frequencies, and relative phase between applied fields. Therefore, the giant Kerr nonlinearity with reduced linear and nonlinear absorption can be obtained under the condition of slow light.

The first- and third-order susceptibilities of a weak probe field are displayed in Fig. 3.2 for various values of the intensity of the applied fields. Here we assume that all of the coupling fields are in exact resonance with the corresponding transitions, so the multiphoton resonance condition is fulfilled, i.e., $\Delta = 0$. Figures 3.2(a) and 3.2(b) show that when $\phi = 0$ and $\Omega_{21} = \Omega_{32} = \Omega_{43} = \Omega_{41} = \gamma$, the first- and third-order susceptibility spectra have three linear and nonlinear absorption peaks. Figure 3.2(b) shows that the maximal Kerr nonlinearity is accompanied by large linear and nonlinear absorption around $\Delta_p = 0$. The slope of linear dispersion is negative at zero probe field detuning, which suggests superluminal light propagation. In this case, the group velocity is negative [Fig. 3.2(c)] and the medium is not suitable for application of low-intensity nonlinear optics due to the absorption losses.

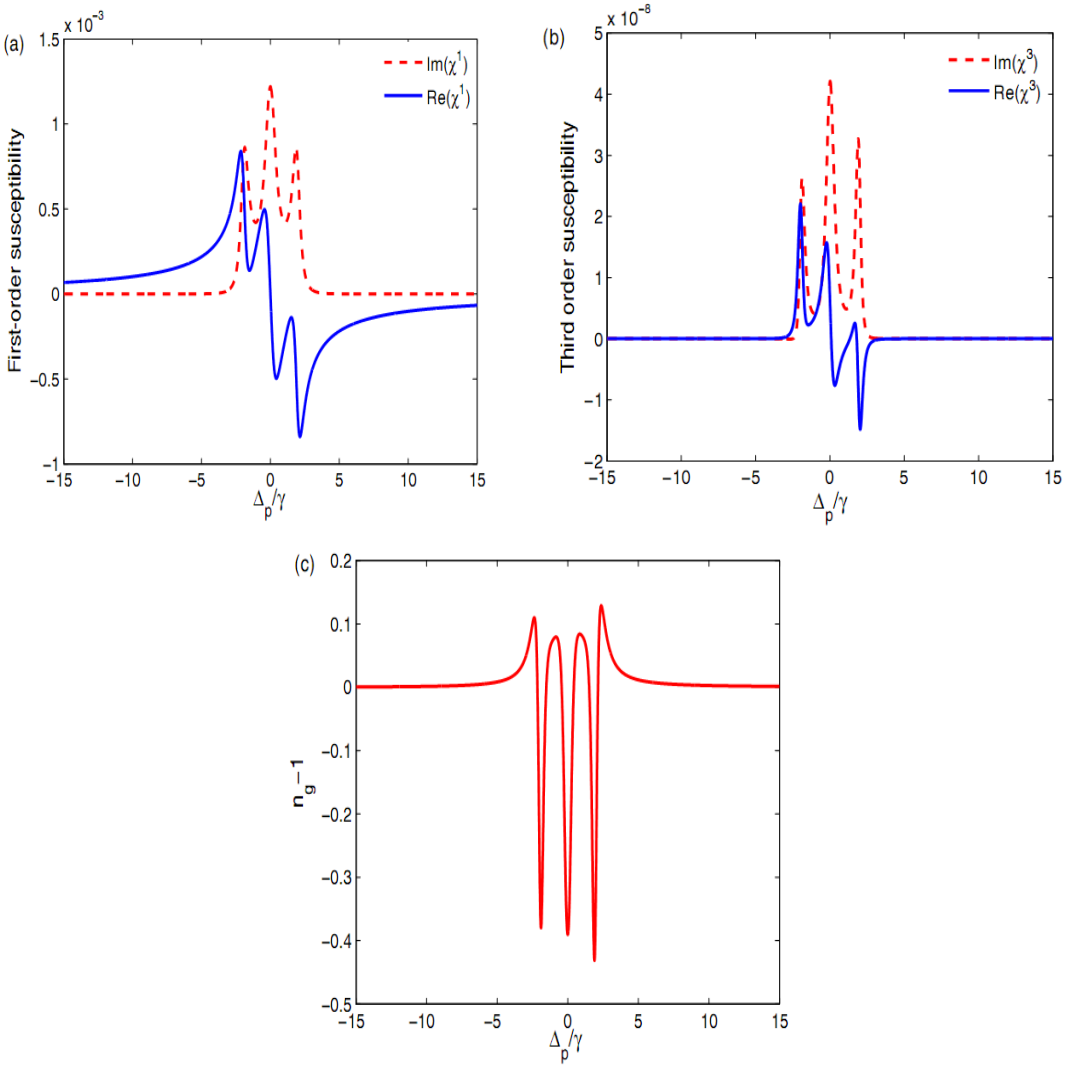

Figure 3.2: Linear and nonlinear susceptibility as well as group index $n_g = c/\nu_g$ versus probe field detuning. (a) Linear absorption (dashed line) and linear dispersion (solid line), (b) nonlinear absorption (dashed line) and Kerr nonlinearity (solid line), and (c) group index. The parameters are $\gamma_{14} = 0.8\gamma$, $\gamma_{12} = \gamma_{23} = 0.1\gamma$, $\gamma_{43} = 0.4\gamma$, $\gamma_{35} = 0.02\gamma$, $\Omega_{21} = \Omega_{32} = \Omega_{43} = \Omega_{41} = \gamma$, $\Delta_{43} = \Delta_{23} = \Delta_{14} = \Delta_{12} = 0$, and $\phi = 0$. All the parameters are scaled with γ.

Figure 3.3 displays the curves for nonequal values of the coupling fields: $\Omega_{21} = 2\gamma$, $\Omega_{41} = 1.1\gamma$, $\Omega_{32} = \gamma$ and $\Omega_{43} = 1.9\gamma$. One can see that the central peaks of the linear and nonlinear absorption are split into four peaks in the absorption spectrum. Compared to Fig. 3.2, now the linear and nonlinear absorption reduce so that three reduced absorption windows appear around $\Delta_p = 0, \pm\delta$. Within these reduced absorption regions the slope of linear dispersion becomes positive. This represents the subluminal light propagation with the positive group velocity [Fig. 3.3(c)]. In addition, the increased Kerr nonlinearity appears inside reduced absorption windows. Thus, by properly adjusting the intensities of driving fields, one could achieve the enhanced Kerr nonlinearity accompanied by reduced absorption under the condition of slow light levels.

A comparison is also made in Fig. 3.4 between the Kerr nonlinear coefficients of the five-level KR5 system with that of the existing four- and three-level cascade-type atomic systems. Note that in the four-level system, level $|2\rangle$ is neglected ($\Omega_{21} = \Omega_{32} = 0$) [see Fig. 3.1(b)], while for the three-level cascade-type system, both atomic levels $|2\rangle$ and $|1\rangle$ are neglected ($\Omega_{21} = \Omega_{32} = \Omega_{41} = 0$) [see Fig. 3.1(c)]. It is realized that the magnitude of Kerr nonlinearity for the five-level KR5 system is larger than that of four- and three- level systems. This indicates an advantage of employing such a scheme in enhancing the Kerr nonlinearity rather than its existing three- and four-level atomic counterparts. Moreover, as mentioned earlier, another type of five-level atomic system has recently been examined for exploring the Kerr-nonlinearity enhancement [36]. In this type of five-level configuration, a weak probe field drives the lower transition, while an intense coupling beam couples simultaneous transitions between the intermediate level and three upper closely spacing states. Then the magnitude of Kerr nonlinearity for such a five-level cascade-type scheme is compared with that of the four- and three-level cascade-type systems. Although compared to the existing four- and three-level schemes this type of five-level configuration can exhibit a wider spectral region of enhanced Kerr nonlinearity with more positive and negative peaks, its maximal Kerr nonlinearity is the same as that of the existing three- and four-level cascade systems.

In fact, both types of five-level KR5 system proposed here and the cascade-type system proposed in Ref. [36] are based on the ladder-type three-level system in which the upper transition is driven by a strong field. However, in Ref. [36] the single upper transition in the ladder-type system is replaced by simultaneous transitions between an intermediate level and three upper closely spacing states.

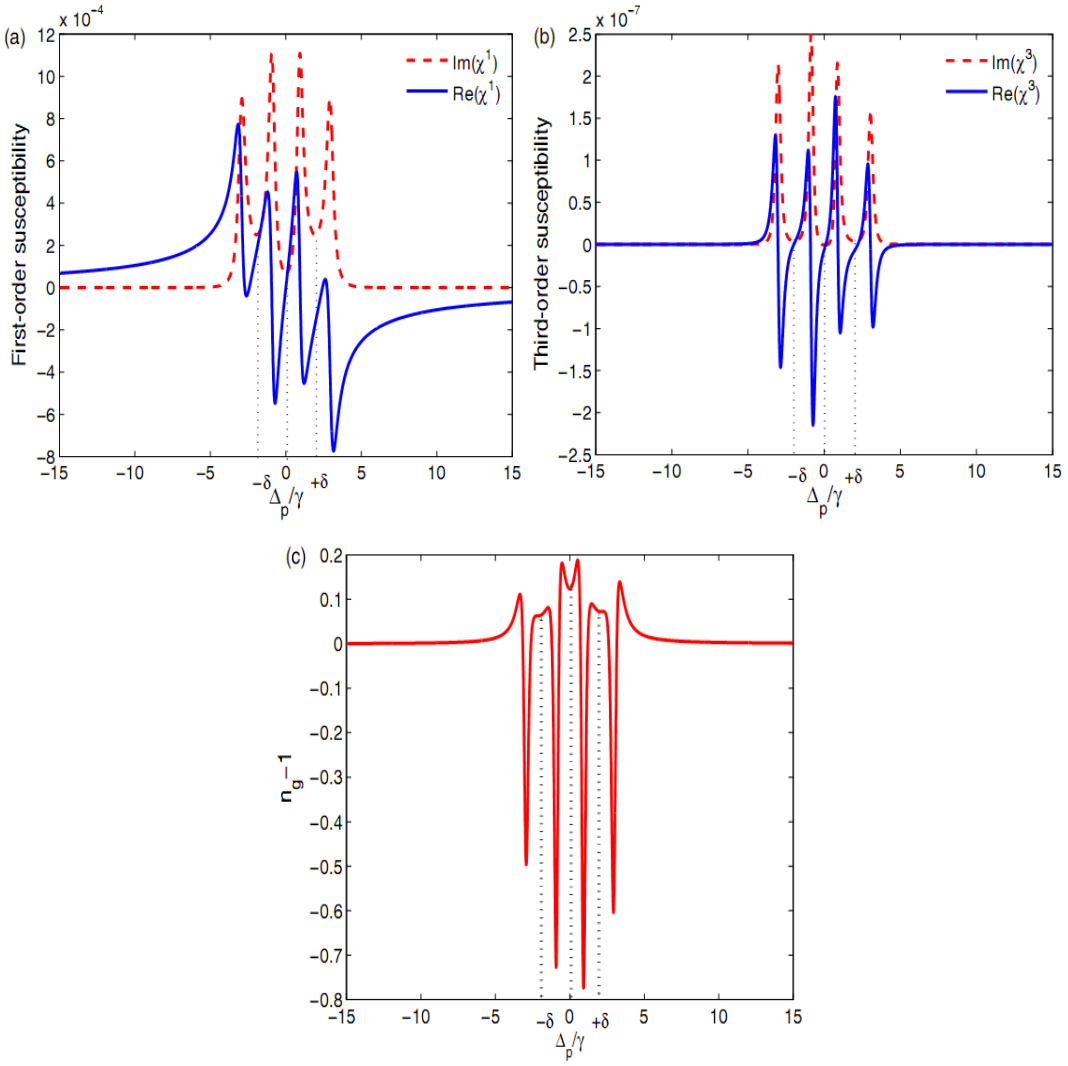

Figure 3.3: Linear and nonlinear susceptibility as well as group index $n_g = c/\nu_g$ versus probe field detuning. (a) Linear absorption (dashed line) and linear dispersion (solid line), (b) nonlinear absorption (dashed line) and Kerr nonlinearity (solid line), and (c) group index. The parameters are $\Omega_{21} = 2\gamma$, $\Omega_{41} = 1.1\gamma$, $\Omega_{32} = \gamma$ and $\Omega_{43} = 1.9\gamma$. The other parameters are the same as in Fig. 3.2.

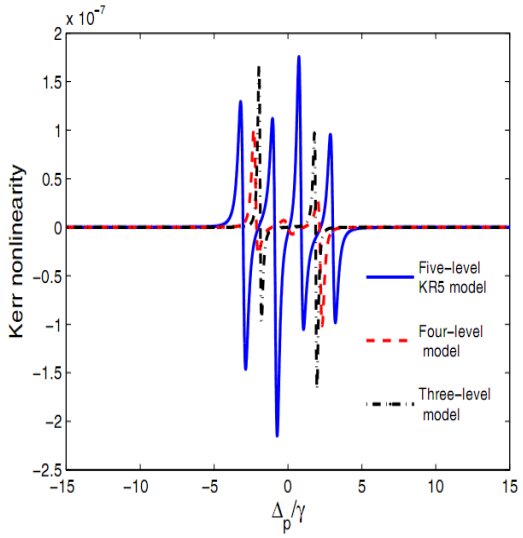

Figure 3.4: Kerr-nonlinear indices in the case of the five-level KR5 system (solid line), the four-level cascade system (dashed line), and the three-level cascade system (dotted line). The parameters are the same as in Fig. 3.3, except those for the four-level case where $\Omega_{21} = \Omega_{32} = 0$, whereas for the three-level case one has $\Omega_{21} = \Omega_{32} = \Omega_{41} = 0$.

In our proposal, the single upper transition is replaced by multiple transitions driven by four laser fields that form a diamond-shape closed-loop structure. We found that by increasing the number of levels in such a way that they form a consequently coupled cyclic chain of four states coupled to the ground state [Figs. 3.1(a)–3.1(c)], it is possible to realize higher orders of nonlinearity, while the same magnitude of Kerr nonlinearity among the three systems was observed in Ref. [36]. This shows an advantage of employing such a five-level system in producing higher Kerr nonlinearity over that considered in Ref. [36].

We consider next the effect of coupling field detunings on the Kerr nonlinearity. Figure 3.5 shows the real (dispersion) and imaginary (absorption) parts of linear and nonlinear susceptibilities versus the relative phase between applied fields. Illustrated in Figs. 3.5(a) and 3.5(b) is a situation where the applied fields are in an exact resonance with the corresponding transitions, i.e., $\Delta_{43} = \Delta_{23} = \Delta_{14} = \Delta_{12} = 0$. One can see that the Kerr nonlinearity is accompanied by large linear and nonlinear absorption. Furthermore, the linear dispersion is negative, which corresponds to the superluminal light propagation. Using the supposition that the fields Ω_{43} and Ω_{32} are not in resonance with the corresponding atomic transitions ($\Delta_{43} = \Delta_{23} = 2\gamma$), we plot the first- and third order susceptibility spectra versus ϕ in Figs. 3.5(c) and 3.5(d). Note that the multiphoton resonance

condition $\Delta = 0$ is still kept. One can see that the giant Kerr nonlinearity is accompanied by the reduced linear and nonlinear absorption for all relative phases ϕ. Also, the linear dispersion is now positive providing the slow light.

3.3 Phase control of Kerr nonlinearity

Expressions (3.27)–(3.29) and Fig. 3.5 show that the linear and nonlinear susceptibilities can be controlled by the relative phase of the applied fields. Now we provide an analytical model to understand such phase control. Four driving fields Ω_{21}, Ω_{41}, Ω_{32} and Ω_{43} acting on the atom build a closed-loop level scheme in which the relative phase ϕ between applied fields affects linear and nonlinear optical properties of the medium. Excluding in Eq. (3.1) the ground (or metastable) state $|5\rangle$, the Hamiltonian of the atom-light interaction for the remaining atomic four-level closed-loop level scheme of diamond shape can be rewritten as

$$H_{4Levels} = -\hbar\Omega \left[|1\rangle \, \mathrm{e}^{i\phi} \, \langle 4| + \Sigma_{j=1}^{3} \, |j+1\rangle \, \langle j| + H.c. \right]. \tag{3.45}$$

In addition, the amplitudes of all Rabi frequencies in Eq. (3.45) are chosen to be the same, i.e.,

$$\Omega_{21} = \Omega_{41} = \Omega_{32} = \Omega_{43} = \Omega. \tag{3.46}$$

The Hamiltonian (3.45) is equivalent to its counterpart involving an infinite number of states

$$H_{4Levels} = -\hbar\Omega \Sigma_{j=-\infty}^{\infty} \, |j+1\rangle \, \langle j| + H.c., \tag{3.47}$$

as long as the coefficients c_j entering any state vector $|...\rangle = \Sigma_j c_j \, |j\rangle$ obey the boundary conditions

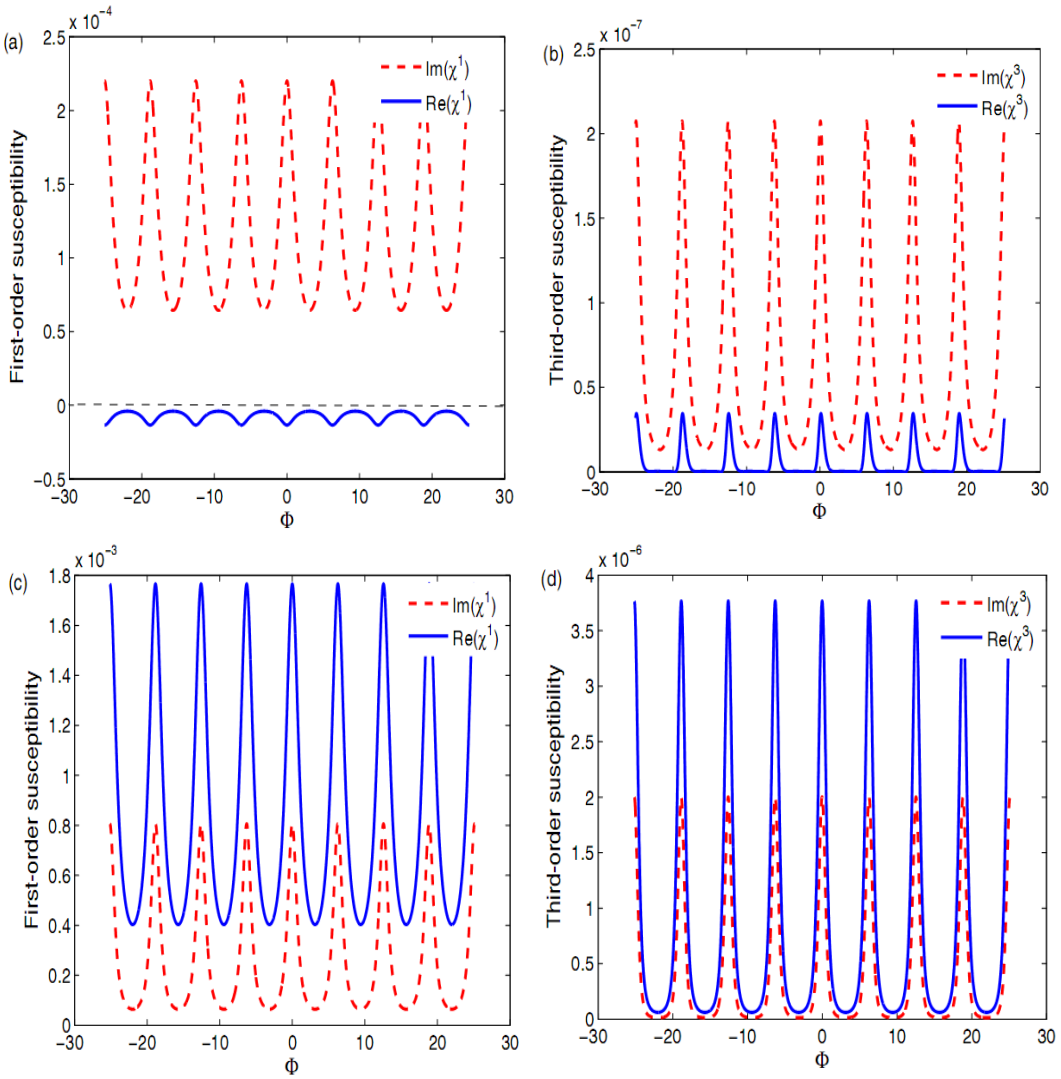

Figure 3.5: (a) and (c) Linear and (b) and (d) nonlinear susceptibility versus relative phase ϕ for (a) and (c) $\Delta_{43} = \Delta_{23} = \Delta_{14} = \Delta_{12} = 0$ and (b) and (d) $\Delta_{43} = \Delta_{23} = 2\gamma$ and $\Delta_{14} = \Delta_{12} = 0$. The parameters are $\Omega_{21} = 5\gamma$, $\Omega_{41} = 3\gamma$, $\Omega_{32} = \gamma$, and $\Omega_{43} = 2\gamma$. The other parameters are the same as in Fig. 3.2.

$$c_{j+4} = \mathrm{e}^{i\phi} c_j. \tag{3.48}$$

For $\phi = 0$, Eq. (3.48) reduces to the usual periodic boundary conditions. On the other hand, for $\phi = \pm\pi$, Eq.(3.48) represents the twisted boundary conditions.

The Hamiltonian given by Eqs. (3.45)–(3.48) can be easily diagonalized [133] and its eigenstates read

$$|n(r)\rangle = \frac{1}{2}\Sigma_{j=1}^{4} |j\rangle \, \mathrm{e}^{iq_n j}, \tag{3.49}$$

with their corresponding eigenenergies

$$E_n = -2\hbar\Omega \cos q_n, \tag{3.50}$$

where $n = 1, 2, 3, 4$. The dimensionless parameter q_n takes a set of values that depends on the relative phase ϕ,

$$q_n = \frac{(n-1)\pi}{2} - \frac{\phi}{4};\ n = 1, 2, 3, 4. \tag{3.51}$$

Let we now analyze the eigenenergies for different phase ϕ by taking $\Omega = 2\gamma$. For condition (i) $\phi = 0$ ($\Omega_{21} = \Omega_{41} = \Omega_{32} = \Omega_{43} = \Omega$), Eq. (3.50) becomes $E_n = -2\hbar\Omega \sin(\frac{n\pi}{2})$, so the eigenenergies are

$$\begin{aligned} E_3 = -E_1 = 2\hbar\Omega, \\ E_2 = E_4 = 0. \end{aligned} \tag{3.52}$$

Three different eigenenergies shown in Fig. 3.1(d) can be attributed to three peaks in the absorption profile in Figs. 3.6(a) and 3.6(b). In this case, the interacting dark resonances will be established.

For condition (ii) $\phi = \frac{\pi}{2}$ ($\Omega_{21} = \Omega_{41} = \Omega_{32} = \Omega_{43} = \Omega$) we have $E_n = -2\hbar\Omega \sin(\frac{n\pi}{2} - \frac{\pi}{8})$, providing the following eigenenergies:

$$\begin{aligned} E_3 &= -E_1 = 4\hbar\Omega \cos\tfrac{\pi}{8}, \\ E_4 &= -E_2 = 4\hbar\Omega \sin\tfrac{\pi}{8}. \end{aligned} \tag{3.53}$$

Now four different eigenenergies are obtained. Thus, four absorption peaks appear for $\phi = \frac{\pi}{2}$, as one can see in Figs. 3.1(e), 3.6(c), and 3.6(d). In other words, the central peaks of linear and nonlinear absorption profiles split and for $\phi = \frac{\pi}{2}$ we have four absorption peaks.

For condition (iii) $\phi = \pi$ ($\Omega_{21} = \Omega_{41} = \Omega_{32} = \Omega_{43} = \Omega$) we have $E_n = -2\hbar\Omega \sin(\frac{n\pi}{2} - \frac{\pi}{4})$, giving the eigenenergies

$$\begin{aligned} E_1 = E_2 &= -\sqrt{2}\hbar\Omega, \\ E_3 = E_4 &= \sqrt{2}\hbar\Omega. \end{aligned} \tag{3.54}$$

It is easy to see that there is a twice degenerate ground level (containing the states with $n = 1$ and 2) and a twice degenerate excited level ($n = 3$ and 4), as shown in Fig. 3.1(f). Therefore, two different eigenenergies are obtained, yielding two peaks in the absorption profile in Figs. 3.6(e) and 3.6(f). Consequently, the double-dark resonance structure is not established for $\phi = \pi$ and just two side peaks are formed in the absorption spectrum.

A three-dimensional plot of the steady-state linear and nonlinear absorption spectra versus Δ_p and ϕ can provide a better perspective of this phenomenon, as shown in Fig. 3.7. One can see that by changing the relative phase ϕ, the medium can have three, four, and two absorption peaks. It should be noted that in Fig. 3.6 the Kerr nonlinearity experiences a large nonlinear absorption. Therefore, we find a wide range of tunability in the linear and nonlinear absorption and dispersion just by adjusting the relative phase of the applied fields.

Using the above analytical model, now we can explain the physical mechanism of the Kerr nonlinearity enhancement obtained in Figs. 3.2 and 3.3. Figure 3.2 is plotted for the parameters satisfying condition (i) ($\Omega_{21} = \Omega_{41} = \Omega_{32} = \Omega_{43} = \gamma$ and $\phi = 0$). Therefore, three absorption peaks observed in Fig. 3.2 reflect

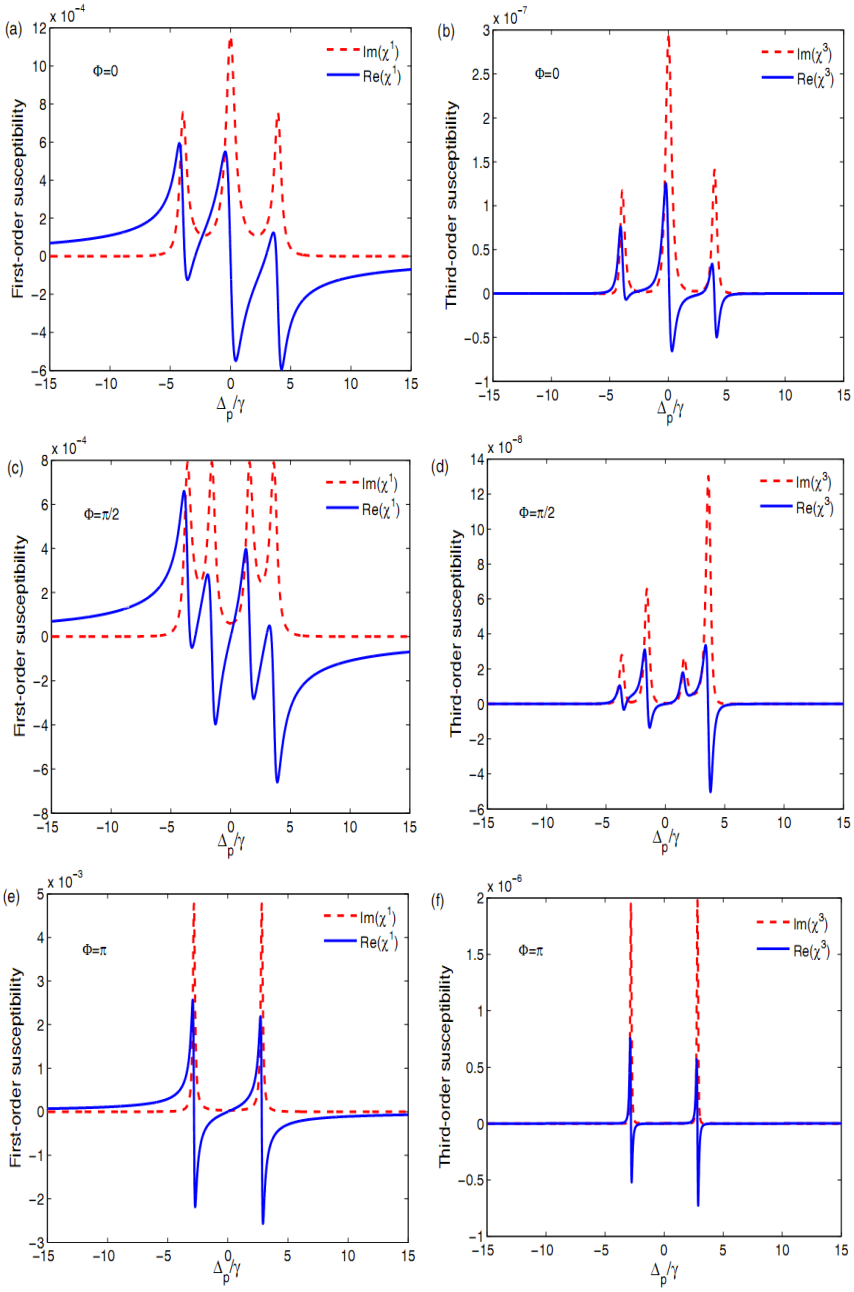

Figure 3.6: Phase control of (a), (c), and (e) linear and (b), (d), and (f) nonlinear susceptibility for (a) and (b) $\phi = 0$, (c) and (d) $\phi = \pi/2$, and (e) and (f) $\phi = \pi$. Here $\Omega_{21} = \Omega_{41} = \Omega_{32} = \Omega_{43} = \Omega = 2\gamma$ and the other parameters are the same as in Fig. 3.2.

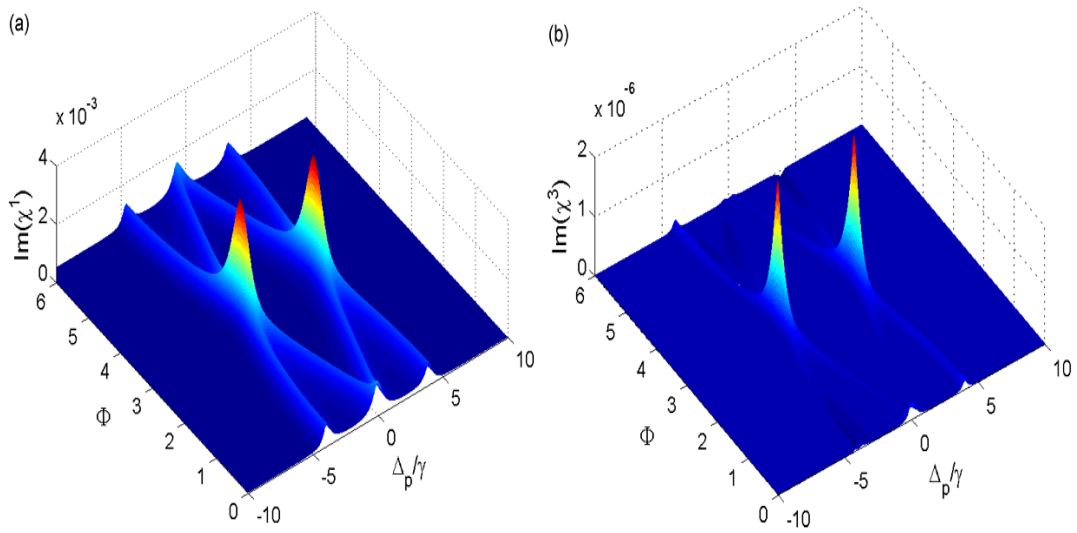

Figure 3.7: Three-dimensional plot of phase control of (a) linear and (b) nonlinear susceptibility Here the parameters are the same as in Fig. 3.6.

the eigenenergies given in Eq. (3.52). The central peaks in both the linear and nonlinear absorption profiles separate two reduced absorption windows and show a double-dark resonance structure, whereas two absorption peaks located on both sides of the central frequency detuning $\Delta_p = 0$ represent one photon transition. In fact, in such a scheme there is coherent population trapping (CPT), which may lead to reduced absorption windows on the left- and right-hand sides of $\Delta_p = 0$. Since an ideal CPT medium does not interact with the light, it also cannot produce any nonlinear effects. When we change the coupling fields to $\Omega_{21} = 2\gamma$, $\Omega_{41} = 1.1\gamma$, $\Omega_{32} = \gamma$ and $\Omega_{43} = 1.9\gamma$ (see the parameter condition used in the plot of Fig. 3.3), the Rabi frequencies of the applied fields exceed those in condition (i). Thus the CPT is disturbed, leading to a strong nonlinear coupling between the electromagnetic fields interacting with the atomic system. In this case, the eigenenergies for the Hamiltonian (3.45) read

$$E_1 = -\frac{(y - m^{1/2})^{1/2}}{2^{1/2}}\,, \tag{3.55}$$

$$E_2 = \frac{(y - m^{1/2})^{1/2}}{2^{1/2}}\,, \tag{3.56}$$

$$E_3 = -\frac{(y + m^{1/2})^{1/2}}{2^{1/2}}\,, \tag{3.57}$$

$$E_4 = \frac{(y + m^{1/2})^{1/2}}{2^{1/2}}\,, \tag{3.58}$$

where

$$\begin{aligned} y &= \Omega_{43}^2 + \Omega_{32}^2 + \Omega_{41}^2 + \Omega_{21}^2, \\ m &= y^2 - 4(\Omega_{41}\Omega_{32} - \Omega_{43}\Omega_{21})^2. \end{aligned} \tag{3.59}$$

Evidently, the four eigenenergies given in Eqs. (3.55)–(3.58) correspond to four absorption peaks in linear and nonlinear susceptibilities. This condition was demonstrated in Fig. 3.3.

3.4 Time-dependent Kerr nonlinearity

In the following we discuss the temporal evolution of the Kerr nonlinearity in the KR5 atomic system and investigate the optical switching time in the nonlinear regime by using the numerical result from the density-matrix equations of motion. Figure 3.8 illustrates the transient behavior of the probe linear absorption and dispersion for various values of the detuning parameters Δ_{43} and Δ_{23}. The selected parameters are the same as in Fig. 3.5, unless $\Delta_p = 0.1\gamma$ and $\phi = \pi$. Figure 3.8 shows an optical switching process in which a weak Kerr index with superluminal absorption switches to the EIT-based slow light giant Kerr nonlinearity by changing $\Delta_{43} = \Delta_{23}$ from 0 to γ. According to Figs. 3.8(a) and 3.8(b), after a short oscillatory behavior, the linear absorption and dispersion curves reach the steady-state limit. However, when the laser beams described by the Rabi frequencies Ω_{43} and Ω_{32} are in resonance ($\Delta_{43} = \Delta_{23} = 0$), the steady-state value of the linear absorption coefficient is positive, while the steady-state value of the linear dispersion is negative. This

condition suggests a superluminal absorption. Similar curves are plotted for the case of nonresonant detuning ($\Delta_{43} = \Delta_{23} = \gamma$). With an increase of time, the steady-state value of the linear absorption is reduced and finally the EIT appears. Furthermore, the steady-state linear dispersion changes its sign to a positive value corresponding to the subluminal light propagation.

A temporal behavior of the Kerr nonlinearity is also displayed in Fig. 3.8(c). It can be seen that the curves for the Kerr-nonlinear coefficient exhibit a transient oscillatory behavior for a short time and then reach a steady-state value. Also, for $\Delta_{43} = \Delta_{23} = \gamma$ the steady-state Kerr nonlinearity is gradually enhanced compared to the case $\Delta_{43} = \Delta_{23} = 0$. Therefore, by going out of resonance, the enhanced Kerr nonlinearity accompanied by subluminal assistant EIT is obtained.

Let us now analyze the phase-sensitive switching feature of the Kerr nonlinearity in the pulsed regime for the KR5 atomic system. Figure 3.9 shows that the oscillation frequency of the Kerr nonlinearity increases as the relative phase changes from $\phi = \pi$ to $\phi = \pi/2$. In a similar manner, the magnitude of the steady-state value of the Kerr nonlinearity can be increased.

We now demonstrate that this system can be used as an optical switch for nonlinear dispersion in which a weak Kerr nonlinearity can be converted to a giant one. It can be seen from Figs. 3.8(c) and 3.9 that the switching time needed to convert a weak nonlinear dispersion into an enhanced one and vice versa equals approximately $15/\gamma$. Considering the D_1 line of the ^{87}Rb atom with the typical decay rate $\gamma \simeq 36MHz$, we can obtain a nonlinear switching time equal to approximately $416ns$.

Thus, we demonstrated that this KR5 medium can be employed as an optical switch in which the propagation of the laser pulse can be controlled by another laser field that is useful for an optically controlled optical device. The results presented may be useful for understanding the switching feature of the EIT-based slow light Kerr nonlinearity, have potential application in optical information processing and transmission, and may be helpful for the realization of fast optical nonlinearities and optically controlled optical devices. A high-speed optical switch is an important technique for quantum information networks [134].

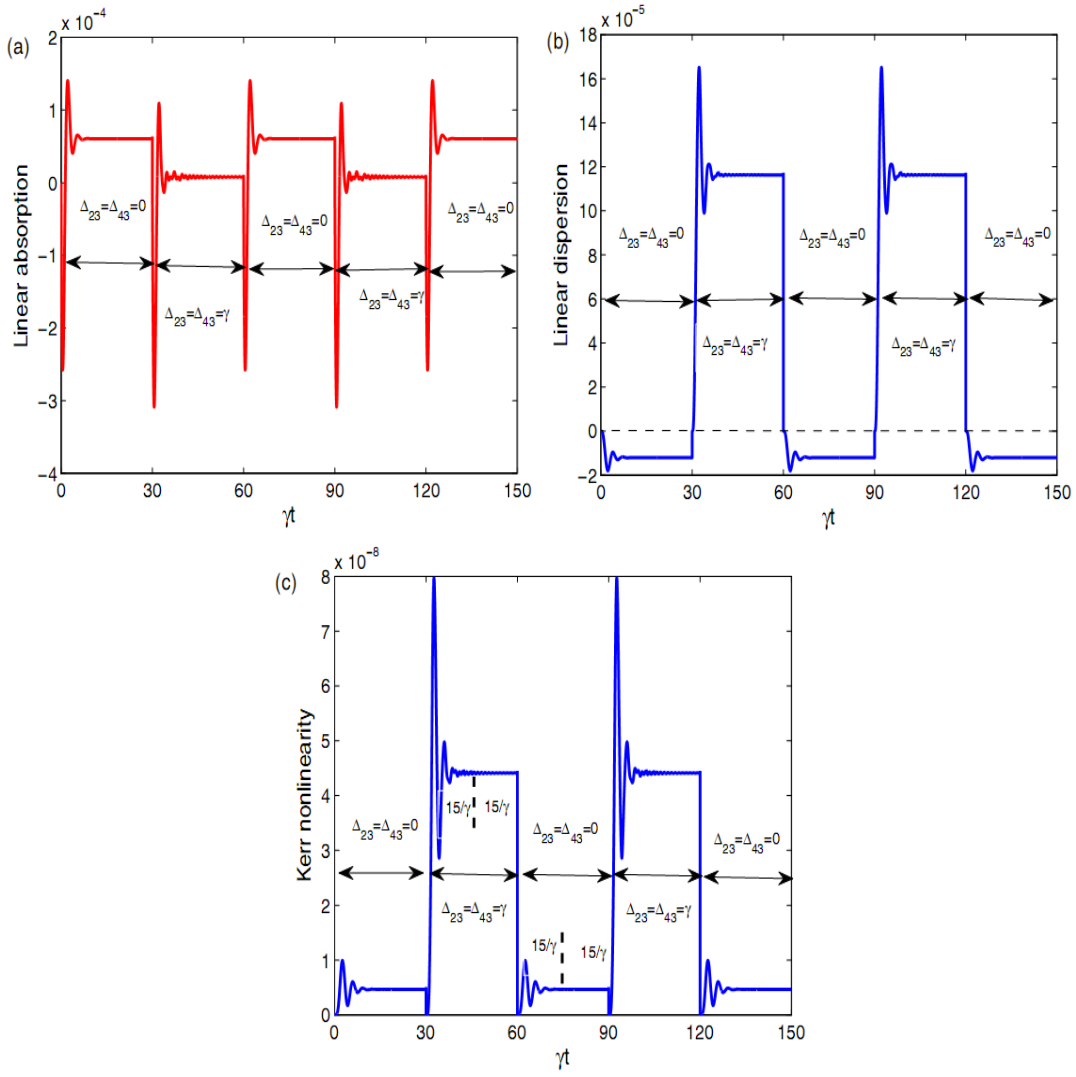

Figure 3.8: Switching process of the (a) linear absorption, (b) linear dispersion, and (c) Kerr nonlinearity for different values of Δ_{43} and Δ_{23}. Here $\Delta_p = 0.1\gamma$ and $\phi = \pi$ and the other parameters are the same as in Fig. 3.5.

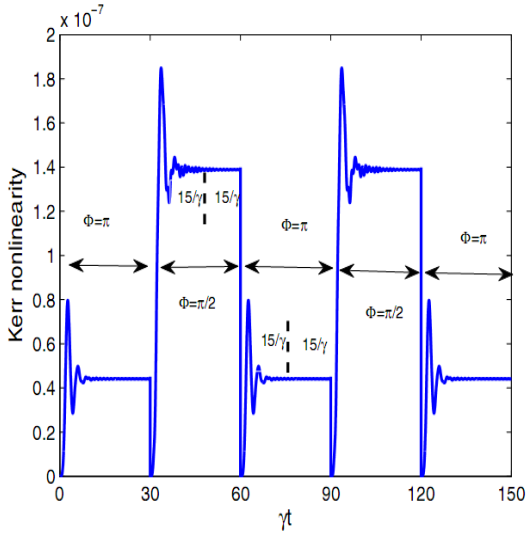

Figure 3.9: Switching process of the Kerr nonlinearity for different values of ϕ. Here $\Delta_{43} = \Delta_{23} = \gamma$ and the other parameters are the same as in Fig. 3.5.

3.5 Doppler broadening and Kerr nonlinearity

At room or higher temperatures there is a broad distribution of atomic velocities. Thus, the Doppler shift cannot be neglected and must be taken into account [135]. The effect of the Doppler broadening due to the atom's thermal velocity ν can be included by replacing Δ_{23}, Δ_{14}, Δ_{12} and Δ_{43} by $\Delta_{23} - k\nu$, $\Delta_{14} - k\nu$, $\Delta_{12} - k\nu$ and $\Delta_{43} - k\nu$, respectively. Here all the laser fields are assumed to copropagate in the same direction $k_1 \simeq k_2 \simeq k_3 \simeq k_4 \simeq k_p = k$, where k_p and k_i $(i = 1, 2, 3, 4)$ are the wave vectors of the probe and driving fields, respectively.

Using the Maxwell velocity distribution, we have

$$\Upsilon(\nu) = (2\pi)^{-1/2}\varpi^{-1}\mathrm{e}^{-\nu^2/\varpi^2}, \tag{3.60}$$

where $\varpi = (\frac{2k_BT}{m})^{1/2}$ is the Doppler width. Relating the probe susceptibility χ to the coherence term ρ_{35} and utilizing Eq.(3.18), the linear and nonlinear susceptibilities of the probe field then read

$$\chi^{(1)}(\Delta_p) = \int_{-\infty}^{\infty} \Upsilon(\nu)\chi^{(1)}(\Delta_p, \nu)d\nu, \tag{3.61}$$

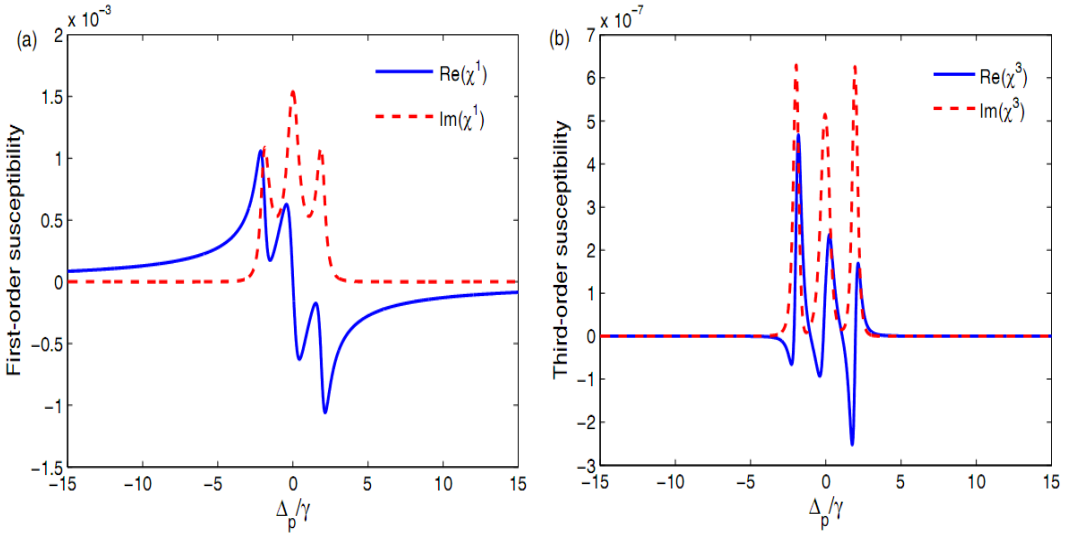

Figure 3.10: (a) Linear and (b) nonlinear susceptibility versus probe field detuning Δ_p including the Doppler broadening $k\varpi = 0.1\gamma$. The parameters are the same as in Fig. 3.2.

$$\chi^{(3)}(\Delta_p) = \int_{-\infty}^{\infty} \Upsilon(\nu)\chi^{(3)}(\Delta_p, \nu)d\nu, \tag{3.62}$$

which gives the first- and third-order susceptibilities in the Doppler-broadened atomic system.

Now we can analyze the behavior of the absorption and dispersion as well as the Kerr nonlinear coefficient inside the Doppler-broadened medium. Figure 3.10 shows the effect of Doppler broadening on the linear and nonlinear susceptibilities. The chosen parameters are the same as those we used to plot Fig. 3.2. In Figs. 3.10(a) and 3.10(b) we chose the Doppler width below the natural linewidth of the probe transition ($k\varpi = 0.1\gamma$). Obviously, the linear susceptibility is very similar in shape to the case without the Doppler broadening [see Fig. 3.2(a)], while a considerable change in shape is observed in the nonlinear susceptibility so that the slope of Kerr nonlinearity becomes positive around $\Delta_p = 0$. This indicates that, compared to the linear response of the KR5 system, the nonlinear response of the medium is more sensitive to the Doppler-broadening effect. Moreover, although the Kerr nonlinearity in Fig. 3.10(b) still experiences strong linear and nonlinear absorption, the Kerr nonlinearity index is greatly enhanced compared to the nonbroadened case shown in Fig. 3.2.

This result is completely different from the Kerr-nonlinearity enhancement due

to EIT, which was presented earlier in this chapter and in most of the relevant studies (see, for instance, [37, 92, 93, 16, 15, 36]). Thus, we could achieve a large nonlinear Kerr coefficient for the probe field while maintaining linear and nonlinear absorption. The main advantage of this method over the EIT is that in the present method there is no need to adjust the laser fields to the strong intensities. However, the disadvantage is that the linear and the nonlinear absorption do not cancel. It should be noted that in order to obtain a Doppler-free arrangement in the room temperature cell, one can adjust the laser direction. However, the best way to eliminate the effect of Doppler broadening is to employ a cold-atom sample.

Chapter 4

Atom Localization in two and three dimensions

Precise localization of atoms has attracted considerable attention in recent years. Earlier theoretical studies for the localization mostly consider 1D atom localization (one-dimensional) based on the atomic coherence and quantum interference effects [13, 26, 136, 137, 64, 75, 74, 76, 138, 66, 139, 140]. More recently, some schemes have been put forward for two-dimensional (2D) atom localization [32, 141, 142, 143]. Ding et al. [142] investigated the atom localization by monitoring the probe absorption in a microwave-driven four-level atomic medium affected by two orthogonal standing-wave fields. They found that the localization behavior is significantly improved due to a joint quantum interference induced by a standing-wave and microwave-driven fields. In another work, a M-type atomic system was proposed by the same group [32] to deal with the 2D atom localization in the subwavelength domain via a controlled spontaneous emission. Wan et al. [143] considered an atomic scheme based on the controlled probe absorption and gain in a four-level double Λ-system. They showed both numerically and analytically that the high-precision atom localization achieved in such a scheme can be attributed to the interference between the one and three-photon excitations. A four-level tripod type atomic system is also proposed to achieve a high precision two dimensional atom localization via measurement of the excited state population [144]. A scheme for two-dimensional (2D) atom localization in a four-level tripod system under an influence of two orthogonal standing-wave fields is also considerd by Ivanov and Rozhdestvensky [141]. Yet the three dimensional (3D) atom localization has been investigated only in few proposals [38, 39, 40]. Compared to the 1D and 2D localization, the 3D localization of an atom gives a more specific information about the position of a moving atom.

In this chapter we present the theoretical model of atom localization in two and three dimensions. There are two different atom-light coupling schemes considered in this chapter. The first one is a five-level atomic configuration in which a diamond-shape subsystem is coupled to a ground level through a weak probe field [44] and the latter is a a modified Λ-type four-level atomic system with three driving fields and a weak probe field [45, 145].

4.1 Scheme 1: Five-level KR5 system

We investigate the 2D and 3D localization of an atom in a five-level configuration in which the laser beams couple the ground level to a four-level closed-loop system. Here we make use of the KR5 scheme to localize atoms in two and three dimensions. We employ three different situations in which the atom could interact with the position-dependent standing-wave fields. In the first two cases all four laser fields represent the standing waves, whereas in the third case only one of the fields is a standing wave, others being propagating waves. It is shown that one can extract information about the position of the atom through measuring the probe absorption. Since the KR5 atomic scheme is phase sensitive, the phase control of atom localization is also possible by adjusting properly the relative phase. In particular, by properly choosing the amplitudes and phases of the driving fields, the atom-light Hamiltonian can have three, four, and two eigenstates, resulting in different localization patterns in the probe absorption spectrum. Subsequently it is demonstrated that the first two atom-field coupling situations are not suitable to achieve a unique atom localization peak. In order to obtain the maximum detection probability of the atom at a certain position in the 2D space, we consider the next situation of coupling between atom and standing waves fields, and illustrate that the maximal probability of finding the atom in one period of standing waves reaches the unity. Eventually, the phase control of the 3D atom localization for this five-level scheme is explored numerically in the 3D space. It is found that the detection probability of finding the atom in a particular volume in 3D space and within one period of standing waves can become 50% [44].

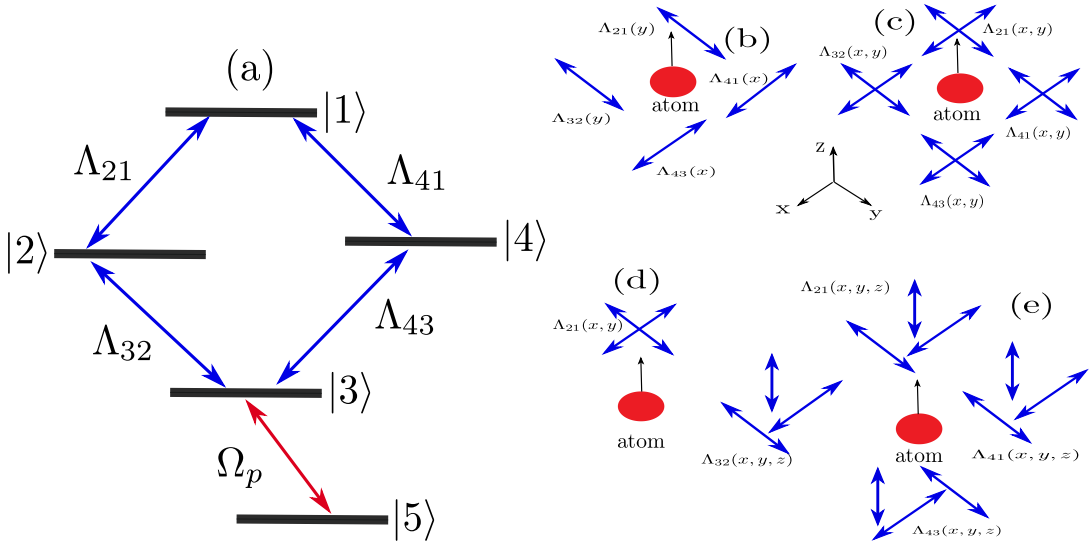

Figure 4.1: (a) Schematic diagram of the five-level quantum system. (b), (c), (d) and (e) Different situations considered in which the atom could interact with the position-dependent standing-wave fields.

4.1.1 Model and equations

The proposed five-level model is similar to that shown in Fig. 3.1(a). Four coherent laser driving components Λ_{43}, Λ_{32}, Λ_{41} and Λ_{21} are applied to couple a pair of atomic internal states $|1\rangle$ and $|3\rangle$ to another pair of states $|4\rangle$ and $|2\rangle$ in all possible ways to form a closed loop scheme of the atom-light interaction. The transition between the states $|3\rangle$ and $|5\rangle$ is dipole-allowed. By applying a weak coherent probe field with a Rabi frequency Ω_p, the diamond-shape system is coupled to a ground or metastable state $|5\rangle$ (Fig. 4.1(a)).

The atom moves along the z direction and interacts with driving laser fields propagating in the $x-y$ plane. The laser radiation can be travelling or standing-waves. In the latter case the strength of the interaction between the atom and the standing-wave fields is spatially dependent. The atom is assumed to move with a high enough velocity, so that its interaction with the driving fields does not affect its motion in z direction. Thus, we may treat the atomic motion classically characterized by a constant velocity in the z direction. On the other hand, the center-of-mass position of the atom along the directions of standing waves (in the $x-y$ plane) can experience only the minor changes and thus remains nearly constant. In this case, one can neglect the kinetic energy term of the atom in the interaction Hamiltonian via the Raman-Nath approximation

[80]. Then, applying the rotating-wave approximation, the resulting interaction Hamiltonian for the whole system in the new notation can be written as

$$H_{5Levels} = -\hbar(\Omega_p \left|3\right\rangle \left\langle 5\right| + \Lambda_{41} \left|1\right\rangle e^{i\phi} \left\langle 4\right| + \Lambda_{21} \left|2\right\rangle \left\langle 1\right| + \Lambda_{32} \left|3\right\rangle \left\langle 2\right| + \Lambda_{43} \left|4\right\rangle \left\langle 3\right|) + H.c., \tag{4.1}$$

where $\phi = \phi_{41} + \phi_{43} - \phi_{32} - \phi_{21}$ is a relative phase of applied fields. The equation of the motion for the density operator of the atomic system is given by Eq. (3.2). Substituting Eq. (4.1) into (3.2), one arrives at the optical Bloch equations for density matrix elements of the five-level system [43, 44].

Our aim is to acquire information about the position of the atom passing through the standing-wave fields from the absorption of the probe field

$$\chi'' = \mathrm{Im}(\chi), \tag{4.2}$$

where

$$\chi = \frac{2N\wp_{53}^2}{\varepsilon_0 \hbar \Omega_p} \rho_{35}, \tag{4.3}$$

is a linear susceptibility of the system for the probe field, and N is the atomic number density. Therefore the absorption measurements allow us to determine the off-diagonal density matrix element ρ_{35} featured in Eq. (4.3).

For a weak intensity of the probe field, the atom populates predominantly the ground state $|5\rangle$, so that $\rho_{55} \approx 1$. Under this condition, the density matrix equations can be simplified by writing them in the matrix form

$$\dot{R} = -MR + A, \tag{4.4}$$

where R, A, and M are given by

$$R = \begin{pmatrix} \rho_{35} \\ \rho_{45} \\ \rho_{25} \\ \rho_{15} \end{pmatrix}, \tag{4.5}$$

$$A = \begin{pmatrix} i\Omega_p \\ 0 \\ 0 \\ 0 \end{pmatrix}, \tag{4.6}$$

and

$$M = \begin{pmatrix} S_1 & -i\Lambda_{43} & -i\Lambda_{32} & 0 \\ -i\Lambda_{43} & S_2 & 0 & -i\Lambda_{41}e^{-i\phi} \\ -i\Lambda_{32} & 0 & S_3 & -i\Lambda_{21} \\ 0 & -i\Lambda_{41}e^{i\phi} & -i\Lambda_{21} & S_4 \end{pmatrix}, \tag{4.7}$$

with $S_1 = \gamma_{35} - i\triangle_p$, $S_2 = i(\triangle_{43} + \triangle_p) - \gamma_{43}$, $S_3 = -[i(\triangle_{23} - \triangle + \triangle_p) - \gamma_{23}]$, and $S_4 = -[i(\triangle_{14} + \triangle_{43} + \triangle_p) - (\gamma_{14} + \gamma_{12})]$ and the detuning parameters are defined in previous chapter. The steady-state solution to Eq.(4.4) reads in the matrix form

$$R = M^{-1}A. \tag{4.8}$$

Using Eq.(4.8), the coherence term ρ_{35} can be expressed as

$$\rho_{35} = i\Omega_p \frac{S_2\Lambda_{21}^2 + S_3\Lambda_{41}^2 + S_2S_3S_4}{Z}, \tag{4.9}$$

where

$$\begin{aligned} Z = {} & 2\Lambda_{41}\Lambda_{32}\Lambda_{43}\Lambda_{21}\cos\phi + S_2S_4\Lambda_{32}^2 - S_3S_4\Lambda_{43}^2 - S_1S_2\Lambda_{21}^2 + S_1S_3\Lambda_{41}^2 \\ & -\Lambda_{43}^2\Lambda_{21}^2 - \Lambda_{41}^2\Lambda_{32}^2 - S_1S_2S_3S_4. \end{aligned} \tag{4.10}$$

It is apparant that the phase factor enters the absorption through the term $2\Lambda_{41}\Lambda_{32}\Lambda_{43}\Lambda_{21}\cos\phi$. Equation (4.9) represents a main result allowing one to measure the position of the atom via the absorption of the atomic system given by the imaginary part of ρ_{35} featured in Eqs. (4.2) and (4.3). Equation (4.9) shows that the absorption depends on the parameters of the system i.e., the amplitudes of the standing wave fields, relative phase of applied fields, as well as the detunings of the probe and driving fields. In what follows we will discuss this issue in more detail. We investigate the localization of atom through numerical results by considering different cases of interaction of atom with the laser fields.

The simulations are displayed in the units of $\frac{2N\wp_{53}^2}{\varepsilon_0\hbar\Omega_p}$. The selected parameters are $\gamma_{14} = \gamma_{12} = \gamma_{23} = \gamma_{43} = \gamma_{35} = \gamma$, and all the parameters are scaled with γ. Note that the wave number of optical waves are selected to be the same and equal to k.

4.1.2 2D atom localization

4.1.2.1 First case: All control fields are position-dependent in one dimension

Considering the case where the different atomic transitions are coupled by different orthogonal standing wave fields (Fig. 4.1(b)), the resulting Rabi-frequencies are

$$\Lambda_{43} = \Lambda_{43}(x, y) = \Omega_{43} f_{11}(x),$$

$$\Lambda_{41} = \Lambda_{41}(x, y) = \Omega_{41} f_{11}(x),$$

$$\Lambda_{32} = \Lambda_{32}(x, y) = \Omega_{32} f_{12}(y),$$

$$\Lambda_{21} = \Lambda_{21}(x, y) = \Omega_{21} f_{12}(y), \tag{4.11}$$

with

$$f_{11}(x, y) = \sin(kx),$$

$$f_{12}(x, y) = \sin(ky). \tag{4.12}$$

It can be seen from Eqs. (4.2), (4.3), (4.9) and (4.11) that the probe absorption χ'' is position dependent. As a result, by measuring probe absorption spectra χ'' one can obtain information about the position of the atom in the $x-y$ plane, as it passes through the standing wave fields. The position of the peak in the probe absorption specifies the location of the atom during its optical detection. Four different patterns of 2D atom localization are illustrated in Fig. 4.2. As it can be seen from Fig. 4.2(a), when $\Omega_{43} = \Omega_{32} = \Omega_{41} = \Omega_{21} = 5\gamma$ and $\phi = 0$, the probe absorption maxima displays four crater-like patterns at each quadrants, and the atom is localzied at these circles. For $\Omega_{32} = \Omega_{21} = \Omega_1 \neq \Omega_2 = \Omega_{43} = \Omega_{41}$ the crater-like patterns gradually move closer to each other and change to the patterns with a shape resembling the number 8. When $\Omega_2 > \Omega_1$ (Fig. 4.2(b)), the patterns are along the x-direction, while as shown in Fig. 4.2(c) for $\Omega_2 < \Omega_1$, they are along the y-direction. As illustrated in Fig. 4.2(d), for $\phi = \pi$, the 2D atom localization pattern changes totaly with respect to Fig. 4.2(a). In all the cases, the maximum probability of atom at a particular position is 1/4.

4.1.2.2 Second case: All control fields are position-dependent in two dimensions

Let us consider now a situation where each standing wave field is obtained from a superposition of two orthogonal standing-wave fields with the same frequency along the directions x and y (Fig. 4.1(c)). As a result, the Rabi-frequencies of standing waves are position dependent and are given by

$$\Lambda_{43} = \Lambda_{43}(x, y) = \Omega_{43} f_2(x, y),$$

$$\Lambda_{41} = \Lambda_{41}(x, y) = \Omega_{41} f_2(x, y),$$

$$\Lambda_{32} = \Lambda_{32}(x, y) = \Omega_{32} f_2(x, y),$$

$$\Lambda_{21} = \Lambda_{21}(x, y) = \Omega_{21} f_2(x, y), \tag{4.13}$$

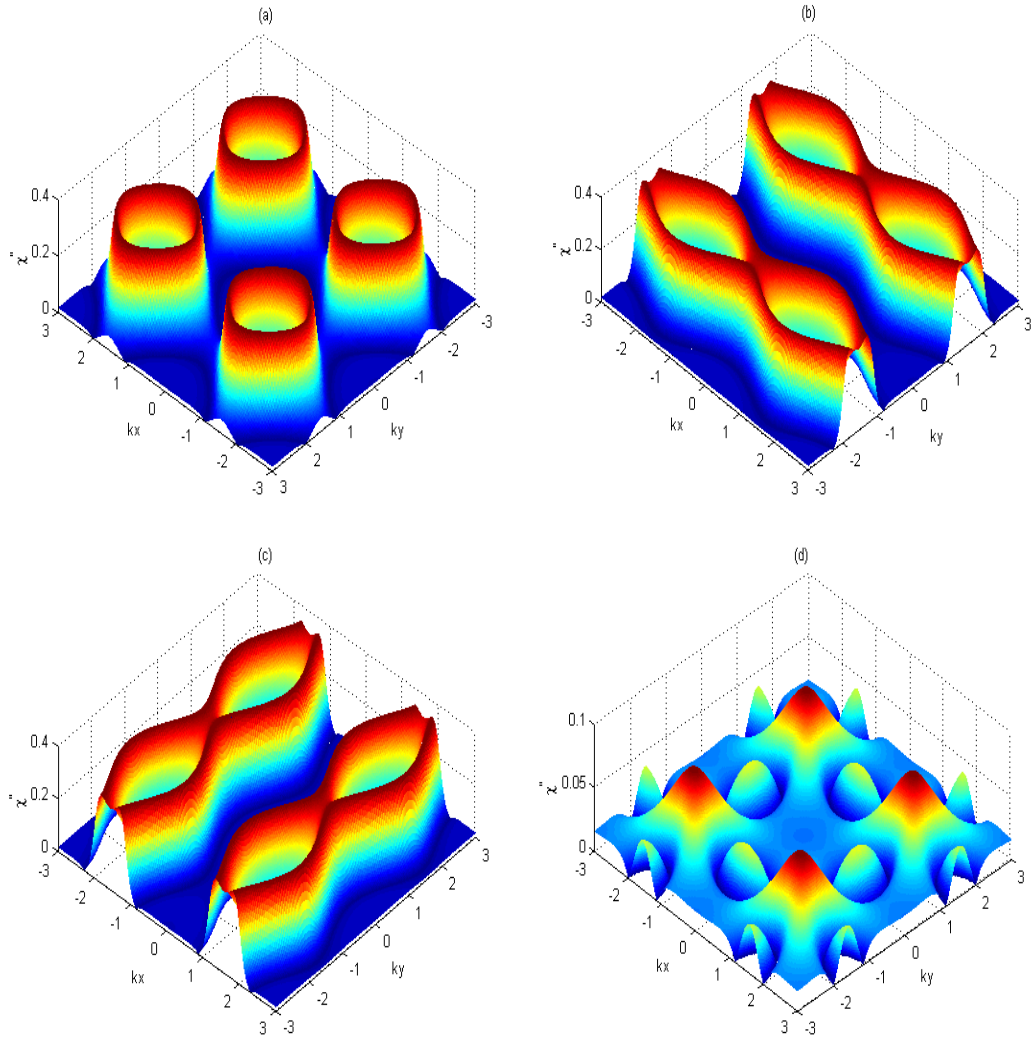

Figure 4.2: Plots of probe absorption χ''versus (kx, ky). The selected parameters are $(\Omega_{43}, \Omega_{32}, \Omega_{41}, \Omega_{21}, \phi)$ = (a) $(5\gamma, 5\gamma, 5\gamma, 5\gamma, 0)$, (b) $(4\gamma, 6\gamma, 4\gamma, 6\gamma, 0)$, (c) $(6\gamma, 4\gamma, 6\gamma, 4\gamma, 0)$, (d) $(5\gamma, 5\gamma, 5\gamma, 5\gamma, \pi)$. The other parameters are $\gamma_{14} = \gamma_{12} = \gamma_{23} = \gamma_{43} = \gamma_{35} = \gamma$, $\triangle = \triangle_{12} = \triangle_{14} = \triangle_{23} = \triangle_{43} = 0$, as well as $\Delta_p = 8\gamma$, $\Omega_p = 0.01\gamma$.

with

$$f_2(x, y) = \sin(kx) + \sin(ky). \tag{4.14}$$

In Fig. 4.3, we show our simulations for the 2D atom localization by proper adjusting the four standing wave fields. As shown in Fig. 4.3(a), for the case where $\Omega_{43} = \Omega_{32} = \Omega_{41} = \Omega_{21} = 10\gamma$, the probe-absorption maxima are distributed in all quadrants of the $x - y$ plane and with a lattice like structure. Setting $(\Omega_{43}, \Omega_{32}, \Omega_{41}, \Omega_{21}) = (8\gamma, \gamma, 10\gamma, 10\gamma)$, the 2D spatial distribution of the atom is almost the same as the one in Fig. 4.3(a), but with two spike-like peaks located in quadrants I and III (Fig. 4.3(b)). We observe that for the condition $\Omega_{43} = \Omega_{32} = \Omega_{41} = \Omega_{21} = 25\gamma$ corresponding to Fig.4.3(c), the resulting absorption spectrum is similar to that in Fig. 4.3(a). For all these cases (Figs. 4.3(a)–4.3(c)), the information on the position of the atom in the $x - y$ plane is ambiguous. A better spatial resolution in the distribution of the probe absorption of the atom can be obtained by adjusting the standing wave intensities to $\Omega_{43} = \Omega_{32} = \Omega_{41} = \Omega_{21} = 2.5\gamma$. In this case, as it can be observed from Fig. 4.3(d), the probe absorption shows two spike-like atom localization peaks in the first and third quadrants. Therefore, the uncertainty in position measurement of the atom is reduced compared to the previous cases shown in Figs. 4.3(a)–4.3(c), and the detection probability of the atom in one period of the standing-wave fields becomes approximately 1/2.

Next, we intend to investigate the influence of relative phase ϕ on precision in the position measurement of the atom in the $x - y$ plane. Equations (4.9) and (4.10) show that the probe absorption is sensitive to the relative phase of the applied fields ϕ through the term $\cos\phi$. Here, we present an analytical model to elucidate such a phase-sensitive property. Four driving fields acting on the atom provide a closed loop (ring coupling) level scheme in which the relative phase between driving fields affects the probe absorption χ''. As discussed in previous chapter, excluding the ground (or metastable) state $|5\rangle$ in Eq. (4.1), the eigenvalues for the remaining four-level Hamiltonian reads (see Eq. (3.50))

$$E_n = -2\Omega \cos q_n(\sin(kx) + \sin(ky)), \tag{4.15}$$

where we have assumed that all the position-dependent Rabi-frequencies are the same; i.e. $\Lambda_{43}(x, y) = \Lambda_{23}(x, y) = \Lambda_{41}(x, y) = \Lambda_{21}(x, y) = \Lambda(x, y) = \Omega(\sin(kx) + \sin(ky))$, while the dimensionless parameter q_n is given by Eq. (3.51).

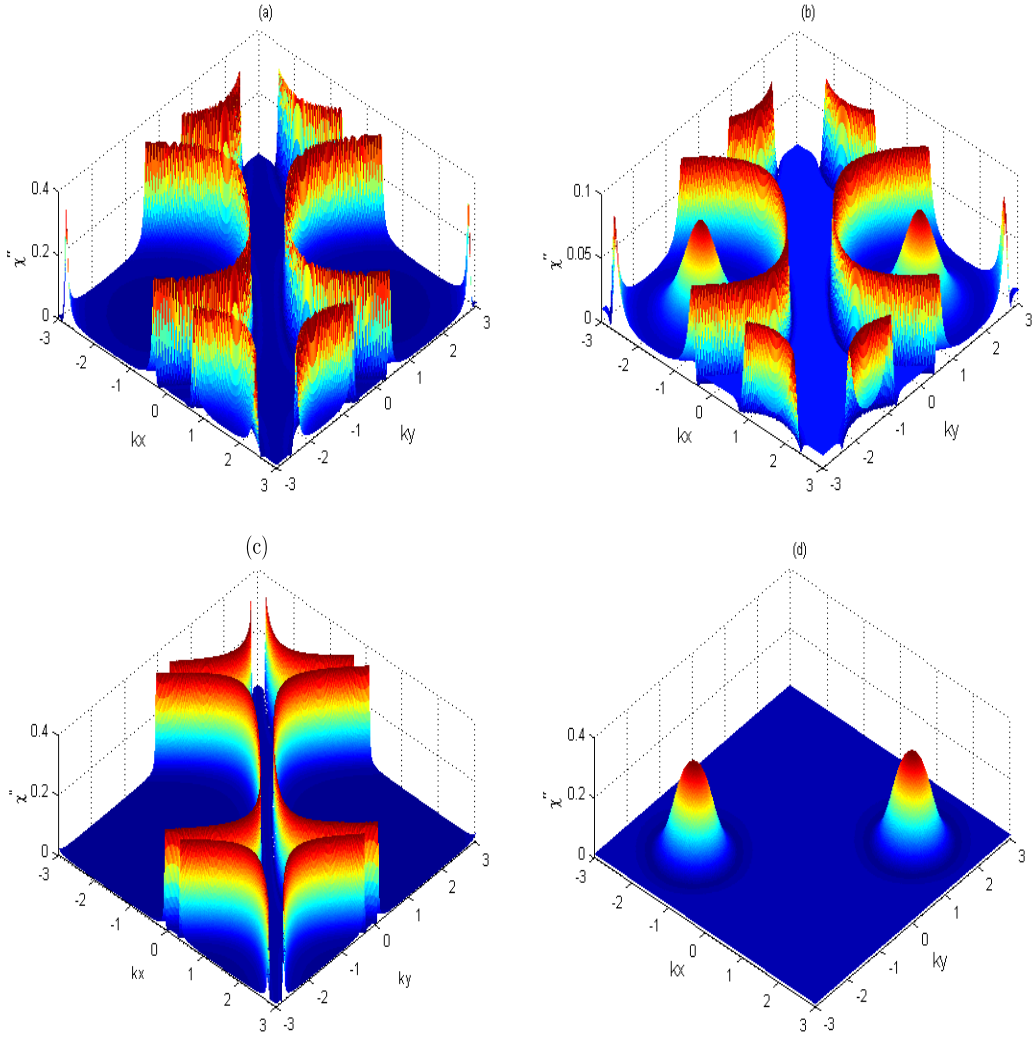

Figure 4.3: Plots of probe absorption χ''versus (kx, ky). The selected parameters are $(\Omega_{43}, \Omega_{32}, \Omega_{41}, \Omega_{21})$ = (a) $(10\gamma, 10\gamma, 10\gamma, 10\gamma)$, (b) $(8\gamma, \gamma, 10\gamma, 10\gamma)$, (c) $(25\gamma, 25\gamma, 25\gamma, 25\gamma)$, (d) $(2.5\gamma, 2.5\gamma, 2.5\gamma, 2.5\gamma)$. Here, $\Delta_p = 10\gamma$, $\phi = 0$. The other parameters are the same as Fig. 4.2.

Let now analyze the eigenenergies for different phase ϕ. For condition $\phi = 0$, Eq. (4.15) changes to

$$E_n = -2\Omega \sin(\frac{n\pi}{2})(\sin(kx) + \sin(ky)), \tag{4.16}$$

Eq. (4.16) results in three eigenenergies $E_3 = -E_1 = 2\Omega(\sin(kx) + \sin(ky))$, and $E_2 = E_4 = 0$. When $\phi = \pi/2$, we obtain

$$E_n = -2\Omega \sin(\frac{n\pi}{2} - \frac{\pi}{8})(\sin(kx) + \sin(ky)), \tag{4.17}$$

Eq. (4.17) gives the following four eigenenergies: $E_3 = -E_1 = 4\Omega(\sin(kx) + \sin(ky))\cos\frac{\pi}{8}$, and $E_4 = -E_2 = 4\Omega(\sin(kx) + \sin(ky))\sin\frac{\pi}{8}$. Finally, for $\phi = \pi$, Eq. (4.15) reduces to

$$E_n = -2\Omega \sin(\frac{n\pi}{2} - \frac{\pi}{4})(\sin(kx) + \sin(ky)), \tag{4.18}$$

In such a case one arrives at two pairs of degenerate eigenenergies $E_1 = E_2 = -\sqrt{2}\Omega(\sin(kx) + \sin(ky))$, and $E_3 = E_4 = \sqrt{2}\Omega(\sin(kx) + \sin(ky))$.

Eqations (4.16)–(4.18) imply that there is a strong phase dependence of the eigenvalues required to achieve maximum in the probe absorption. It can be seen that the number of absorption peaks varies by changing ϕ. Obviously, three, four and two absorption peaks appear for $\phi = 0$, $\phi = \pi/2$, and $\phi = \pi$, respectively (see Figs. 3.6(a)-(f)).

Another interesting illustration of our results can be described using the right hand side of Eqs. (4.16)–(4.18). For a given probe detuning, the maximum conditions would be satisfied just when the curves of the probe detuning intersect with the curves obtained from the solutions of Eqs. (4.16)–(4.18). There are certain positions in $x - y$ plane at which probe absorption maxima take place. The position of intersections depend strongly on the value of the arbitrary selected detunings, as well as on the relative phase ϕ of the applied fields. In this case, the positions of intersections correspond to the probe absorption maxima in the 2D localization patterns illustrated in Fig. 4.4.

The above discussion implies the dependence of probe absorption χ'' on the relative phase ϕ resulting in different patterns in 2D localization profile of an atom as demonstrated in Fig. 4.4. It is found from Figs. 4.4(a) and 4.4(b) that for $\phi = 0$ and $\phi = \pi/3$, the behavior of the 2D atom localization is pretty much similar to that presented in Figs. 4.3(a) and 4.3(b). For $\phi = \pi/2$, two crater-like patterns are formed within the half-crater patterns in the first and third quadrants (Fig. 4.4(c)). For these cases, the absorption measurement provide little information of the atomic position in the $x - y$ plane. Adjusting $\phi = \pi$, the radii of the craters and half-craters are reduced and merge together in the absorption profile so that two crater-like patterns appear in the first and third quadrants, and the atom is localized at the circular edges of the two craters (Fig. 4.4(d)). In this case, the uncertainty of the position probability distribution is significantly reduced and the detecting probability of the atom is increased compared to the cases illustrated in Figs. 4.4(a)–4.4(c). Yet the spatial resolution of the atom position is not good enough, so this atom-light coupling condition is not suitable for detecting with high probability in the 2D atom localization.

In the following, we shall analyze another situation aimed at reducing the number of localization peaks in the $x - y$ plane and achieving a unique detecting probability of the atom in the $x - y$ plane.

4.1.2.3 Third case: Only one control field is position-dependent

Let us next consider a case where only one of the control fields $\Lambda_{21} = \Lambda_{21}(x, y)$ is position-dependent. This field is a combination of two orthogonal standing-wave fields with the same frequency, other laser fields being the traveling-waves (Fig. 4.1(d)):

$$\Lambda_{21} = \Lambda_{21}(x, y) = \Omega_{21}(\sin(kx) + \sin(ky)),$$

$$\Lambda_{43} = \Omega_{43},$$

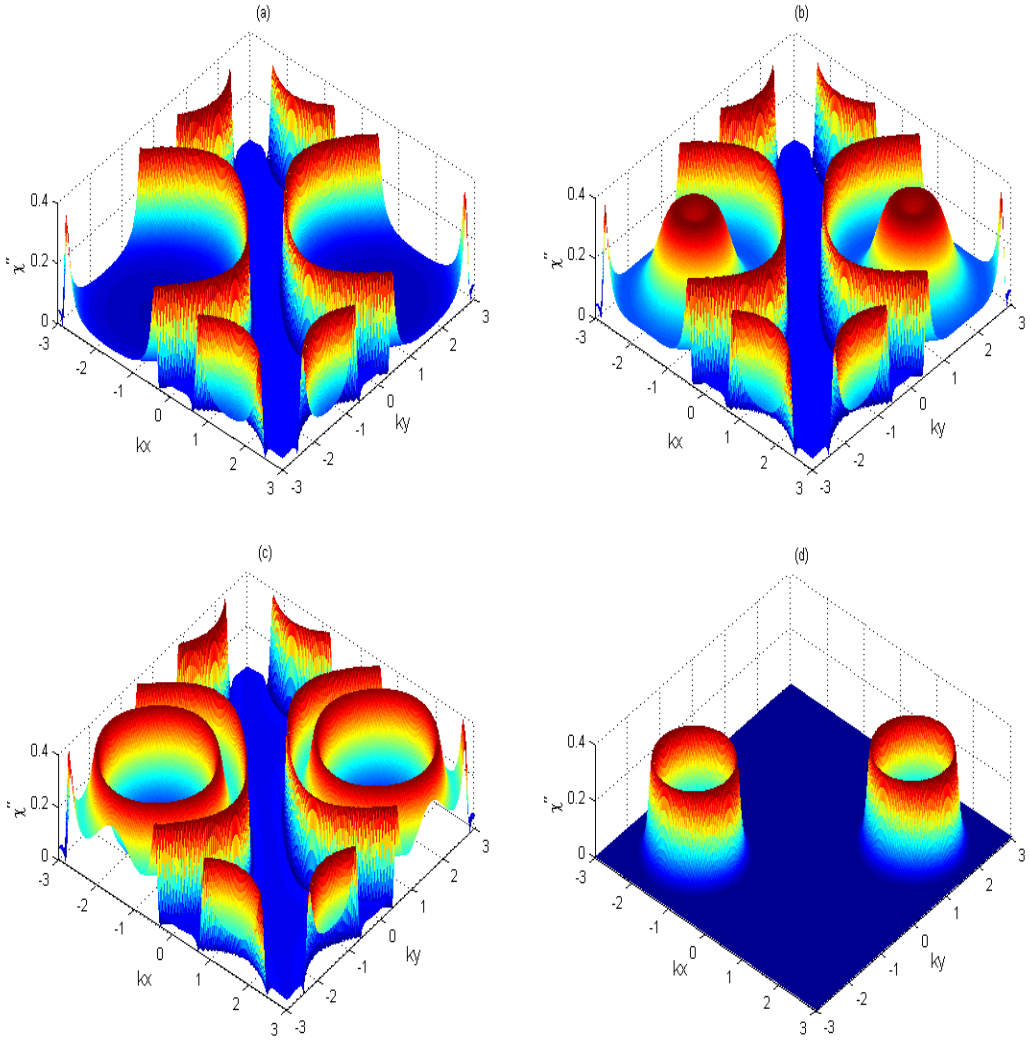

Figure 4.4: Plots of probe absorption χ''versus (kx, ky). The selected parameters are (a) $\phi = 0$, (b) $\phi = \pi/3$, (c) $\phi = \pi/2$, (d) $\phi = \pi$. Here, $(\Omega_{43}, \Omega_{32}, \Omega_{41}, \Omega_{21}) = (5\gamma, 5\gamma, 5\gamma, 5\gamma)$, $\Delta_p = 5\gamma$. The other parameters are the same as Fig. 4.2.

$$\Lambda_{41} = \Omega_{41},$$

$$\Lambda_{32} = \Omega_{32}, \tag{4.19}$$

where no phase factors are contained in the Rabi frequencies Λ_{43}, Λ_{41} and Λ_{32} by assuming that these fields propagate perpendicular to the $x-y$ plane positioned at $z = 0$.

Let us firstly explore an impact of the driving fields Ω_{ij} on the position-dependent probe absorption. For $\Omega_{43} = \Omega_{32} = \Omega_{41} = \Omega_{21} = 10\gamma$, the maxima of the probe absorption are situated mainly in the first quadrant, but with a low precision (Fig. 4.5(a)), i.e. the absorption peak is blurred. The next plots of χ'' are presented for different values of Ω_{ij}. The plots are for $\Omega_{41} = 20\gamma$ and $\Omega_{43} = \Omega_{32} = \Omega_{21} = 10\gamma$ (Fig. 4.5(b)), for $\Omega_{32} = 20\gamma$ and $\Omega_{43} = \Omega_{41} = \Omega_{21} = 10\gamma$ (Fig. 4.5(c)), for $\Omega_{43} = 18\gamma$ and $\Omega_{32} = \Omega_{41} = \Omega_{21} = 10\gamma$(Fig. 4.5(d)), as well as for $\Omega_{21} = 14.8\gamma$ and $\Omega_{43} = \Omega_{32} = \Omega_{41} = 10\gamma$ (Fig. 4.5(e)). It is clear that by increasing each of Ω_{ij}, different spatial distribution and localization patterns are obtained. As one can see in Fig. 4.5(b), the probe-absorption maxima are distributed on the diagonal in the second and fourth quadrants, with a lattice-like pattern showing a uniform position probability distribution across diagonals corresponding to $kx + ky = 2m\pi$ (or $kx - ky = (2n + 1)\pi$) (m, n are integers). When the intensity of driving field Ω_{32} is increased to $\Omega_{32} = 20\gamma$, the maxima of all absorption peaks are located in the third quadrant with a crater-like pattern, and the atom is localized at the circular edge of the crater (Fig. 4.5(c)). Increasing the Rabi frequency Ω_{43} to 18γ results in localization of the atom in the first quadrant with a spike-like pattern, whereas in the third quadrant there is a very weak crater-like pattern. Therefore the localization precision of the first quadrant is much higher than that of the third quadrant (Fig. 4.5(d)). Although compared to Figs. 4.5(a)–4.5(c), in the current situation there is an improvement of the information of the atomic position in the $x - y$ plane, but there is still not a perfect atom localization. A best result appears in Fig. 4.5(e) in which one can observe that by increasing the intensity of standing wave field Ω_{21} to 14.8γ the probability of finding the atom is significantly increased and the atom is localized nearly at a certain position (i.e., $(kx, ky) \approx (\pi/2, \pi/2)$). Therefore, the detection probability of finding the atom in one period of the standing-wave fields reaches almost 100%.

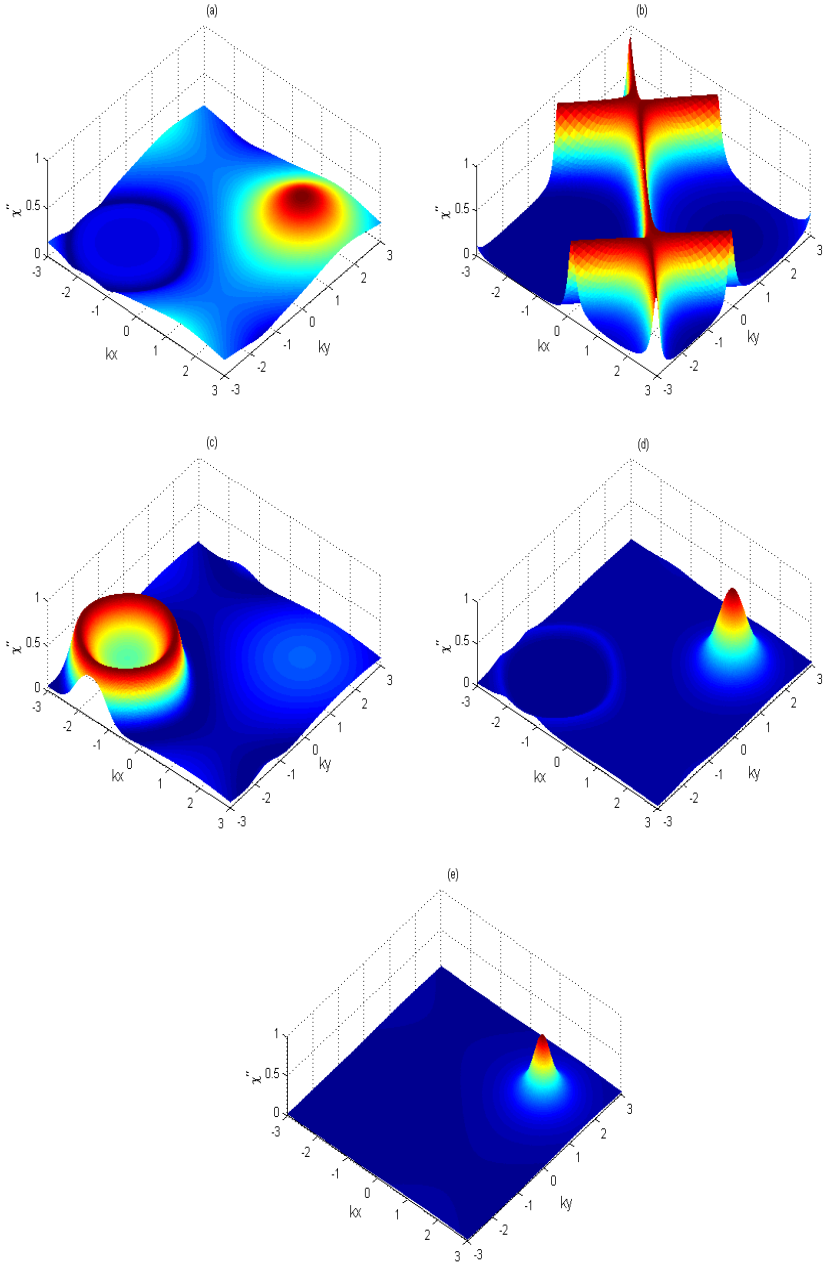

Figure 4.5: Plots of probe absorption χ''versus (kx, ky). The selected parameters are $(\Omega_{43}, \Omega_{32}, \Omega_{41}, \Omega_{21})$ =(a) $(10\gamma, 10\gamma, 10\gamma, 10\gamma)$, (b) $(10\gamma, 10\gamma, 20\gamma, 10\gamma)$, (c) $(10\gamma, 20\gamma, 10\gamma, 10\gamma)$, (d) $(18\gamma, 10\gamma, 10\gamma, 10\gamma)$, and (e) $(10\gamma, 10\gamma, 10\gamma, 14.8\gamma)$. Here, $\triangle_{12} = \triangle_{14} = \triangle_{23} = \triangle_{43} = 10\gamma$, $\Delta_p = 0$, and the other parameters are the same as Fig. 4.2.

Finally, we discuss the phase dependence of atom localization in the KR5 quantum system for the third situation described above. Figure 4.6 displays the atom localization patterns of the probe absorption as a function of the positions (kx, ky) for different values of the relative phase ϕ. When $\phi = 0$, one spike-like localization peak appears in the first quadrant providing the high-precision atom localization (Fig. 4.6(a)). In this case, the probability of finding the atom within one period of the standing-wave fields reaches the unity. Adjusting the phase parameter to $\phi = \pi/4$, as it can be seen in Fig. 4.6(b), the spatial distribution of the probe absorption has a crater-like pattern located in the first quadrant. As we further increase the relative phase to $\phi = \pi/2$, it can be observed from Fig. 4.6(c) that another crater-like localization peak appears in the third quadrant, so that the peak maxima of the probe absorption exhibits two symmetric crater-like patterns, and the uncertainty of finding an atom in one period increases accordingly. Thus we can find atom at circular edges around $(kx, ky) \approx (\pi/2, \pi/2)$ or $(kx, ky) \approx (-\pi/2, -\pi/2)$ in quadrants I or III, respectively. For the case $\phi = 3\pi/4$, it can be found from Fig. 4.6(d) that the localization peak in the first quadrant has completely vanished, and the detection uncertainty is reduced correspondingly. As can bee seen in Fig. 4.6(e), for $\phi = \pi$ the localization peak shifts to the third quadrant and thus, the pattern of the probe absorption becomes a mirror image of the localization pattern for $\phi = 0$ (illustrated in Fig. 4.6(a)) with respect to the line $y = -x$ in the $x-y$ plane. Therefore, it is quite obvious that the relative phase plays an important role to achieve the perfect detection probability of an atom at a particular position within one period of standing-wave fields.

The origin of such an efficient localization stems from the quantum interference induced by two possible ways of going from the ground level $|5\rangle$ to upper level $|1\rangle$, involving $|5\rangle \overset{\Omega_p}{\longmapsto} |3\rangle \overset{\Omega_{32}}{\longmapsto} |2\rangle \overset{\Omega_{21}}{\longmapsto} |1\rangle$ and $|5\rangle \overset{\Omega_p}{\longmapsto} |3\rangle \overset{\Omega_{43}}{\longmapsto} |4\rangle \overset{\Omega_{41}}{\longmapsto} |1\rangle$ pathways. This affects the absorption of the probe field for such a closed-loop quantum system and results in a perfect atom localization. In Eqs. (4.9) and (4.10) for the susceptability, the quantum interference is represented by the term $2\Lambda_{41}\Lambda_{32}\Lambda_{43}\Lambda_{21}\cos\phi$ playing the main role in formation of the atom localization patterns.

In the first case where the atom-light coupling is described by Eqs. (4.11) and (4.12), the interference term reduces $2\Omega_{41}\Omega_{32}\Omega_{43}\Omega_{21}\cos\phi\sin^2(kx)\sin^2(ky)$. The position-dependent absorption spectrum remains then unchanged under the transformations $(x, y) \leftrightarrow (-x, -y)$, $(x, y) \leftrightarrow (x, -y)$, $(-x, y) \leftrightarrow (x, -y)$,

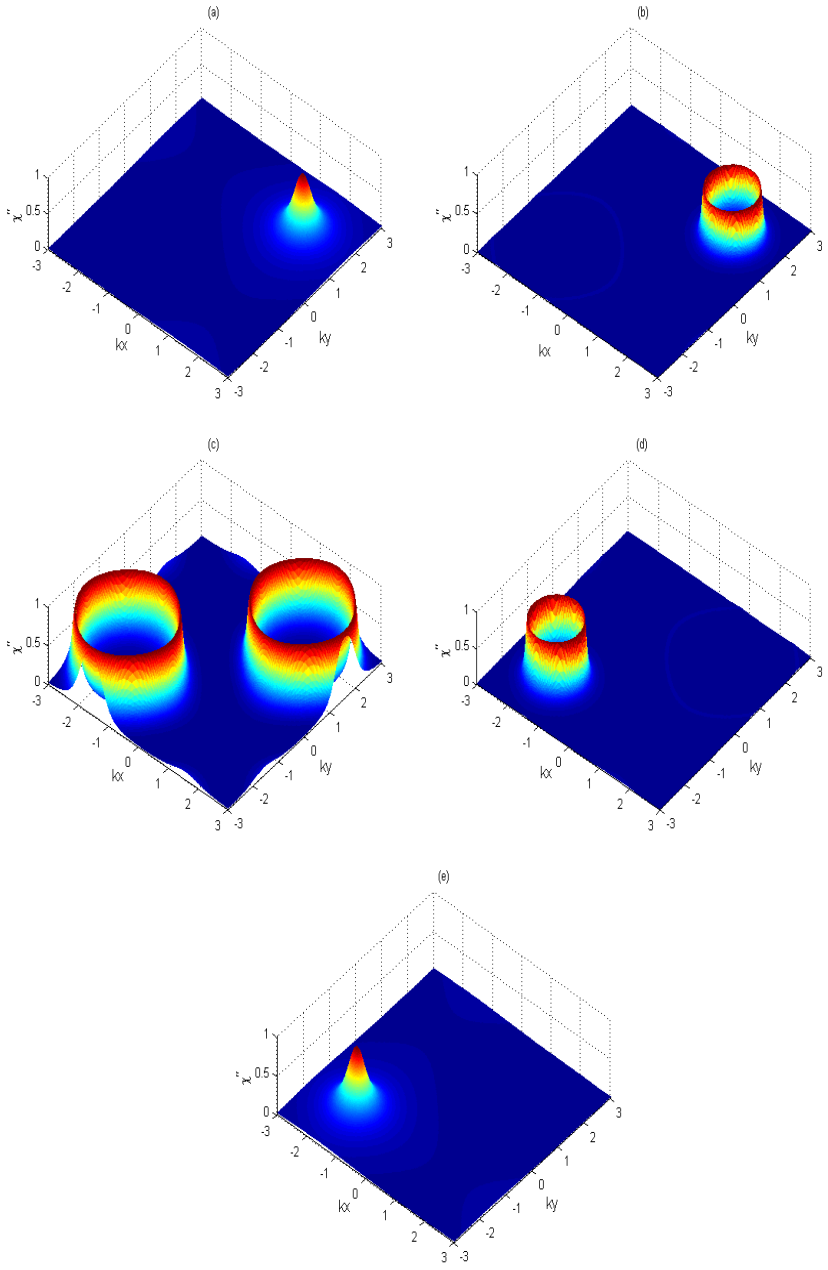

Figure 4.6: Plots of probe absorption χ''versus (kx, ky). The selected parameters are (a) $\phi = 0$, (b) $\phi = \pi/4$, (c) $\phi = \pi/2$, (d) $\phi = 3\pi/4$, (e) $\phi = \pi$. Here, $(\Omega_{43}, \Omega_{32}, \Omega_{41}, \Omega_{21}) = (10\gamma, 10\gamma, 10\gamma, 14.8\gamma)$. The other selected parameters are the same as Fig. 4.5.

and $(-x, y) \leftrightarrow (-x, -y)$. Thus for a given probe detuning the immaginary part of the susceptibility reads $\chi''(x, y) = \chi''(-x, -y)$, $\chi''(x, y) = \chi''(x, -y)$, $\chi''(-x, y) = \chi''(x, -y)$, and $\chi''(-x, y) = \chi''(-x, -y)$. In such a situation the probe absorption is the same in each of four quadrants, so the localization is not perfect.

In the second case described by Eqs. (4.13) and (4.14), the quantum interference term reads $2\Omega_{41}\Omega_{32}\Omega_{43}\Omega_{21}\cos\phi(\sin(kx) + \sin(ky))^4$. The resulting probe absorption spectrum is invariant only with respect to the transformations $(x, y) \leftrightarrow (-x, -y)$, and $(-x, y) \leftrightarrow (x, -y)$, giving $\chi''(x, y) = \chi''(-x, -y)$, and $\chi''(-x, y) = \chi''(x, -y)$. Consequently the probability distribution is the same in quadrants I and III, as well as in quadrants II and IV, leading to a higher detection probability than in the first case. Finaly in the third case of the atom-light coupling corresponding to Eq. (4.19), the interference term reads $2\Omega_{41}\Omega_{32}\Omega_{43}\Omega_{21}\cos\phi(\sin(kx) + \sin(ky))$. In such a situation there is no symmetry under which the interference term (and hence the position-dependent absorption spectrum) could remain unchanged. The probability distribution of the absorption peaks is then not equal in all four quadrants, so one arrives at a nealy perfect atom localization by properly adjusting the system parameters, as one can see in Figs. 4.5(d), 4.6(a) and 4.6(e).

Let us now discuss the phase effects. When the relative phase of applied fields is $\phi = \pi/2$, the interference term vanishes in Eqs. (4.9) and (4.10). In the third case the probe absorption spectrum then does not alter under the transformation $(x, y) \leftrightarrow (-x, -y)$, giving $\chi''(x, y; \phi = \pi/2) = \chi''(-x, -y; \phi = \pi/2)$. Therefore, one should observe two absorption maxima with the same probability distribution in the quadrants I and III (see Fig. 4.6(c)). On the other hand, for $\phi = 0$ and $\phi = \pi$ the interference term becomes maximum. Thus the absorption spectrum remains again unchanged under the transformation $(x, y, \phi = 0) \leftrightarrow (-x, -y, \phi = \pi)$. That is why for $\phi = \pi$ the probe absorption becomes a mirror image of the localization pattern for $\phi = 0$, as one can see in Figs. 4.6(a) and (e).

4.1.3 3D atom localization

Let us now investigate the phase control of atom localization in three dimensions for our proposed scheme. For this situation, each standing wave field is obtained

from a superposition of three orthogonal standing wave fields with the same frequency (Fig. 4.1(e)). The Rabi-frequencies corresponding to such standing waves read

$$\Lambda_{43} = \Lambda_{43}(x, y, z) = \Omega_{43} f_3(x, y, z),$$

$$\Lambda_{41} = \Lambda_{41}(x, y, z) = \Omega_{41} f_3(x, y, z),$$

$$\Lambda_{32} = \Lambda_{32}(x, y, z) = \Omega_{32} f_3(x, y, z),$$

$$\Lambda_{21} = \Lambda_{21}(x, y, z) = \Omega_{21} f_3(x, y, z), \tag{4.20}$$

with

$$f_3(x, y, z) = \sin(kx) + \sin(ky) + \sin(kz). \tag{4.21}$$

One can see from Eqs. (4.9) and (4.10) that the atom localization in 3D space depends crucially on the atom-field coupling featured in Eq. (4.20) via the relative phase factor ϕ. Figure 4.7 illustrates the isosurface plot of the probe absorption as a function of the position (kx, ky, kz) for different values of the relative phase ϕ. It can be observed that the effect of the relative phase ϕ leads to different absorptions structures in 3D space. When $\phi = 0$, the probe absorption is distributed in eight different subspaces of the 3D space (Fig. 4.7(a)). In particular, we observe that for $\phi = \pi/3$, two spheres appear in the subspaces $0 \leqslant kx, ky, kz \leqslant \pi$ and $-\pi \leqslant kx, ky, kz \leqslant 0$ with maximum detecting probability of the atom in one of these regions being approximately 1/2 (Fig. 4.7(b)). By setting the relative phase ϕ to $\pi/2$, the volume of two spheres in each subspace becomes larger as can be seen in Fig. 4.7(c) so that the uncertainty in position measurement of the atom is increased. Finally for $\phi = \pi$, the probe absorption spectrum is mostly located in the subspaces $0 \leqslant kx, ky, kz \leqslant \pi$ and $-\pi \leqslant kx, ky, kz \leqslant 0$ with little in the other regions. Therefore, we could show that different 3D localization patterns can be obtained in 3D space through manupulating the relative phase ϕ. However, the maximum detection probability of finding the atom in the particular region is around 1/2 for the atom-field

coupling described by Eq. (4.20). Note that in this 3D scheme, the probe field Ω_p is assumed to propagate along the z direction allowing us to monitor the 3D localization of an atom [39].

4.2 Scheme 2: Four-level system with twofold lower levels

Now we propose a scheme for phase sensitive 3D atom localization by the measurement of the absorption of the weak probe field. The scheme is applied to a four-level atomic system with three orthogonal standing wave fields and a weak probe field. Because of the space-dependent atom-field interaction in three dimensions, the position probability distribution of the atom passing through the standing wave fields can be straightforwardly determined by measuring the probe absorption spectra of the probe laser field. Focusing on the signatures of the relative phase of applied fields stemming from the closed loop structure of the system, we observe that different periodic isosurface patterns of localization can be obtained in 3D space [45].

4.2.1 Model and equations

Figure 4.8(a) shows a four-level system interacting with a weak probe field and three perpendicular standing wave fields. The probe field of Rabi-frequency Ω_p mediates the transition between the ground level $|a\rangle$ and the upper level $|b\rangle$. The upper level $|b\rangle$ is coupled to the atomic level $|c\rangle$, and further the level $|c\rangle$ is connected to level $|d\rangle$, and then the level $|d\rangle$ is coupled to the upper level $|b\rangle$ via standing wave fields $\Omega_c(x)$, $\Omega_m(y)$ and $\Omega_d(z)$, respectively. Such a scheme is equivalent to a modified Λ-type level structure with an extra atomic level and additional driving fields forming a complete loop of atom-light interaction as shown in Fig. 4.8(a). We consider a situation in which three standing waves drive different atomic tranistions. The coupling of the laser fields with the atom is represented by the Rabi-frequencies (4.8(b))

$$\Omega_c(x) = \Omega_c \sin k_x x,$$

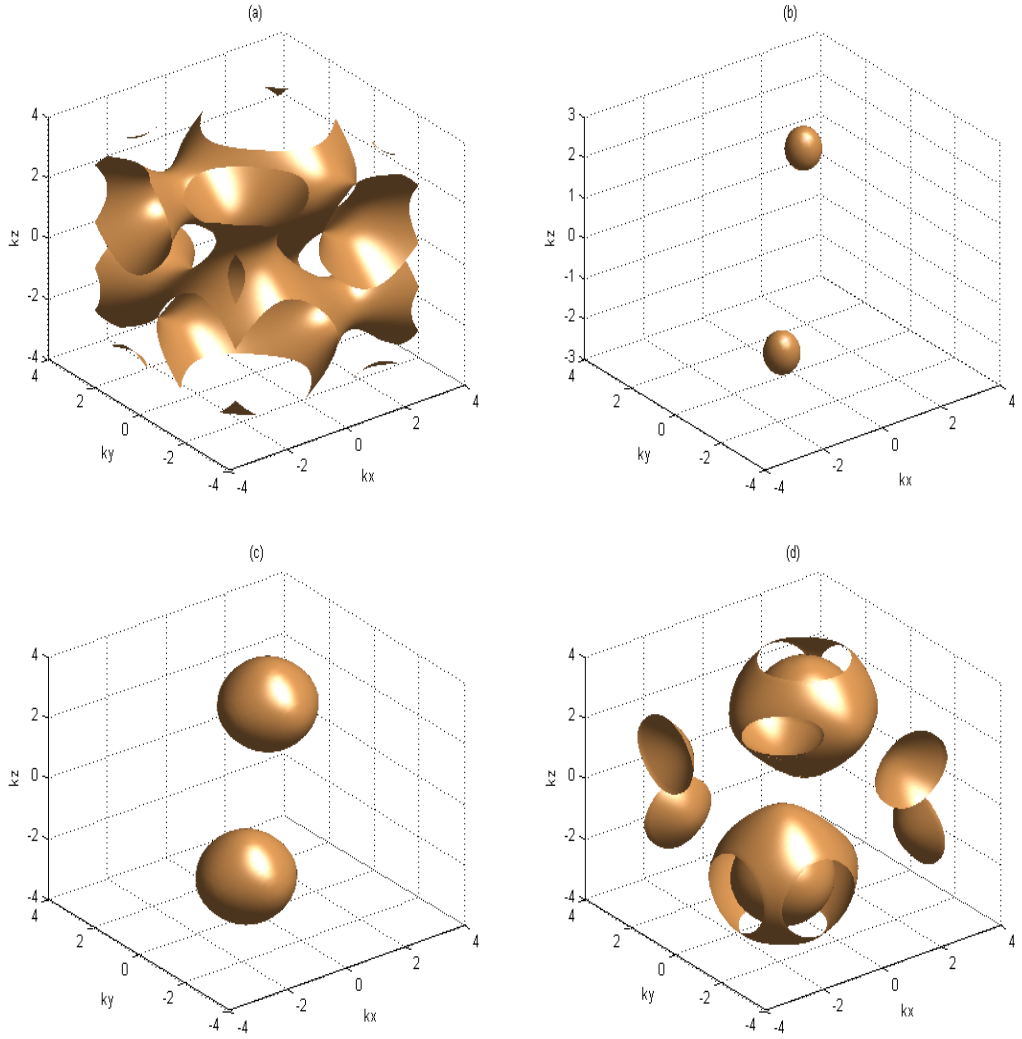

Figure 4.7: Isosurface plots of probe absorption χ''versus (kx, ky, kz). The selected parameters are (a) $\phi = 0$, (b) $\phi = \pi/3$, (c) $\phi = \pi/2$, and (d) $\phi = \pi$. Here, $(\Omega_{43}, \Omega_{32}, \Omega_{41}, \Omega_{21}) = (10\gamma, 10\gamma, 10\gamma, 10\gamma)$,$\triangle_{12} = \triangle_{14} = \triangle_{23} = \triangle_{43} = \Delta_p = 10\gamma$. The other selected parameters are the same as Fig. 4.2.

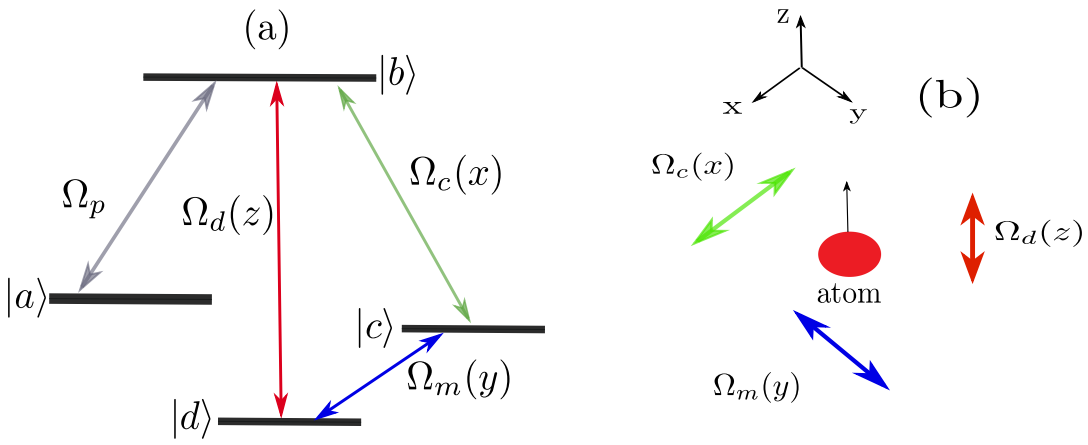

Figure 4.8: (a) Schematic diagram for the four-level atomic system with twofold lower levels. (b) A situation in which the atom could interact with the position-dependent standing wave fields.

$$\Omega_m(y) = \Omega_m \sin k_y y,$$

$$\Omega_d(z) = \Omega_d \sin k_z z, \tag{4.22}$$

where k_x, k_y and k_z are the corresponding wave vectors. Since the Rabi-frequencies of the standing wave fields are position dependent, so the interaction between the atom and laser fields becomes position dependent.

Under the Raman-Nath approximation [80] and applying the rotating-wave approximation, the resulting interaction Hamiltonian for the system reads

$$H_I = -\hbar(\Omega_p \left|b\right\rangle \left\langle a\right| + \Omega_c(x) \left|b\right\rangle \left\langle c\right| + \Omega_m(y) \left|c\right\rangle \left\langle d\right| + \Omega_d(z) \left|b\right\rangle \left\langle d\right|) + H.c. \tag{4.23}$$

Using the Liouville equation (2.33), the optical Bloch equations for the off-diagonal density matrix elements for the system are given by

$$\dot{\rho}_{ba} = -(\gamma_{ba} + i\Delta_p)\rho_{ba} + i\Omega_c(x)\rho_{ca} + i\Omega_p(\rho_{aa} - \rho_{bb}) + i\Omega_d(z)\rho_{da}, \tag{4.24}$$

$$\dot{\rho}_{ca} = -(\gamma_{ca} + i(\Delta_p - \Delta_c))\rho_{ca} + i\Omega_c(x)\rho_{ba} - i\Omega_p\rho_{cb} + i\Omega_m(y)\mathrm{e}^{i\phi}\rho_{da.}, \tag{4.25}$$

$$\dot{\rho}_{da} = -(\gamma_{da}+i(\Delta_p-\Delta_c-\Delta_m))\rho_{da}-i\Omega_p\rho_{db}+i\Omega_m(y)\mathrm{e}^{-i\phi}\rho_{ca.}+i\Omega_d(z)\rho_{ba}, \tag{4.26}$$

$$\begin{aligned}\dot{\rho}_{bc} = -(\gamma_{bc} + i\Delta_c)\rho_{bc} - i\Omega_c(x)(\rho_{bb} - \rho_{cc}) + i\Omega_p\rho_{ac} - i\Omega_m(y)\mathrm{e}^{-i\phi}\rho_{bd.} \\ +i\Omega_d(z)\rho_{dc},\end{aligned} \tag{4.27}$$

$$\begin{aligned}\dot{\rho}_{bd} = -(\gamma_{bd} + i(\Delta_c + \Delta_m))\rho_{bd} + i\Omega_c(x)\rho_{cd} + i\Omega_p\rho_{ad} - i\Omega_m(y)\mathrm{e}^{i\phi}\rho_{bc.} \\ +i\Omega_d(z)(\rho_{dd} - \rho_{bb}),\end{aligned} \tag{4.28}$$

$$\dot{\rho}_{cd} = -(\gamma_{cd} + i\Delta_m)\rho_{cd} + i\Omega_c(x)\rho_{bd} - i\Omega_m(y)\mathrm{e}^{i\phi}(\rho_{dd} - \rho_{cc}) - i\Omega_d(z)\rho_{cb}, \tag{4.29}$$

where the detuning parameters are defined as $\Delta_p = \omega_{ba} - \nu_p$, $\Delta_c = \omega_{bc} - \nu_c$ and $\Delta_m = \omega_{cd} - \nu_m$, while γ_{ij} denote the spontaneous decay rates of the upper level $|i\rangle$ to the lower level $|j\rangle$. Owning to the closed-loop structure of the subsystem interacting with the ground level $|a\rangle$, such a medium is phase sensitive. The relative phase of applied fields is determined by $\phi = \phi_c + \phi_m - \phi_d$, where $\phi_i\,(i = c, m, d)$ denotes the initial phase of laser fields. Assuming the atom is predominantly populated in the initial ground state $|a\rangle$, the steady state solution of the coherence term ρ_{ba} reads

$$\rho_{ba} = \frac{i\Omega_p(YZ + \Omega_m^2(y))}{\Omega_m^2(y)X + \Omega_d^2(z)Y + \Omega_c^2(x) - Q}\,, \tag{4.30}$$

where

$$\begin{aligned} X &= \gamma_{ba} + i\Delta_p, \\ Y &= \gamma_{ca} + i(\Delta_p - \Delta_c), \\ Z &= \gamma_{da} + i(\Delta_p - \Delta_c - \Delta_m), \end{aligned} \tag{4.31}$$

with the quantum interference term represented by

$$Q = 2i\Omega_c(x)\Omega_m(y)\Omega_d(z)\cos\phi. \tag{4.32}$$

As shown in Fig. 4.8(a), there exist two possible transition pathways from ground state $|a\rangle$ to upper state $|b\rangle$: the direct one $|a\rangle \overset{\Omega_p}{\longmapsto} |b\rangle$ and the indirect one $|a\rangle \overset{\Omega_p}{\longmapsto} |b\rangle \overset{\Omega_c}{\longmapsto} |c\rangle \overset{\Omega_m}{\longmapsto} |d\rangle \overset{\Omega_d}{\longmapsto} |a\rangle$. Then the effect of the relative phase ϕ on absorption characteristics of the weak probe field in such a configuration with the closed-loop subsystem can be explained from quantum interference term Q featured in Eq. (4.32).

4.2.2 Phase control of 3D atom localization

The coherence term ρ_{ba} featured in Eq. (4.30) is directly related to the susceptibility of the probe field $\chi = \chi^{'} + i\chi^{''} = \frac{2N\wp_{ab}^2}{\varepsilon_0\hbar\Omega_p}\rho_{ba}$. It can be seen from Eq. (4.32) that the phase ϕ enters the susceptibility expression through the quantity Q.

In what follows, we explore how the relative phase ϕ affects the 3D spatial distribution of probe absorption. We take $\gamma_{ba} = \gamma_{ca} = \gamma_{da} = \gamma$, and reduce all the parameters to the dimensionless units through scaling by γ. Figure 4.9 illustrates the isosurface plot of probe absorption in 3D space for different values of ϕ. We have selected the detunings as $\Delta_c = \Delta_m = 0$ and $\Delta_p = 5\gamma$. It is clear that the 3D atom localization is very sensitive to the relative phase of applied fields. When ϕ is zero, the isosurface plot of probe absorption exhibits four spheres located at subspaces ($0 \leqslant k_x x \leqslant \pi, 0 \leqslant k_y y \leqslant \pi, 0 \leqslant k_z z \leqslant \pi$)), ($-\pi \leqslant k_x x \leqslant 0, -\pi \leqslant k_y y \leqslant 0, 0 \leqslant k_z z \leqslant \pi$)), ($-\pi \leqslant k_x x \leqslant 0, 0 \leqslant k_y y \leqslant \pi, -\pi \leqslant k_z z \leqslant 0$)), and ($0 \leqslant k_x x \leqslant \pi, -\pi \leqslant k_y y \leqslant 0, -\pi \leqslant k_z z \leqslant 0$)). For this case, the maximum detecting probability of the atom in one of these regions is approximately 1/4 (Fig. 4.9(a)). In this case, the interference term becomes $Q = 2i\Omega_c\Omega_m\Omega_d \sin k_x x \sin k_y y \sin k_z z$.

The position-dependent absorption spectrum remains then unchanged under the transformations $(x, y, z) \leftrightarrow (-x, -y, z)$, $(-x, y, -z)$, and $(x, -y, -z)$. Thus for a given probe detuning the immaginary part of the susceptibility reads $\chi''(x, y, z) = \chi''(-x, -y, z) = \chi''(-x, y, -z) = \chi''(x, -y, -z)$. As we change the relative phase ϕ to $\pi/2$, eight diamond-like spheres take place (Fig. 4.9(b)). In this case, the detection probability of finding the atom is reduced to 1/8. For this situation, the quantum interfererence term vanishes, resulting in the same detection probability in each of subspaces $(\pm x, \pm y, \pm z)$. By setting $\phi = \pi$, the quantum interference term becomes $Q = -2i\Omega_c\Omega_m\Omega_d \sin k_x x \sin k_y y \sin k_z z$, making the probe absorption being a mirror image of the localization pattern for $\phi = 0$, as illustrated in Figs. 4.9(c). In this case, four spheres appears at subspaces $(-\pi \leqslant k_x x \leqslant 0, -\pi \leqslant k_y y \leqslant 0, -\pi \leqslant k_z z \leqslant 0))$, $(0 \leqslant k_x x \leqslant \pi, 0 \leqslant k_y y \leqslant \pi, -\pi \leqslant k_z z \leqslant 0))$, $(0 \leqslant k_x x \leqslant \pi, -\pi \leqslant k_y y \leqslant 0, 0 \leqslant k_z z \leqslant \pi))$, and $(-\pi \leqslant k_x x \leqslant 0, 0 \leqslant k_y y \leqslant \pi, 0 \leqslant k_z z \leqslant \pi))$ with the detection probability again being 1/4. Results indicate that there is a strong correlation between 3D atom localization and the relative phase of applied fields.

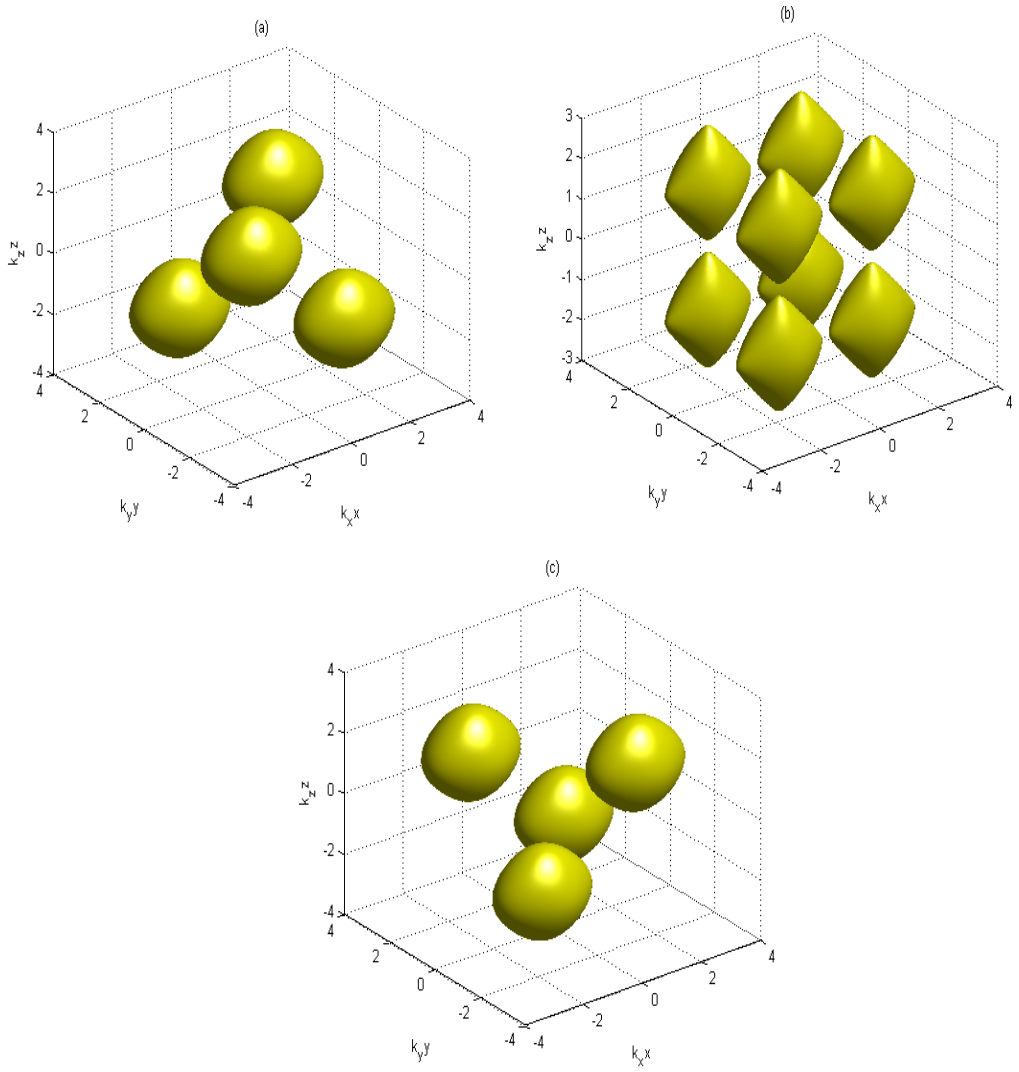

Figure 4.9: Isosurface plots of probe absorption χ''versus $(k_x x, k_y y, k_z z)$. The selected parameters are (a) $\phi = 0$, (b) $\phi = \pi/2$, and (c) $\phi = \pi$. The selected parameters are $\gamma_{ba} = \gamma_{ca} = \gamma_{da} = \gamma$, $\Delta_c = \Delta_m = 0$, $\Delta_p = 5\gamma$ and $\Omega_c = \Omega_d = \gamma$ and $\Omega_m = 4\gamma$.

Chapter 5

Linear and nonlinear effects in five-level double-ladder systems

During the recent years there have been remarkable activities in studying the slow light [10, 8, 58, 146] stimulated by applications to low-light-level nonlinear optics [84, 86] and quantum information manipulation [147]. It was demonstrated that a weak probe beam of light in an atomic medium driven by a stronger control laser propagates as slowly as several of tens of meters per second [58]. The resonant and opaque medium becomes transparent for the probe beam in presence of the control laser beam due the effect of EIT [124, 7]. The slow light forming due to the EIT can also enhance significantly the interaction of light and matter enabling the nonlinear optical processes to achieve significant efficiency even at single-photon level [86]. EIT effect can modify the propagation dynamics of the medium through altering the absorptive and dispersive characteristics [144, 26, 10, 11, 148] and induces nonlinear optical phenomena such as an enhanced Kerr nonlinearity [15, 16] as well as formation of stable slow optical solitons [100, 114]. Probe field strength in such nonlinear optical phenomena is assumed to be strong enough to consider the coherence only up to the third order of the probe susceptibility.

The work presented in this chapter is concerned with linear and nonlinear optical phenomena in a five-level double-ladder atom light coupling scheme. We explore the effect of a control field Ω_d on linear and nonlinear optical properties of a probe field in such a medium by using the semi-classical density matrix method. In the absence of the control field, it is realized that the system is opaque for the probe field. When the control field is turned on, the medium switches to transparency for the probe field. In this case, the subluminal light propagates in the medium. In addition to analytical solutions, numerical results are given in terms of a Gaussian intensity profile of the probe field to elucidate such optical

switching [46].

This chapter is also aimed at modeling the enhanced Kerr nonlinearity for such an atom light coupling scheme. We find that a giant Kerr nonlinearity can be achieved along with zero absorption by properly manipulating the Rabi frequency of control field [47].

5.1 Model and equations

We shall consider the light-matter interaction in an ensemble of atoms using a five-level double ladder-type (inverted Y-type) coupling scheme illustrated in Fig. 5.1(a). A weak probe field with the Rabi-frequency Ω_p is applied to the transition $|1\rangle \leftrightarrow |3\rangle$. In addition, three strong laser beams wirh Rabi frequencies Ω_d, Ω_c and Ω_s induce atomic transitions $|2\rangle \leftrightarrow |3\rangle$, $|4\rangle \leftrightarrow |3\rangle$, and $|4\rangle \leftrightarrow |5\rangle$, respectively. In the interaction picture, the resulting interaction Hamiltonian describing the atom-field interaction for the system can be written as ($\hbar = 1$)

$$\begin{aligned} H = (\Delta_p - \Delta_d)\,|2\rangle\langle 2| + \Delta_p\,|3\rangle\langle 3| + (\Delta_p + \Delta_c)\,|4\rangle\langle 4| + (\Delta_p + \Delta_c + \Delta_s)\,|5\rangle\langle 5| \\ -(\Omega_p\,|3\rangle\langle 1| + \Omega_d\,|3\rangle\langle 2| + \Omega_c\,|4\rangle\langle 3| + \Omega_s\,|5\rangle\langle 4| + H.c.). \end{aligned} \tag{5.1}$$

The detunings of the transitions from the corresponding laser frequencies are defined as $\Delta_p = \omega_{31} - \omega_p$, $\Delta_d = \omega_{32} - \omega_d$, $\Delta_c = \omega_{43} - \omega_c$, and $\Delta_s = \omega_{54} - \omega_s$, where the transition frequencies between the energy levels $|3\rangle$ and $|1\rangle$, $|3\rangle$ and $|2\rangle$, $|4\rangle$ and $|3\rangle$, and $|5\rangle$ and $|4\rangle$ are ω_{31}, ω_{32}, ω_{43}, and ω_{54}, respectively.

Having determined the Hamiltonian Eq. (5.1) and under the rotating wave approximation, the optical Bloch equations for density matrix elements of the five-level atomic system are obtained by the Liouville equation (2.33)

$$\dot{\rho}_{11} = \gamma_{31}\rho_{33} + \gamma_{51}\rho_{55} + i\Omega_p(\rho_{31} - \rho_{13}), \tag{5.2}$$

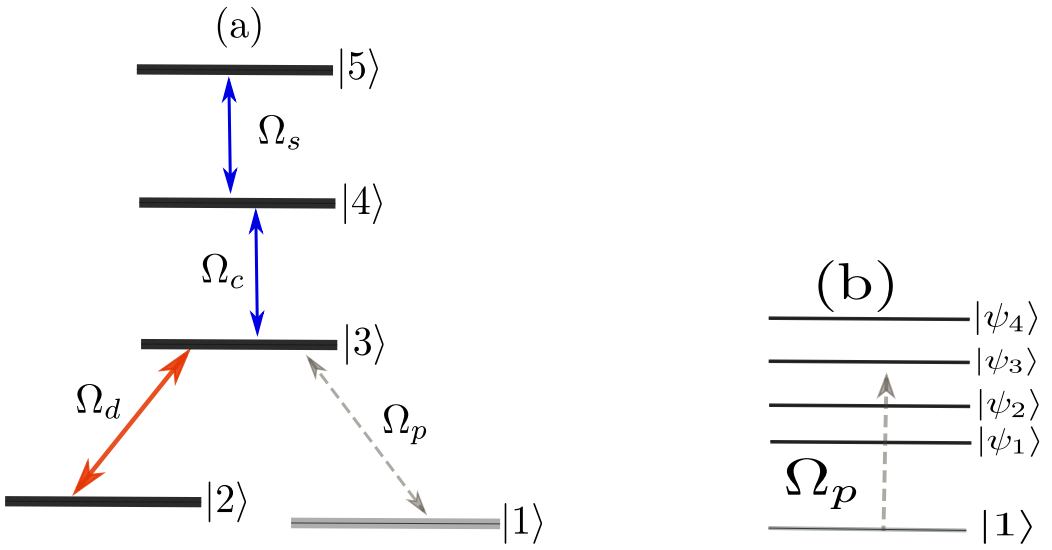

Figure 5.1: (a) Five-level atomic system in a double-ladder configuration. (b) The atom–field states in the dressed state basis.

$$\dot{\rho}_{22} = \gamma_{32}\rho_{33} + \gamma_{52}\rho_{55} + i\Omega_d(\rho_{32} - \rho_{23}), \tag{5.3}$$

$$\begin{aligned}\dot{\rho}_{33} = -(\gamma_{31} + \gamma_{32})\rho_{33} + \gamma_{43}\rho_{44} - i\Omega_p(\rho_{31} - \rho_{13}) + i\Omega_d(\rho_{23} - \rho_{32}) \\ +i\Omega_c(\rho_{43} - \rho_{34}),\end{aligned} \tag{5.4}$$

$$\dot{\rho}_{44} = -\gamma_{43}\rho_{44} + \gamma_{54}\rho_{55} - i\Omega_c(\rho_{43} - \rho_{34}) + i\Omega_s(\rho_{54} - \rho_{45}), \tag{5.5}$$

$$\dot{\rho}_{21} = -i(\Delta_p - \Delta_d)\rho_{21} + i\Omega_d\rho_{31} - i\Omega_p\rho_{23}, \tag{5.6}$$

$$\dot{\rho}_{31} = -\left(i\Delta_p + \frac{\gamma_{31} + \gamma_{32}}{2}\right)\rho_{31} + i\Omega_p(\rho_{11} - \rho_{33}) + i\Omega_c\rho_{41} + i\Omega_d\rho_{21}, \tag{5.7}$$

$$\dot{\rho}_{41} = -\left(i(\Delta_p + \Delta_c) + \frac{\gamma_{43}}{2}\right)\rho_{41} + i\Omega_s\rho_{51} + i\Omega_c\rho_{31} - i\Omega_p\rho_{43}, \tag{5.8}$$

$$\dot{\rho}_{51} = -\left(i(\Delta_p + \Delta_c + \Delta_s) + \frac{\gamma_{51} + \gamma_{52} + \gamma_{54}}{2}\right)\rho_{51} + i\Omega_s\rho_{41} - i\Omega_p\rho_{53}, \quad (5.9)$$

$$\dot{\rho}_{32} = -\left(i\Delta_d + \frac{\gamma_{31} + \gamma_{32}}{2}\right)\rho_{32} + i\Omega_p(\rho_{22} - \rho_{33}) + i\Omega_p\rho_{12} + i\Omega_c\rho_{42}, \quad (5.10)$$

$$\dot{\rho}_{42} = -\left(i(\Delta_p + \Delta_c) + \frac{\gamma_{43}}{2}\right)\rho_{42} + i\Omega_c\rho_{32} - i\Omega_d\rho_{43} + i\Omega_s\rho_{52}, \quad (5.11)$$

$$\dot{\rho}_{52} = -\left(i(\Delta_d + \Delta_c + \Delta_s) + \frac{\gamma_{51} + \gamma_{52} + \gamma_{54}}{2}\right)\rho_{52} + i\Omega_s\rho_{42} - i\Omega_d\rho_{53}, \quad (5.12)$$

$$\begin{aligned}\dot{\rho}_{43} = -\left(i\Delta_c + \tfrac{\gamma_{31}+\gamma_{32}+\gamma_{43}}{2}\right)\rho_{43} + i\Omega_c(\rho_{33} - \rho_{44}) + i\Omega_s\rho_{53} - i\Omega_p\rho_{41} \\ -i\Omega_d\rho_{42},\end{aligned} \quad (5.13)$$

$$\begin{aligned}\dot{\rho}_{53} = -\left(i(\Delta_c + \Delta_s) + \tfrac{\gamma_{51}+\gamma_{52}+\gamma_{54}+\gamma_{31}+\gamma_{32}}{2}\right)\rho_{53} + i\Omega_s\rho_{43} - i\Omega_p\rho_{51} \\ -i\Omega_d\rho_{52} - i\Omega_c\rho_{54},\end{aligned} \quad (5.14)$$

$$\dot{\rho}_{54} = -\left(i\Delta_s + \frac{\gamma_{51} + \gamma_{52} + \gamma_{54} + \gamma_{43}}{2}\right)\rho_{54} - i\Omega_c\rho_{53} + i\Omega_s(\rho_{44} - \rho_{55}), \quad (5.15)$$

$$\rho_{11} + \rho_{22} + \rho_{33} + \rho_{44} + \rho_{55} = 1, \quad (5.16)$$

where the spontaneous decay rates between level $|i\rangle$ and level $|j\rangle$ are denoted by γ_{ij}. Also, the relaxation rates of coherence between level $|1\rangle$ and level $|2\rangle$ are neglected.

5.2 Linear and nonlinear susceptibilities

It is required to obtain the steady-state solution of the density matrix equations in Eqs. (5.2)–(5.16) in order to derive the linear and nonlinear susceptibilities $\chi^{(1)}$ and $\chi^{(3)}$. Assuming that the coupling fields Ω_c, Ω_s, Ω_d are much stronger than the probe field Ω_p and applying the perturbation approach (Eq. (2.109)) the zeroth order solution is $\rho_{11}^{(0)} = 1$, while other elements are equal to zero. Then under the weak-probe field limit we get the first- and third-order density matrix elements $\rho_{31}^{(1)}$ and $\rho_{31}^{(3)}$

$$\rho_{31}^{(1)} = -i\Omega_p B_3(B_4B_2 + \Omega_s^2)/W, \tag{5.17}$$

$$\begin{aligned}\rho_{31}^{(3)} = -i\Omega_p B_3(B_2B_4 + \Omega_s^2)(\rho_{11}^{(2)} - \rho_{33}^{(2)})/W - iB_3\Omega_p\Omega_c\Omega_s\rho_{53}^{(2)}/W \\ -\Omega_p\Omega_d(B_2B_4 + \Omega_s^2)\rho_{23}^{(2)}/W,\end{aligned} \tag{5.18}$$

with

$$W = B_1B_2B_3B_4 + B_2B_4\Omega_d^2 + B_3B_4\Omega_c^2 + B_1B_3\Omega_s^2 + \Omega_d^2\Omega_s^2, \tag{5.19}$$

$$\begin{aligned}B_1 &= i\Delta_p + \tfrac{\gamma_{31}+\gamma_{32}}{2}, \\ B_2 &= i(\Delta_p + \Delta_c) + \tfrac{\gamma_{43}}{2}, \\ B_3 &= i(\Delta_p - \Delta_d), \\ B_4 &= i(\Delta_d + \Delta_c + \Delta_s) + \tfrac{\gamma_{51}+\gamma_{52}+\gamma_{54}}{2}.\end{aligned} \tag{5.20}$$

Having obtained the first- and third-order density matrix elements $\rho_{31}^{(1)}$ and $\rho_{31}^{(3)}$, the linear and nonlinear susceptibilities $\chi^{(1)}$ and $\chi^{(3)}$ can be determined by

$$\chi^{(1)} = \frac{2N\wp_{13}^2}{\epsilon_0\hbar\Omega_p}\rho_{31}^{(1)}, \tag{5.21}$$

$$\chi^{(3)} = \frac{2N\wp_{13}^4}{3\epsilon_0\hbar^3\Omega_p^3}\rho_{31}^{(3)}, \tag{5.22}$$

where $\wp_{13}$ is the transition dipole moment between $|3\rangle$ and $|1\rangle$.

As the real and the imaginary parts of $\chi^{(3)}$ ($\chi^{(1)}$) correspond to the nonlinear (linear) dispersion and absorption, respectively, one can control the nonlinear (linear) response of the medium by properly adjusting the system parameteres. In what follows, we investigate the linear and nonlinear optical characteristics of the five-level double ladder-type atom-light coupling scheme through equations (5.21) and (5.22). Note that in all simulations for the first- and third-order susceptibilities, the curves are plotted in the units of $\frac{2N\wp_{13}^2}{\epsilon_0\hbar\Omega_p}$ and $\frac{2N\wp_{13}^4}{3\epsilon_0\hbar^3\Omega_p^3}$, respectively.

5.3 Dressed-states approach

To understand the physical origin of linear and nonlinear optical effects for the probe field, it is useful to consider the dressed-state approach [Fig. 5.1(b)]. Under the resonance condition and assuming $\Omega_s = \Omega_c = \Omega_d = \Omega$, we obtain the eigenstates by excluding in Eq. (5.1) the ground level $|1\rangle$

$$|\psi_1\rangle = s_1|2\rangle + t_1 s_1|3\rangle + \left(t_1^2 - 1\right) s_1|4\rangle + \left(t_1 - \frac{1}{t_1}\right) s_1|5\rangle, \tag{5.23}$$

$$|\psi_2\rangle = s_3|2\rangle + t_3 s_3|3\rangle + \left(t_3^2 - 1\right) s_3|4\rangle + \left(t_3 - \frac{1}{t_3}\right) s_3|5\rangle, \tag{5.24}$$

$$|\psi_3\rangle = s_4|2\rangle - t_3 s_4|3\rangle + \left(t_3^2 - 1\right) s_4|4\rangle - \left(t_3 - \frac{1}{t_3}\right) s_4|5\rangle, \tag{5.25}$$

$$|\psi_4\rangle = s_2|2\rangle - t_1 s_2|3\rangle + \left(t_1^2 - 1\right) s_2|4\rangle - \left(t_1 - \frac{1}{t_1}\right) s_2|5\rangle, \tag{5.26}$$

with the corresponding eigenenergies

$$e_1 = \Omega\left(\frac{\sqrt{5}}{2}+\frac{3}{2}\right)^{1/2}, \tag{5.27}$$

$$e_2 = \Omega\left(-\frac{\sqrt{5}}{2}+\frac{3}{2}\right)^{1/2}, \tag{5.28}$$

$$e_3 = -\Omega\left(-\frac{\sqrt{5}}{2}+\frac{3}{2}\right)^{1/2} = -e_2, \tag{5.29}$$

$$e_4 = -\Omega\left(\frac{\sqrt{5}}{2}+\frac{3}{2}\right)^{1/2} = -e_1, \tag{5.30}$$

where

$$s_1 = \left(1+t_1^2+(t_1^2-1)^2+(t_1-\frac{1}{t_1})^2\right)^{-1/2}, \tag{5.31}$$

$$s_2 = \left(1-t_1^2+(t_1^2-1)^2-(t_1-\frac{1}{t_1})^2\right)^{-1/2}, \tag{5.32}$$

$$s_3 = \left(1+t_3^2+(t_3^2-1)^2-(t_3-\frac{1}{t_3})^2\right)^{-1/2}, \tag{5.33}$$

$$s_4 = \left(1-t_3^2+(t_3^2-1)^2-(t_3-\frac{1}{t_3})^2\right)^{-1/2}, \tag{5.34}$$

and $t_{1(3)} = e_{1(3)}/\Omega$. The dressed-states representation presented in this section will be used below to elucidate the linear and nonlinear optical properties of the medium for the weak probe field.

5.4 Absorptive-dispersive optical characteristics

To trace the linear optical properties of the medium one has to investigate the first order linear susceptibility of the medium featured in Eq. (5.21). Figure 5.2 illustrates typical linear probe absorption ($\mathrm{Im}(\chi^{(1)})$) and dispersion ($\mathrm{Re}(\chi^{(1)})$) spectra against probe field detuning Δ_p. Note that for simplicity in all numerical results we take $\gamma_{32} = \gamma_{31} = \gamma_{51} = \gamma_{52} = \gamma_{54} = \gamma_{43} = \gamma$, and all the parameters are scaled with dimensionless parameter γ.

First we consider the case in which the control field is absent (i.e., $\Omega_d = 0$). In this situation the medium reduces to a four-level ladder-type system [12] involving four atomic levels $|1\rangle$, $|3\rangle$, $|4\rangle$ and $|5\rangle$. As can be seen in Fig. 5.2(a), three absorption peaks appear with a low transmission at resonance which pertains to double dark resonances [12]. In this case, the superluminal light propagates through the three anomalous dispersive windows accompanied by noticeable absorption. When the control field Ω_d is introduced on the transition $|2\rangle \leftrightarrow |3\rangle$ satisfying $\Omega_d = \Omega_c = \Omega_s = 3\gamma$, the central absorption peak is split into doublet so that four absorption peaks occur (Fig. 5.2(b)). Hence, the medium switches to the transparency on resonance. Subsequently, subluminality takes place at zero probe detuning instead of superluminality. The corresponding dressed-state representation is that the bare states $|2\rangle$, $|3\rangle$, $|4\rangle$ and $|5\rangle$ form dressed-states $|\psi_i\rangle$ ($i = 1, 2, 3, 4$) (see equations (5.23)–(5.30)). The four absorption peaks appear as a result of the interactions between the ground state $|1\rangle$ with one of the four dressed states (through the pathways $|1\rangle \overset{\Omega_p}{\rightarrow} |\psi_1\rangle$, $|1\rangle \overset{\Omega_p}{\rightarrow} |\psi_2\rangle$, $|1\rangle \overset{\Omega_p}{\rightarrow} |\psi_3\rangle$ and $|1\rangle \overset{\Omega_p}{\rightarrow} |\psi_4\rangle$ as can be seen in Fig. 5.1(b)).

5.5 Linear pulse propagation

It was shown in the previous section that the absorption of probe field on resonance can be efficiently eliminated through the effect of control field Ω_d. This feature may be used to realize an optical switch where a laser field controls absorption of another laser field. In this section we present numerical results by solving Maxwell-Bloch equations to describe such an optical switching in terms of a Gaussian intensity profile of the probe field.

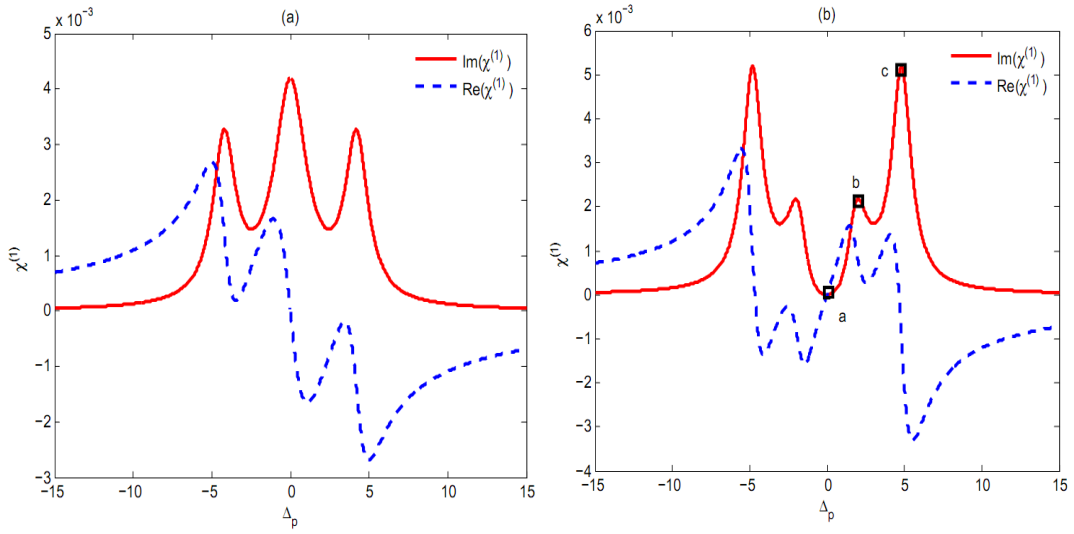

Figure 5.2: (a) Linear and (b) nonlinear susceptibility versus probe field detuning Δ_p for (a) $\Omega_d = 0$, (b) $\Omega_d = 3\gamma$. The selected parameters are $\gamma_{32} = \gamma_{31} = \gamma_{51} = \gamma_{52} = \gamma_{54} = \gamma_{43} = \gamma$, $\Omega_p = 0.01\gamma$, $\Omega_s = \Omega_d = 3\gamma$ and $\Delta_s = \Delta_c = \Delta_d = 0$.

We study the linear propagation of probe field through the medium. The Maxwell wave equation in the slowly varying envelope approximation is required along the propagating direction of $\hat{z}$ (see Eq. (2.128))

$$\frac{\partial \Omega_p(z,t)}{\partial z} + \frac{1}{c}\frac{\partial \Omega_p(z,t)}{\partial t} = i\beta\rho_{31}^{(1)}(z,t), \tag{5.35}$$

where $\beta = \frac{2N\omega_p|\wp_{13}|^2}{\hbar c}$ is the propagation constant. We use the retarded coordinates where $\zeta = z$ and $\tau = t - z/c$. Let us consider propagation of a Gaussian-shaped probe pulse of the form

$$\Omega_p(0,\tau) = \Omega_p^0 e^{-[(\tau-\tau_0)/\sigma]^2},$$

where Ω_p^0 is a real constant characterizing the maximal value of the Rabi frequency before the pulse enters the medium, σ denotes the temporal width of the input pulse and τ_0 gives the peaks location. Figure 5.3 shows the propagation of a Gaussian pulse through the medium. Obviously, when Ω_d is not switched on, the weak probe pulse propagates with significant absorption and broadening inside the medium (Fig. 5.3(a)). As the control field is switched on satisfying $\Omega_d = \Omega_c = \Omega_s = 3\gamma$, the output pulse remains equally intense as that of the input pulse which is due to the transparency generated by the control field Ω_d

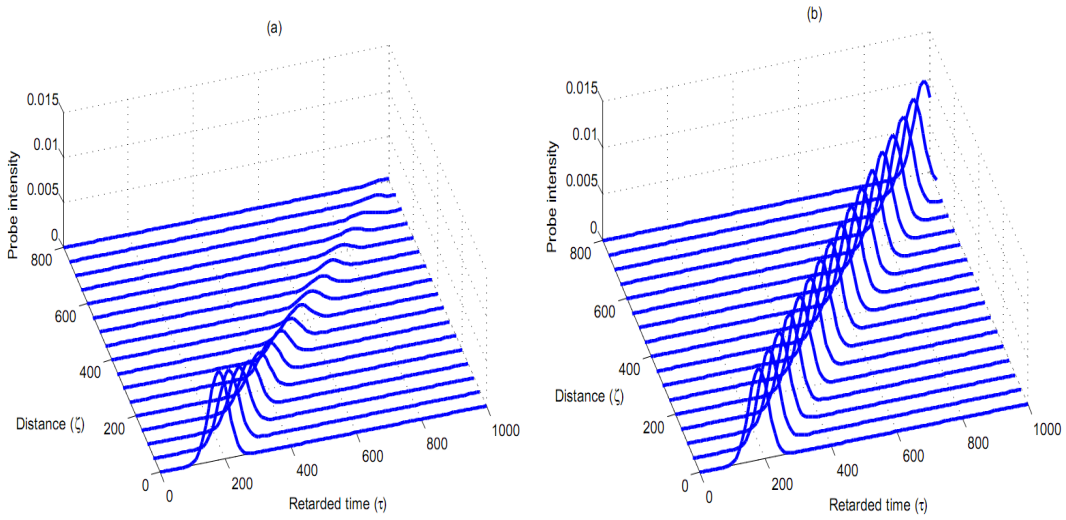

Figure 5.3: Plots of probe field intensity in the medium against retarded time and distance for $\sigma = 30/\gamma$, $\tau_0 = 180/\gamma$ and (a) $\Omega_d = 0$, (b) $\Omega_d = 3\gamma$. Here, $\Delta_p = 0$, and the other parameters are the same as Fig. 5.2.

(Fig. 5.3(b)). Obviously, the medium works as an optical switch where the propagation of the weak probe field can be fully controlled by another coupling field of larger intensity.

We observed in Fig. 5.2(b) that the absorption of the system for the probe field is gradually increased by going out of resonance ($\mathrm{Im}(\chi^{(1)})|_c > \mathrm{Im}(\chi^{(1)})|_b > \mathrm{Im}(\chi^{(1)})|_a$). In terms of the propagation of the Gaussian-shaped probe pulse, it can be seen from Fig. 5.4 that there is overall broadening and loss of intensity when increasing the value of the probe detuning. The probe pulse is attenuated in shorter characteristic propagation distances as Δ_p increases further to the larger values.

5.6 Giant Kerr nonlinearity for the double-ladder model

Now, we study numerically the third-order susceptibility behavior of the five-level double-ladder type atomic system. The selected parameters are $\gamma_{32} = \gamma_{31} = \gamma$, $\gamma_{51} = \gamma_{52} = \gamma_{54} = 0.02\gamma$ and $\gamma_{43} = 0.13\gamma$, while all the parameters are scaled with the dimensionless parameter γ.

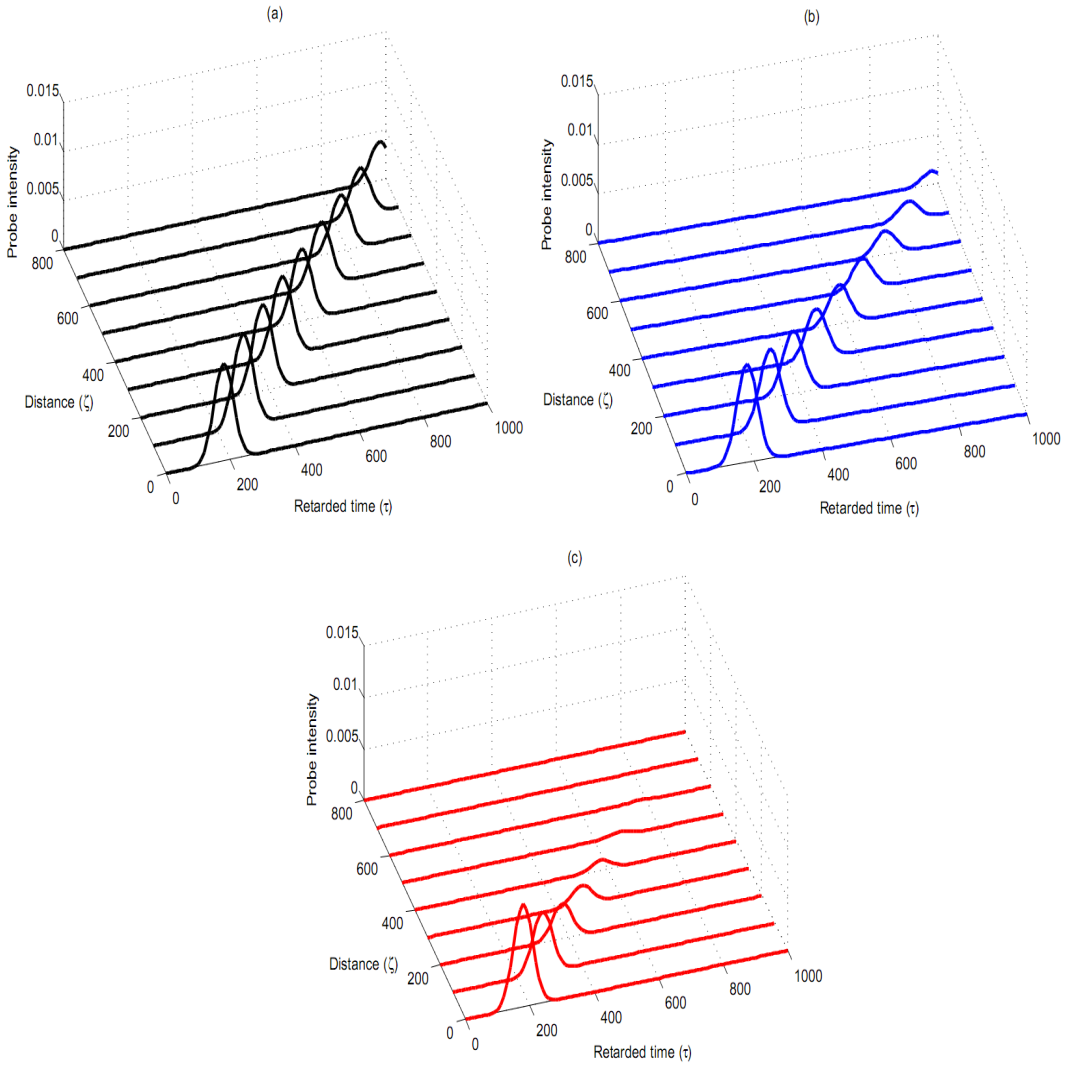

Figure 5.4: Plots of probe field intensity in the medium against retarded time and distance for (a) $\Delta_p = \gamma$, (b) $\Delta_p = 2\gamma$, and (c) $\Delta_p = 5\gamma$. The other parameters are the same as Fig. 5.2.

As shown in Eqs. (5.17)–(5.22), the linear and nonlinear susceptibilities depend on the system parameters such as the intensity and frequency detuning of coupling fields. This enables us to investigate the influence of system parameters on the nonlinear response of the medium and explore the possible giant Kerr nonlinearity along with negligible absorption for the weak probe field.

As known, EIT can suppress the absorption of the medium through destructive quantum interference in an absorbing medium. Here, we show that suppression of the probe absorption can be effectively used through the coherent field Ω_d to enhance the Kerr nonlinearity in the proposed five-level medium.

As illustrated in Fig. 5.5(a), for $\Omega_d = 0.1\gamma$ and when the applied fields are in resonance with the corresponding atomic transitions (i.e., $\Delta_d = \Delta_c = \Delta_s = 0$), although the medium experiences four linear absorption peaks (dashed line), yet the two central absorption peaks are not well seperated, and hence, the medium experiences strong linear absorption at $\Delta_p = 0$. Figure. 5.5(b) illustrates that the magnitude of the Kerr nonlinearity (dashed line) is about 0.4×10^{-4} at line center. In this situation the medium is not suitable for the application of low-intensity nonlinear optics due to field losses [20]. Setting Ω_d to 3γ the separation between two central absorption peaks increases (see solid line in Fig. 5.5(a)) making the medium transparent at zero probe field detuning. Note that the emergence of four absorption peaks can be underestood by means of the dressed-state analysis given in equations (5.23)–(5.30). As shown in in Fig. 5.5(b), the magnitude of the Kerr index enhances simultaneously and reaches to about 0.8×10^{-4} resulting in an enhancement of Kerr nonlinearity on resonance of the probe field, i.e., $\Delta_p = 0$. This is an important feature, for instance, in generation of stable optical solitons where the distortionless propagation of the probe pulse is possible via an enhanced Kerr nonlinearity.

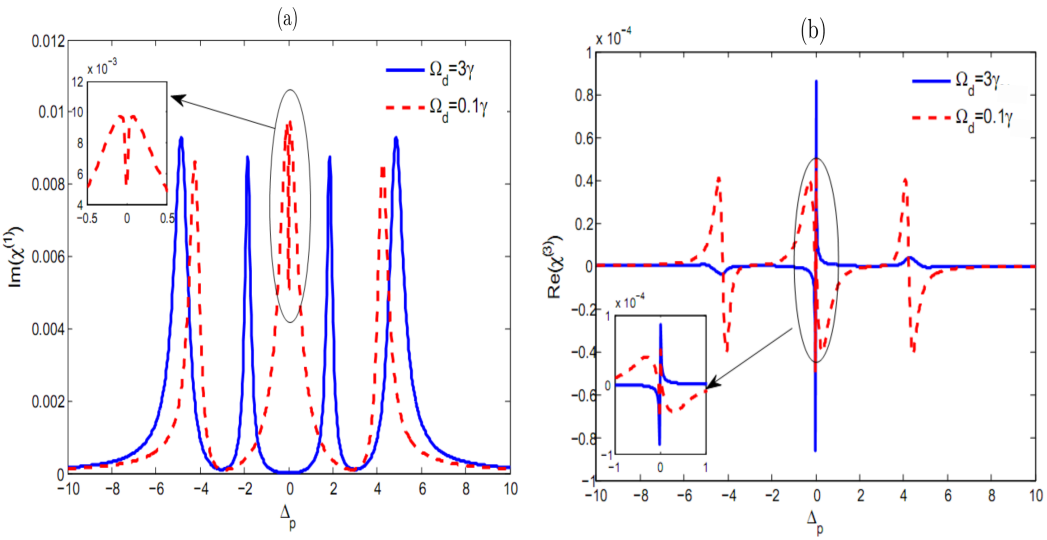

Figure 5.5: (a) Linear absorption and (b) nonlinear dispersion as functions of probe detuning Δ_p for $\Omega_d = 0.1\gamma$ (dashed line) and $\Omega_d = 3\gamma$ (solid line). Selected parameters are $\Omega_p = 0.01\gamma$,$\Omega_c = \Omega_s = 3\gamma$, $\gamma_{32} = \gamma_{31} = \gamma$, $\gamma_{51} = \gamma_{52} = \gamma_{54} = 0.02\gamma$and $\gamma_{43} = 0.13\gamma$, and $\Delta_d = \Delta_c = \Delta_s = 0$.

Chapter 6

Electromagnetically induced transparency and nonlinear pulse propagation

In this chapter, we consider propagation of a probe pulse in an atomic medium characterized by a combined tripod and Lambda (Λ) clossed-loop atom-light coupling scheme. Closed-loop quantum configurations [149, 43, 42, 150, 151, 152] represent a class of atom-light coupling schemes in which the driving fields acting on atoms build closed paths for the transitions between atomic levels. The interference between different paths makes the system sensitive to relative phases of the applied fields. In our proposal illustrated in Fig. 6.1, the atom-light coupling represents a five-level combined Lambda-tripod scheme, in which three atomic ground states are coupled to two excited states by four control and one probe laser fields. In other words, the scheme involves four atomic levels coupled between each other by four control fields and interacting with a ground level through a weak probe field. It is demonstrated that dark states can be formed for such an atom-light coupling. This is essential for formation of the electromagnetically induced transparency (EIT) and slow light. In the limiting cases the scheme reduces to conventional Λ- or N-type atom-light couplings providing the EIT or absorption, respectively. Thus the atomic system can experience a transition from the EIT to the absorption by changing the amplitudes or phases of control lasers. Subsequently the scheme is employed to analyze the nonlinear pulse propagation using the coupled Maxwell-Bloch equations. It is shown that generation of stable slow light optical solitons is possible in such a five-level combined tripod and Λ atomic system.

6.1 Formulation and theoretical background

6.1.1 The system

Let us consider a probe pulse described by a Rabi frequency Ω_p. Additional laser fields described by Rabi frequencies Ω_1, Ω_2, Ω_3 and Ω_4 control propagation of the probe pulse. The probe and the control fields are assumed to co-propagate along the z direction. We shall analyze the light-matter interaction in an ensemble of atoms using a five-level Lambda-tripod scheme shown in Fig. 6.1. The atoms are characterized by three ground levels $|a\rangle$, $|c\rangle$ and $|d\rangle$, as well as two excited states $|b\rangle$ and $|e\rangle$. Four coherent control fields with the Rabi frequencies Ω_1, Ω_2, Ω_3 and Ω_4 induce dipole-allowed transitions $|b\rangle \longleftrightarrow |c\rangle$, $|b\rangle \longleftrightarrow |d\rangle$, $|e\rangle \longleftrightarrow |c\rangle$, and $|e\rangle \longleftrightarrow |d\rangle$, respectively. As a result, the control fields couple two excited states $|b\rangle$ and $|e\rangle$ via two different pathways $|b\rangle \overset{\Omega_1^*}{\rightarrow} |c\rangle \overset{\Omega_3}{\rightarrow} |e\rangle$ and $|b\rangle \overset{\Omega_2^*}{\rightarrow} |d\rangle \overset{\Omega_4}{\rightarrow} |e\rangle$ making a four level closed-loop coherent coupling scheme described by the Hamiltonian ($\hbar = 1$)

$$H_{4\text{Levels}} = -\Omega_1^*|c\rangle\langle b| - \Omega_2^*|d\rangle\langle b| - \Omega_3^*|c\rangle\langle e| - \Omega_4^*|d\rangle\langle e| + \text{H.c.}\,. \tag{6.1}$$

Furthermore, the tunable probe field with the Rabi frequency Ω_p induces a dipole-allowed optical transition $|a\rangle \longleftrightarrow |b\rangle$. The total Hamiltonian of the system involving all five atomic levels of the combined Λ and tripod level scheme is given by

$$H_{5\text{Levels}} = -\left(\Omega_p^*|a\rangle\langle b| + \Omega_p|b\rangle\langle a|\right) + H_{4\text{Levels}}\,. \tag{6.2}$$

Note that the complex Rabi frequencies of the four control fields can be written as $\Omega_j = |\Omega_j|\mathrm{e}^{i\phi_i}$, with $j = 1, 2, 3, 4$, where $|\Omega_j|$ and ϕ_j are the amplitude and phase of each applied field. As it will be explored below, in this scheme the destructive interference between different transition pathways induced by the the control and probe beams can make the medium transparent for the resonant probe beams in a narrow frequency range due to the EIT. We define $\phi = (\phi_1 - \phi_2) - (\phi_3 - \phi_4)$ to be a relative phase among the four control fields forming a closed-loop coherent coupling. By changing ϕ, one can substantially modify the transparency and absorption properties for the probe field in such a Lambda-tripod scheme.

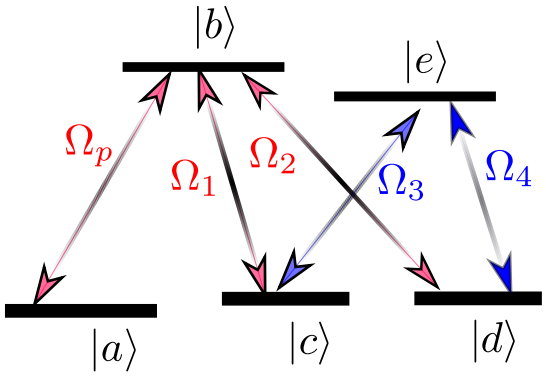

Figure 6.1: Schematic diagram of the five-level Lambda-tripod quantum system.

6.1.2 Equations of motion

The dynamics of the probe field propagating through the atomic medium is described by the Maxwell-Bloch equations. To the first-order of Ω_p the equations have the form

$$\dot{\rho}_{ba}^{(1)} = d_1\rho_{ba}^{(1)} + i\Omega_1\rho_{ca}^{(1)} + i\Omega_2\rho_{da}^{(1)} + i\Omega_p, \tag{6.3}$$

$$\dot{\rho}_{ca}^{(1)} = d_2\rho_{ca}^{(1)} + i\Omega_1^*\rho_{ba}^{(1)} + i\Omega_3^*\rho_{ea}^{(1)}, \tag{6.4}$$

$$\dot{\rho}_{da}^{(1)} = d_2\rho_{da}^{(1)} + i\Omega_2^*\rho_{ba}^{(1)} + i\Omega_4^*\rho_{ea}^{(1)}, \tag{6.5}$$

$$\dot{\rho}_{ea}^{(1)} = d_3\rho_{ea}^{(1)} + i\Omega_3\rho_{ca}^{(1)} + i\Omega_4\rho_{da}^{(1)}, \tag{6.6}$$

and

$$\frac{\partial\Omega_p}{\partial z} + c^{-1}\frac{\partial\Omega_p}{\partial t} = i\eta\rho_{ba}^{(1)}, \quad \text{with} \quad \eta = \frac{2N\omega_p|\wp_{ba}|^2}{\hbar c}, \tag{6.7}$$

where $\rho_{u,v}^{(1)}$ are the first-order matrix elements of the density materix operator $\rho = \sum|u\rangle\rho_{uv}\langle v|$. The optical Bloch equations (6.3)–(6.6) imply the probe field to be much weaker than the control ones. In that case most atomic population is in the ground state $|a\rangle$, and one can treat the probe field as a perturbation. Therefore, we can apply the perturbation expansion $\rho_{ij} = \Sigma_k\rho_{ij}^{(k)}$, where $\rho_{ij}^{(k)}$ represents the kth order part of ρ_{ij} in terms of probe field Ω_p. Since $\Omega_p \ll \Omega_i$ $(i = 1, 2, 3, 4)$, the zeroth-order solution is $\rho_{aa}^{(0)} = 1$, while other elements being zero ($\rho_{bb}^{(0)} = \rho_{cc}^{(0)} = \rho_{dd}^{(0)} = \rho_{ee}^{(0)} = 0$). All fast-oscillating exponential factors associated with central frequencies and wave vectors have been eliminated from the equations, and only the slowly-varying amplitudes are retained.

The wave equation (6.7) describes propagation of the probe field Ω_p influenced by the atomic medium, where $\wp_{ba}$ is an electric dipole matrix element corresponding to the transition $|b\rangle \longleftrightarrow |a\rangle$, N is the atomic density and ω_p is the frequency of the probe field. The density matrix equations (6.3)–(6.6) describe the evolution of the atomic system affected by the control and probe fields. They follow from the general quantum Liouville equation for the density matrix operator [18]

$$\dot{\rho} = -\frac{i}{\hbar}[H_{5\text{Levels}}, \rho] + L_\rho, \tag{6.8}$$

where the damping operator L_ρ describes the decay of the system described by parameters $d_1 = -\Gamma_b/2 + i\Delta_p$, $d_2 = i(\Delta_p - \Delta_2)$ and $d_3 = -\Gamma_e/2 + i(\Delta_p + \Delta_3 - \Delta_2)$ in Eqs. (6.3)–(6.6). We have defined the detunings as: $\Delta_2 = \Delta_{bc} = \Delta_{bd}$, and $\Delta_3 = \Delta_{ec} = \Delta_{ed}$, with $\Delta_{bc} = \omega_1 - \omega_{bc}$, $\Delta_{bd} = \omega_2 - \omega_{bd}$, $\Delta_{ec} = \omega_3 - \omega_{ec}$, $\Delta_{ed} = \omega_4 - \omega_{ed}$, and $\Delta_p = \omega_p - \omega_{ba}$, where ω_i is a central frequency of the corresponding control field. Two excited states $|b\rangle$ and $|e\rangle$ decay with rates Γ_b and Γ_e, respectively.

6.1.3 Transition to a new basis

The Hamiltonian for the atomic four-level subsystem (6.1) can be represented as

$$H_{4\text{Levels}} = -\beta|D_e\rangle\langle b| - \alpha|B_e\rangle\langle b| - \Omega|B_e\rangle\langle e| + \text{H.c.}, \tag{6.9}$$

where

$$|D_e\rangle = \frac{1}{\Omega}\left(\Omega_4|c\rangle - \Omega_3|d\rangle\right), \tag{6.10}$$

$$|B_e\rangle = \frac{1}{\Omega}\left(\Omega_3^*|c\rangle + \Omega_4^*|d\rangle\right), \tag{6.11}$$

are the internal dark and bright states for the Λ-scheme made of the two ground states states $|c\rangle$ and $|d\rangle$, as well as an excited states $|e\rangle$. One can also introduce another set of dark and bright states corresponding to the Λ-scheme made of the same pair of ground states states $|c\rangle$ and $|d\rangle$, yet a different excited state

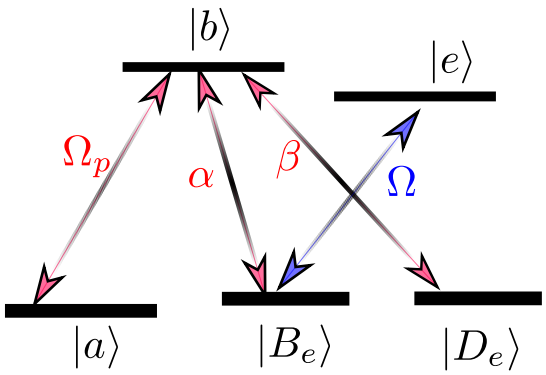

Figure 6.2: Five-level quantum system in the transformed basis for $\beta \neq 0$ and $\alpha \neq 0$.

$|b\rangle$:

$$|D_b\rangle = \frac{1}{\Omega}\left(\Omega_2|c\rangle - \Omega_1|d\rangle\right), \tag{6.12}$$

$$|B_b\rangle = \frac{1}{\Omega}\left(\Omega_1^*|c\rangle + \Omega_2^*|d\rangle\right). \tag{6.13}$$

In writing Eq. (6.9), the coefficient

$$\beta = \langle D_b|B_e\rangle = \langle D_e|B_d\rangle = \frac{1}{\Omega}(\Omega_1^*\Omega_4^* - \Omega_2^*\Omega_3^*) \tag{6.14}$$

represents the quantum inteference between the four control fields playing the main role in tuning dispersion and absorption properties in the combined tripod and Λ scheme. In addition, we define

$$\alpha = \langle D_b|D_e\rangle = \langle B_e|B_d\rangle = \frac{1}{\Omega}(\Omega_1^*\Omega_3 + \Omega_2^*\Omega_4) \tag{6.15}$$

and the total Rabi frequency

$$\Omega = \sqrt{|\Omega_3|^2 + |\Omega_4|^2}\,. \tag{6.16}$$

By changing the quantum interference coefficient β and the coefficient α one arrives at three different situations. For each of them we shall plot the level schemes in the basis involving the transformed states $|B_e\rangle$ and $|D_e\rangle$.

6.1.3.1 Situation (a): $\beta \neq 0$ and $\alpha \neq 0$

In the case when both coefficients α and β are nonzero, the five-level tripod and Λ scheme shown in Fig. 6.2 looks similar to the original scheme (Fig. 6.1) in the transformed basis, but the coupling between the states $|D_e\rangle$ and $|e\rangle$ is missing. The coefficient β is nonzero when $\Omega_1\Omega_4 \neq \Omega_2\Omega_3$. The condition $\beta \neq 0$ is valid provided $|\Omega_1||\Omega_4| \neq |\Omega_2||\Omega_3|$ and phase ϕ is arbitrary, or $|\Omega_1||\Omega_4| = |\Omega_2||\Omega_3|$ with $\phi \neq 0$.

When both α and β are nonzero, one can define a global dark state $|D\rangle$ for the whole atom-light coupling scheme

$$|D\rangle = \beta|a\rangle - \Omega_p|D_e\rangle\,. \tag{6.17}$$

The dark state is an eigenstate of the full atom-light Hamiltonian with a zero eigen-energy: $H_{5\text{Levels}}|D\rangle = 0$. The state $|D\rangle$ has no contribution by the ground state superpositon $|B_e\rangle$, as well as no contribution by the bare excited states $|e\rangle$ and $|b\rangle$. As a result, there is no transition from the state $|D\rangle$ to the excited states $|e\rangle$ and $|b\rangle$, making the five-level closed-loop scheme transparent to the electromagnetic field. This is a new mechanism for EIT transparency compared with the Λ [7, 8], tripod [14, 25, 41], or double tripod schemes [42, 29].

It is known that the real and imaginary parts of $\rho_{ba}^{(1)}$ correspond to the probe dispersion and absorption, respectively. A steady-state solution to the density matrix element $\rho_{ba}^{(1)}$ reads under the resonance condition $\Delta_2 = \Delta_3 = 0$

$$\begin{aligned}\rho_{ba}^{(1)} = \Omega_p\Delta_p \Bigg(|\Omega_3|^2 + |\Omega_4|^2 + i\Delta_p\left(-\frac{\Gamma_e}{2} + i\Delta_p\right)\Bigg) \\ \times \Bigg[\beta^2\Omega^2 + i\Delta_p\left(-\frac{\Gamma_e}{2} + i\Delta_p\right)(|\Omega_1|^2 + |\Omega_2|^2) \\ + i\Delta_p\left(-\frac{\Gamma_b}{2} + i\Delta_p\right)\left(|\Omega_3|^2 + |\Omega_4|^2 + i\Delta_p\left(-\frac{\Gamma_e}{2} + i\Delta_p\right)\right)\Bigg]^{-1},\end{aligned} \tag{6.18}$$

where the interference term β is involved.

A denominator of Eq. (6.18) represents the fourth order polynomial which contains zero points at four different detunings Δ_p of the probe field from the EIT resonance. This provides four maxima in the absorption profile of the system, as one can see in Fig. 6.5(a). Furthermore the EIT window is formed for zero

detuning. In Appendix A we have presented eigenstates and the corresponding eigenvalues of the Hamiltonian (6.9) describing the four-level subsystem. One can see that all four eigenstates $|n_i\rangle$ characterzed by the eigenvalues λ_i contain contributions due to the excited state $|b\rangle$. This results in four peaks in absorption profile of the system.

6.1.3.2 Situation (b): $\beta = 0$ and $\alpha \neq 0$

The condition $\beta = 0$ is fulfilled if $\Omega_1\Omega_4 = \Omega_2\Omega_3$, or equivalently $|\Omega_2||\Omega_3| = |\Omega_1||\Omega_4|$ and $\phi = 0$. In that case the state $|D_e\rangle$ is not involved, so the interaction Hamiltonian Eq. (6.9) for the four-level subsystem can be rewritten as

$$H_{4\text{Levels}} = -\alpha|B_e\rangle\langle b| - \Omega|B_e\rangle\langle e| + \text{H.c.}\,. \tag{6.19}$$

Consequently the five-level tripod and Λ scheme becomes equivalent to a conventional N-type atomic system [15, 98] shown in Fig. 6.3.

Since the quantum interference term β vanishes, Eq. (6.18) simplifies to

$$\begin{aligned}\rho_{ba}^{(1)} = \Omega_p \Bigg(|\Omega_3|^2 + |\Omega_4|^2 + i\Delta_p \left(-\frac{\Gamma_e}{2} + i\Delta_p\right)\Bigg) \\ \times \Bigg[i\left(-\frac{\Gamma_e}{2} + i\Delta_p\right)(|\Omega_1|^2 + |\Omega_2|^2) \\ + i\left(-\frac{\Gamma_b}{2} + i\Delta_p\right)\left(|\Omega_3|^2 + |\Omega_4|^2 + i\Delta_p\left(-\frac{\Gamma_e}{2} + i\Delta_p\right)\right)\Bigg]^{-1}.\end{aligned} \tag{6.20}$$

The denominator of $\rho_{ba}^{(1)}$ in Eq. (6.20) is now a cubic polynomial, providing three absorption maxima. The eigenstates and eigenvalues corresponding to this situation are presented in Appendix B. The eigenvector $|n_2\rangle$ characterized by a zero eigen-energy coincides with the dark state $|D_e\rangle$ and is decoupled from the radiation fields. Only the remaining three eigenvectors $|n_1\rangle$, $|n_3\rangle$ and $|n_4\rangle$ contain the contribution due to an excited state $|b\rangle$. This leads to three absorption peaks displayed in Fig. 6.5(b). In this way, the absence of quantum interference term β between the control fields destroys one of the peaks in the absorption profile leading to three absorption maxima.

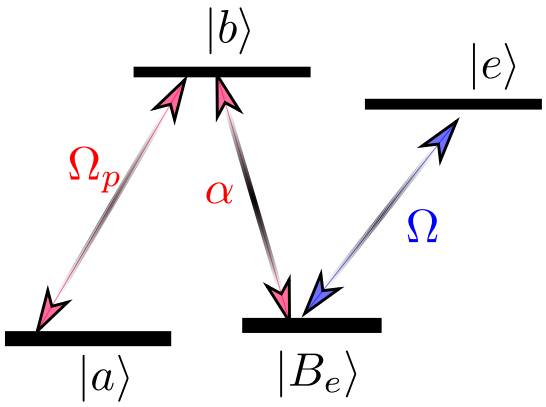

Figure 6.3: The level scheme in the transformed basis for $\beta = 0$ and $\alpha \neq 0$. The ground state superposition $|D_e\rangle$ (now shown in the figure) is decoupled from the remaining four states.

6.1.3.3 Situation (c): $\beta \neq 0$ and $\alpha = 0$

When the coefficient β is nonzero but the coefficient α is zero, the interaction Hamiltonian (6.9) can be represented as

$$H_{\text{4Levels}} = -\beta|D_e\rangle\langle b| - \Omega|B_e\rangle\langle e| + \text{H.c.}\,. \tag{6.21}$$

As illustrated in Fig. 6.4, the five-level tripod and Λ scheme is then equivalent to a conventional Λ-type atomic system [7, 19] which is decoupled from the two-level system involving the states $|B_e\rangle$ and $|e\rangle$.

In the following we consider a symmetric case where $|\Omega_1| = |\Omega_2|$, $|\Omega_3| = |\Omega_4|$ and $\phi = \pi$. In such a situation the conditions $\beta \neq 0$ and $\alpha = 0$ are fulfilled, with $\beta^2 = 2|\Omega_1^2|$. Equation (6.18) for $\rho_{ba}^{(1)}$ then is simplifies considerably, giving

$$\rho_{ba}^{(1)} = \Omega_p \frac{\Delta_p}{|\beta|^2 + i\Delta_p\left(-\frac{\Gamma_b}{2} + i\Delta_p\right)}\,. \tag{6.22}$$

Obviously, the polynominal in denominator becomes quadratic in Δ_p resulting in two absorption peaks or a single EIT window, which is a characteristic feature of the Λ scheme (Fig. 6.5(c)). Furthermore, the probe absorption and dispersion do not dependent on Ω, only β contributes to the optical properties. This is

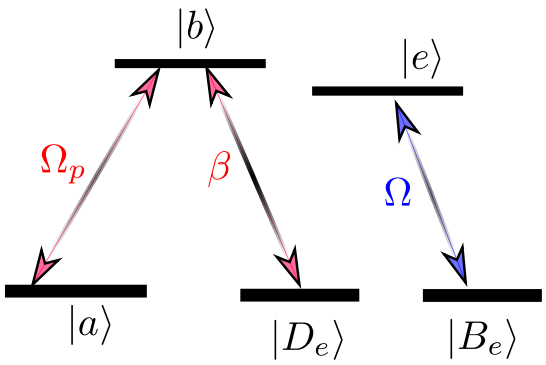

Figure 6.4: Schematic diagram of the five-level quantum system associated with situation (c).

because the Λ-type scheme is now decoupled from the transition $|B_e\rangle \xrightarrow{\Omega} |e\rangle$, and the system behaves as a three-level Λ-type scheme containing $|a\rangle$, $|b\rangle$, and $|D_e\rangle$ (see also Appendix C).

In the following we summarize our results for the behavior of real and imaginary parts of $\rho_{ba}^{(1)}$ corresponding to the probe dispersion and absorption for different situations (a)–(c) described above. Without a loss of generality, we take $\Gamma_e = \Gamma_b = \gamma$ for all the simulations. The other frequencies are scaled by γ which should be in the order of MHz for cesium (Cs) atoms. Figure 6.5 shows that our model provides a high control of dispersive-absorptive optical properties of the probe field. The absorption profile has four, three and two peaks featured in Figs. 6.5(a)–6.5(c), respectively. There is the resulting change in the sign of the slope of the dispersion at $\Delta_p = 0$ for different situations (a)–(c). This gives rise to switching in the group velocity of the probe pulse from subluminal to superluminal or visa versa. In particular, for the choice of parameters satisfying situation (a) and (c), there is the subluminality accompanied by EIT at line center. On the other hand, the superluminality accompanied by a considerable absorption is observed for the parametric condition satisfying the situation (b).

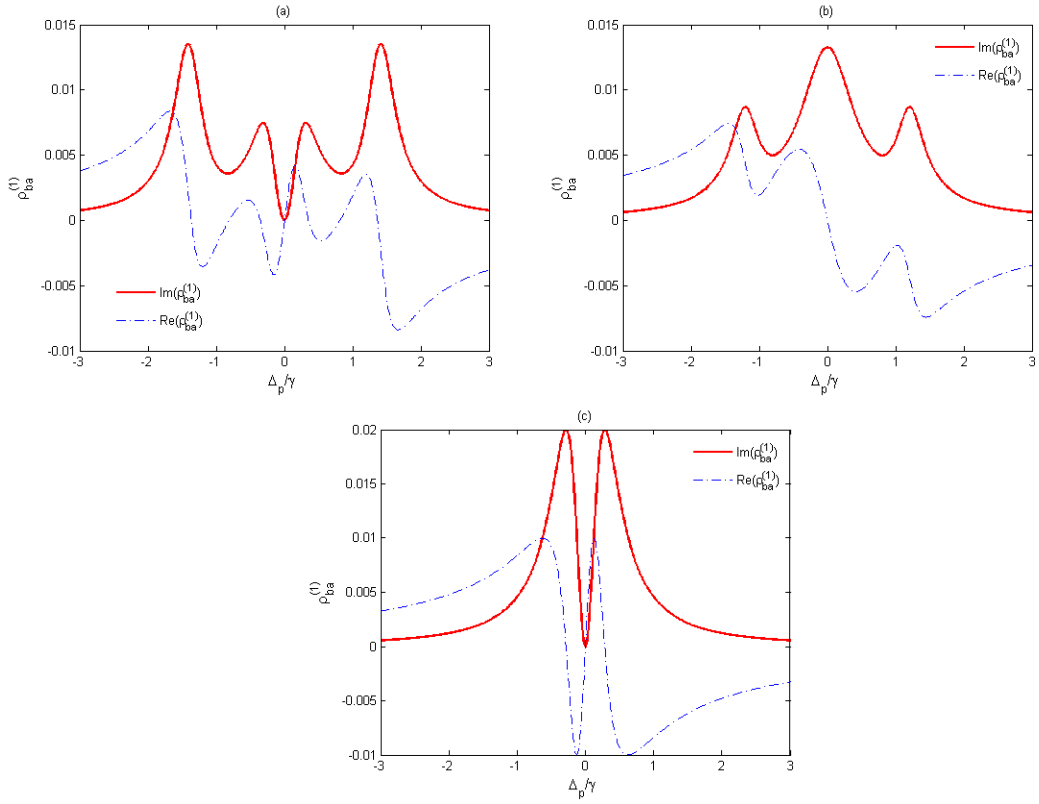

Figure 6.5: Probe absorption ($\mathrm{Im}(\rho_{ba}^{(1)})$) versus Δ_p for (a) $\Omega_1 = 0.9\gamma$, $\Omega_2 = 0.7\gamma$, $\Omega_3 = 0.4\gamma, \Omega_4 = 0.8\gamma$, and $\phi = 0$ corresponding to the first situation, (b) $\Omega_1 = \Omega_2 = 0.5\gamma$, $\Omega_3 = \Omega_4 = 0.7\gamma$ and $\phi = 0$ corresponding to the second situation, and (c) $\Omega_1 = \Omega_2 = 0.2\gamma$, $\Omega_3 = \Omega_4 = 0.1\gamma$ and $\phi = \pi$ corresponding to the third situation. Other parameters are $\Gamma_e = \Gamma_b = \gamma$, $\Delta_2 = \Delta_3 = 0$, and $\Omega_p = 0.01\gamma$. Note that all frequencies are scaled by γ which should be in the order of MHz, like for cesium (Cs) atoms.

6.2 Linear and nonlinear pulse propagation in combined tripod and Λ scheme

In this section we consider propagation of the probe pulse in the proposed tripod and Λ scheme. Performing the time Fourier transform of Eqs. (6.3)–(6.7) one can obtain

$$t_1(\omega)F_{ba} + \Omega_1 F_{ca} + \Omega_2 F_{da} + \Lambda_p = 0, \tag{6.23}$$
$$t_2(\omega)F_{ca} + \Omega_1^* F_{ba} + \Omega_3^* F_{ea} = 0, \tag{6.24}$$
$$t_2(\omega)F_{da} + \Omega_2^* F_{ba} + \Omega_4^* F_{ea} = 0, \tag{6.25}$$
$$t_3(\omega)F_{ea} + \Omega_3 F_{ca} + \Omega_4 F_{da} = 0, \tag{6.26}$$

and

$$\frac{\partial \Lambda_p}{\partial z} - i\frac{\omega}{c}\Lambda_p = i\eta F_{ba}, \tag{6.27}$$

where $t_1(\omega) = \omega + i\Gamma_b/2 + \Delta_p$, $t_2(\omega) = \omega + \Delta_p - \Delta_2$, and $t_3(\omega) = \omega + i\Gamma_e/2 + \Delta_p - \Delta_2 + \Delta_3$. Note that F_{ij} and Λ_p represent the Fourier transforms of $\rho_{ij}^{(1)}$ and Ω_p, respectively, where ω is a deviation from the central frequency.

The solution of Eq. (6.27) is a plane wave of the form

$$\Lambda_p(z,\omega) = \Lambda_p(0,\omega)e^{i\kappa(\omega)z}, \tag{6.28}$$

where

$$\kappa = \frac{\omega}{c} - \frac{\eta S_1(\omega)}{Q(\omega)}, \tag{6.29}$$

describes the linear dispersion relation of the system. Expanding κ in power series around the center frequency of the probe pulse ($\omega = 0$) and taking only the first three terms, we get

$$\kappa = \kappa_0 + \kappa_1\omega + \kappa_2\omega^2, \tag{6.30}$$

where the detailed expressions for the coefficients κ_0, κ_1 and κ_2 are given in Appendix D, while $S_1(\omega)$ and $Q(\omega)$ can be found in Appendix E. In Eq. (6.30), $\kappa_i = \frac{d^j\kappa(\omega)}{d\omega^j}|_{\omega=0}$ with $j = 0, 1, 2$ are the dispersion coefficients in different orders. In general, the real part of $\kappa_0 = \Upsilon + i\chi/2$ defines the phase shift Υ per unit length, while the imaginary part indicates the linear absorption χ of the probe pulse. The group velocity v_g is given by $1/\kappa_1$, whereas the quadratic term κ_2 is associated with the group velocity dispersion which causes the pulse distortion.

In the linear regime, we take an incoming probe pulse to be of the Gausian shape, $\Omega_p(0,t) = \Omega_p^0 e^{-(t/\tau_0)^2}$, with a duration τ_0. The subsequent time evolution is obtained from Eq. (6.28) by carrying out an inverse Fourier transform [54, 100]

$$\Omega_p(z,t) = \frac{\Omega_p^0}{\sqrt{L_z}} \exp\left[i\kappa_0 z - \frac{(t-\kappa_1 z)^2}{L_z\tau_0^2}\right], \tag{6.31}$$

with $L_z = s_1(z) - is_2(z)$, $s_1(z) = 1 + 4z\mathrm{Re}(\kappa_2)/\tau_0^2$ and $s_2(z) = 4z\mathrm{Im}(\kappa_2)/\tau_0^2$. In this way, even if there is no absorption due to EIT ($\mathrm{Im}(\kappa_i) = 0$, $i = 0, 1, 2$), the dispersion effects can contribute to the pulse attenuation and spreading during propagation.

Our goal is to obtain shape preserving optical pulses which can propagate without significant distortion and loss in our medium. The idea is to include the optical Kerr nonlinearity of the probe laser field into the light propagation, and show that the Kerr nonlinear effect can compensate the dispersion effects and result in shape preserving optical pulses. To balance the dispersion effects and optical nonlinearity, in the following a theoretical model is employed based on the coupled Maxwell-Bloch equations for the nonlinear pulse propagation. Following the Ref. [100], we take a trial function

$$\Lambda_p = \tilde{\Lambda}_p e^{i\kappa_0 z}. \tag{6.32}$$

Substituting Eq. (6.32) into wave equation (6.27) and using Eq. (6.30) we get

$$\frac{\partial \Lambda_p}{\partial z} e^{i\kappa_0 z} = i(\kappa_1 \omega + \kappa_2 \omega^2)\Lambda_p e^{i\kappa_0 z}, \tag{6.33}$$

where we have replaced $\tilde{\Lambda}_p$ with Λ_p for the sake of convenience. Here we only keep terms up to the order ω^2 in expanding the dispersion relarion κ_j.

In deriving the linearized wave equation (6.7), the nonlinear polarization due to the optical Kerr nonlinearity of the probe field has been neglected. Now we turn to investigate the nonlinear propagation of light due to the Kerr effect. To incorporate the nonlinear optical terms in the pulse propagation, the right hand side of wave equation (6.7) must be rewritten as $i\eta\rho_{ba}^{(1)} - i\eta\text{Kerr}$. The Kerr nonlinear term has an opposite sign than the linear term $i\eta\rho_{ba}^{(1)}$ and the probe absorption and dispersion are proportional to imaginary and real parts of $\rho_{ba}^{(1)}$, respectively. Consequently a large optical nonlinearity can cancel the dispersion and suppress the absorption of probe field, effectively. The Kerr nonlinear term is given by (see Appendix F)

$$\text{Kerr} = \rho_{ba}^{(1)}(|\rho_{ba}^{(1)}|^2 + |\rho_{ca}^{(1)}|^2 + |\rho_{da}^{(1)}|^2 + |\rho_{ea}^{(1)}|^2). \tag{6.34}$$

As F_{ij} is the Fourier transform of $\rho_{ij}^{(1)}$, the coefficients for $\rho_{ij}^{(1)}$ can be obtained by taking $\omega = 0$ in the coefficients given in Appendix E. Replacing the coefficients for $\rho_{ij}^{(1)}$ in this way into Eq. (6.34) yields

$$\text{Kerr} = \frac{-S_1}{Q|Q|^2}\left(|S_1|^2 + |S_2|^2 + |S_3|^2 + |S_4|^2\right). \tag{6.35}$$

Performing the inverse Fourier transform and using the expression (6.35) for Kerr, we arrive at the nonlinear wave equation for the slowly varing envelope Ω_p

$$-i\left[\frac{\partial}{\partial z} + \kappa_1 \frac{\partial}{\partial t}\right]\Omega_p + \kappa_2 \frac{\partial^2}{\partial t^2}\Omega_p = \Theta e^{-\alpha\zeta}|\Omega_p|^2\Omega_p, \tag{6.36}$$

where $\Theta = -\eta\text{Kerr}$, and

$$\alpha = 2\text{Im}(\kappa_0) = 2\eta\text{Im}\left(\frac{-S_1}{Q}\right), \tag{6.37}$$

Using new coordinates $\zeta = z$ and $\eta = t - z/v_g$, Eq. (6.36) acquires the following form

$$i\frac{\partial}{\partial\zeta}\Omega_p - \kappa_2\frac{\partial^2}{\partial\eta^2}\Omega_p = \Theta e^{-\alpha\zeta}|\Omega_p|^2\Omega_p. \tag{6.38}$$

Equation (6.38) contains generally complex coefficients. However, for suitable set of system parameters, the absorption coefficent α may be very small, i.e., $\chi \simeq 0$, and imaginary parts of coefficients Θ and κ_2 may be made very small in comparison to their real parts, i.e.,

$$\kappa_2 = \kappa_{2r} + i\kappa_{2i} \approx \kappa_{2r}, \tag{6.39}$$

and

$$\Theta = \Theta_r + i\Theta_i \approx \Theta_r\,. \tag{6.40}$$

In this case, Eq. (6.38) can be written as

$$i\frac{\partial}{\partial\zeta}\Omega_p - \kappa_{2r}\frac{\partial^2}{\partial\eta^2}\Omega_p = \Theta_r|\Omega_p|^2\Omega_p. \tag{6.41}$$

This corresponds to the conventional nonlinear Schrodinger equation (NLSE) which governs the nonlinear evolution of probe pulse and allows bright and dark soliton solutions. The nature of the soliton solution is determined by the sign of product $\kappa_{2r}\Theta_r$. A bright soliton is obtained when $\kappa_{2r}\Theta_r > 0$, and is given by

$$\Omega_p = \Omega_{p0}\mathrm{sech}(\eta/\tau)\exp\left(-i\zeta\Theta_r|\Omega_p|^2/2\right)\,. \tag{6.42}$$

When $\kappa_{2r}\Theta_r < 0$, one can obtain the dark solion solution of the form

$$\Omega_p = \Omega_{p0}\tanh(\eta/\tau)\exp\left(-i\zeta\Theta_r|\Omega_p|^2/2\right)\,. \tag{6.43}$$

Note that here, Ω_{p0} represents an amplitude of the probe field and τ is the typical pulse duration (soliton width). They are arbitrary constants subjected

only to the constraint $\Omega_{p0}\tau = \sqrt{|\kappa_{2r}/\Theta_r|}$.

In the following, we explore a possibility for the formation of the shape preserving optical solitons in this combined tripod and Λ scheme for a realistic atomic system and present numeric calculations. The proposed scheme involving the five-level combined tripod and Λ structure can be experimentally implemented using the cesium (Cs) atom vapor. In our proposal, the levels $|c\rangle$, $|d\rangle$ and $|e\rangle$ can correspond to $|6S_{1/2}, F = 3, M_F = +1\rangle$, $|6S_{1/2}, F = 3, M_F = +3\rangle$ and $|6P_{3/2}, F = 2, M_F = +2\rangle$, respectively. In addition, the levels $|b\rangle$ and $|a\rangle$ can correspond to $|6P_{3/2}, F = 4\rangle$ and $|6S_{1/2}, F = 4\rangle$, respectively. The two excited states are assumed to decay with the rates $\Gamma_e = \Gamma_b = \gamma = 2\pi \times 5.2\,\mathrm{MHz}$.

Assuming the parameteric situation (a) described in the previous section, we take $|\Omega_1| = |\Omega_2| = 1.97 \times 10^9\,\mathrm{s}^{-1}$, $|\Omega_3| = 2.3 \times 10^9\,\mathrm{s}^{-1}$, $|\Omega_4| = 16.4 \times 10^7\,\mathrm{s}^{-1}$, $\Delta_2 = 6.4 \times 10^9\,\mathrm{s}^{-1}$, $\Delta_p = 5.9 \times 10^9\,\mathrm{s}^{-1}$ and $\Delta_3 = 82 \times 10^7\,\mathrm{s}^{-1}$. Consequentlhy we obtain $\kappa_0 \approx (3.9 - 0.008i)\,\mathrm{cm}^{-1}$, $\kappa_1 \approx (4.7 - 2.1 \times 10^{-2}i)10^{-9}\,\mathrm{cm}^{-1} \cdot \mathrm{s}$, $\kappa_2 \approx (-8.06 - 3.6 \times 10^{-2}i)10^{-17}\,\mathrm{cm}^{-1} \cdot \mathrm{s}^2$, and $\Theta \approx (3.6 - 1.12 \times 10^{-2}i)10^{-19}\,\mathrm{cm}^{-1} \cdot \mathrm{s}^2$. In this case, the standard nonlinear Schrodinger equation (6.41) with $\kappa_{2r}\Theta_r < 0$ is well characterized, leading to the formation of dark solitons in the proposed system. With this set of parameters, the fundamental soliton has a width and amplitude satisfying $|\Omega_{p0}\tau| = \sqrt{\kappa_{2r}/\Theta_r} \simeq 4.7$. As shown in Fig. 6.6, the dark soliton of this type remains fairly stable during propagation, which is due to the balance between the group-velocity dispersion and Kerr-type optical nonlinearity. According to Eq. (5.9) in Appendix D, the group velocity v_g has a general form $v_g^{-1} = c^{-1} + \eta(-g_1/Q + S_1 g_2/Q^2)$, with all coefficients given in Appendix D. With the above system parameters, one can find $v_g \approx 7 \times 10^{-3}c$, indicating that the soliton propagates with a slow velocity.

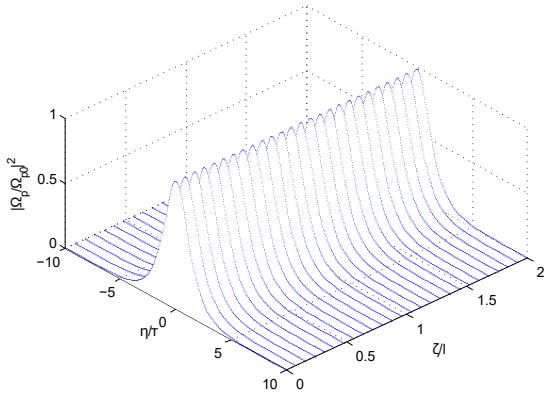

Figure 6.6: Propagation dynamics of an ultraslow optical soliton with $\tau = 10^{-7}\,\mathrm{s}$, $l = 1\,\mathrm{cm}$, and $\eta = 1.0 \times 10^{10}\,\mathrm{cm}^{-1} \cdot \mathrm{s}^{-1}$ and the parameters given in the main text.

Chapter 7

Conclusions and Outlook

1. The Kerr nonlinearity behavior of a five-level KR5 quantum system has been investigated theoretically. It is shown that an enormous Kerr coefficient with reduced absorption can be obtained under the condition of the subluminal light propagation by properly tuning of the applied fields. When the multiphoton resonance condition is established, one can achieve large subluminal Kerr nonlinearities with a negligible absorption in a wide range of relative phases by adjusting the detuning parameters. It is shown that the nonlinear dispersion and absorption of this system involving the closed-loop atomic transitions are strongly susceptible to the relative phase of the applied fields. An analytical model is presented to elucidate such phase control of the Kerr nonlinearity. We made a comparison between the nonlinear Kerr coefficients for the five-level KR5 scheme with that of the existing three- and four-level cascade-type systems. We found that the magnitude of Kerr nonlinearity is larger than that of the three- and four-level counterparts. This means that increasing the number of levels can lead the higher orders of nonlinearity. Finally, the influence of the Doppler broadening on linear and nonlinear susceptibilities was discussed.

2. We have proposed a scheme of high-precision 2D and 3D atom localization in a five-level atom-light coupling configuration. A pair of atomic internal states are coupled to another pair of states via four strong laser components in all possible pathways in a closed loop (ring coupling) configuration of the atom-light coupling. We considered situations where one or more radiation field is position-dependent, so the imaginary part of the probe susceptibility is also position-dependent. Therefore, it is possible to acquire information about the position of atom through measuring the

resulting absorption spectra. Specifically, the effect of the relative phase of the applied fields due to the closed-loop structure of the diamond-shape subsystem has been explored. An analytical solution is presented to elucidate such a phase-sensitivity. It is found that there exists a significant phase dependence of the eigenvalues required to obtain maxima in the probe absorption spectrum. Through appropriate adjusting the amplitudes and phases of the driving fields, the atom-light Hamiltonian can experience three, four, and two eigenstates, leading to different localization patterns for the atom. The situations for the optimum atom localization have been identified.

3. A four-level atomic system is proposed to investigate the 3D atom localization. Since the interaction between the atom and the laser fields is position dependent, the resulting probe absorption spectra gives information about the position of atom in the 3D space of the standing wave fields. It is demonstrated that he relative phase ϕ of applied fields can control the 3D atom localization behaviour of the system. In particular, we observed that compared to the case of $\phi = \pi/2$, the detecting probability of finding the atom at a particular volume in 3D space is increased when $\phi = 0$ or $\phi = \pi$.

4. We have demonstrated the possibility of coherent control of linear and nonlinear optical properties of a weak probe field in a five-level double-ladder atom light coupling scheme. We have shown that as the control field Ω_d is introduced on the transition $|2\rangle \leftrightarrow |3\rangle$ satisfying $\Omega_s = \Omega_c = \Omega_d = \Omega$, a transparency window appears in the otherwise opaque medium. As a result, the control field Ω_d can work as a knob to switch from the absorption to the transparency. We have presented numerical results in terms of a Gaussian intensity profile of the probe field to explain such optical switching. We further have investigated the possibility of giant enhancement of Kerr nonlinear coefficient in such an atomic configuration. It was found that an enhanced Kerr nonlinearity with negligible linear absorption can be obtained by proper tuning of the control field.

5. We have demonstrated the existence of dark states which are essential for appearance of electromagnetically induced transparency (EIT) for a situation where the atom-light interaction represents a five-level combined tripod and Λ configuration. The EIT is possible in the combined tripod

and Λ scheme when the Rabi frequencies of the control fields obey the condition $\beta \neq 0$, $\alpha \neq 0$, where β and α given by Eqs. (6.14)–(6.15) characterize the relative amplitudes and phases of the four control fields. Under this condition, the medium supports the lossless propagation of slow light. It is analytically demonstrated that combined tripod and Λ scheme can reduce to simpler atom light-coupling configurations under various quantum interference situations. In particular, this scheme is equivalent to a four-level N-type scheme when $\beta = 0$ and $\alpha \neq 0$. On the other hand, for $\beta \neq 0$ but $\alpha = 0$, a three-level Λ-type atom-light coupling scheme can be established. As a result, by changing the Rabi frequencies of control fields, it is possible to make a transition from one limiting case to the another one. This can lead to switching from subluminality accompanied by EIT to superluminality along with absorption and visa versa. Based on the coupled Maxwell-Bloch equations, a nonlinear equation governing the evolution of the probe pulse envelope is then obtained. This leads to formation of stable optical solitons with a slow propagating velocity due to the balance between dispersion and Kerr nonlinearity of the system.

In 2014, a group of researchers from Taiwan and Lithuania suggested a novel five-level double-tripod (DT) atom-light coupling scheme to realize the spinor (two-component) slow light based on the EIT effect [29]. The DT scheme involves three atomic ground states coupled to two excited states by two probe fields as well as four control fields. An interesting idea is to investigate the possibility of formation of slow light soliton pairs in the DT system.

Recently, much attention has been paid to optical vortices since the pioneering experiment by Gramila et al. [153]. Indeed, beams carrying orbital angular momentum (OAM) [154, 155, 156] possess remarkable potential applications in quantum computation and quantum information [154, 156, 157]. The intensity of optical vortices vanishes at the beam center and, at the same time, the beam remains localized propagating in the form of a ringlike beam. The OAM represents a new degree of freedom and provides additional possibilities in manipulating the slow light [158, 159, 19, 14, 42]. Several proposals have been suggested for the vortex slow light [19, 14, 42]. Vortex spatial solitons have been demonstrated experimentally in Kerr [160], photorefractive [161], and photovoltaic [162] nonlinear media. Yet it would be appealing to realize existence of the vortex spatial solitons in the cold multi-level atomic configurations.

Appendix A

Eigenstates and eigenvalues for situation (a)

The expressions for the eigenstates and their corresponding eigenvalues for situaion (a) are:

$$|n_1\rangle = \frac{\alpha^*(S-Y)}{\Omega(X-Y)}|b\rangle - \frac{\sqrt{S-Y}}{\sqrt{2}\Omega}|B_e\rangle - \frac{\alpha^*\beta\sqrt{2(S-Y)}}{\Omega(X-Y)}|D_e\rangle + |e\rangle\,, \tag{A.1}$$

$$|n_2\rangle = \frac{\alpha^*(S-Y)}{\Omega(X-Y)}|b\rangle + \frac{\sqrt{S-Y}}{\sqrt{2}\Omega}|B_e\rangle + \frac{\alpha^*\beta\sqrt{2(S-Y)}}{\Omega(X-Y)}|D_e\rangle + |e\rangle\,, \tag{A.2}$$

$$|n_3\rangle = \frac{\alpha^*(S+Y)}{\Omega(X+Y)}|b\rangle - \frac{\sqrt{S+Y}}{\sqrt{2}\Omega}|B_e\rangle - \frac{\alpha^*\beta\sqrt{2(S+Y)}}{\Omega(X+Y)}|D_e\rangle + |e\rangle\,, \tag{A.3}$$

$$|n_4\rangle = \frac{\alpha^*(S+Y)}{\Omega(X+Y)}|b\rangle + \frac{\sqrt{S+Y}}{\sqrt{2}\Omega}|B_e\rangle + \frac{\alpha^*\beta\sqrt{2(S+Y)}}{\Omega(X+Y)}|D_e\rangle + |e\rangle\,, \tag{A.4}$$

with eigenvalues

$$\lambda_1 = -\frac{\sqrt{S-Y}}{\sqrt{2}}\,, \tag{A.5}$$

$$\lambda_2 = \frac{\sqrt{S-Y}}{\sqrt{2}}\,, \tag{A.6}$$

$$\lambda_3 = -\frac{\sqrt{S+Y}}{\sqrt{2}}\,, \tag{A.7}$$

$$\lambda_4 = \frac{\sqrt{S+Y}}{\sqrt{2}}\,, \tag{A.8}$$

where

$$S = |\alpha|^2 + |\beta|^2 + \Omega^2\,, \tag{A.9}$$

$$X = |\alpha|^2 - |\beta|^2 + \Omega^2\,, \tag{A.10}$$

$$Y = \sqrt{S^2 - 4|\beta|^2\Omega^2}\,. \tag{A.11}$$

Appendix B

Eigenstates and eigenvalues for situation (b)

The expressions for the eigenstates and their corresponding eigenvalues for situaion (b) are:

$$|n_1\rangle = -\frac{\Omega}{\alpha}|b\rangle + |e\rangle\,, \tag{B.1}$$

$$|n_2\rangle = |D_e\rangle\,, \tag{B.2}$$

$$|n_3\rangle = \frac{\alpha^*}{\Omega}|b\rangle - \frac{\sqrt{|\alpha|^2+\Omega^2}}{\Omega}|B_e\rangle + |e\rangle\,, \tag{B.3}$$

$$|n_4\rangle = \frac{\alpha^*}{\Omega}|b\rangle + \frac{\sqrt{|\alpha|^2+\Omega^2}}{\Omega}|B_e\rangle + |e\rangle\,, \tag{B.4}$$

with eigenvalues

$$\lambda_1 = 0\,, \tag{B.5}$$

$$\lambda_2 = 0\,, \tag{B.6}$$

$$\lambda_3 = -\sqrt{|\alpha|^2+\Omega^2}\,, \tag{B.7}$$

$$\lambda_4 = \sqrt{|\alpha|^2+\Omega^2}\,. \tag{B.8}$$

Appendix C

Eigenstates and eigenvalues for situation (c)

$$|n_1\rangle = -|b\rangle + |D_e\rangle\,, \tag{C.1}$$
$$|n_2\rangle = |b\rangle + |D_e\rangle\,, \tag{C.2}$$
$$|n_3\rangle = -|B_e\rangle + |e\rangle\,, \tag{C.3}$$
$$|n_4\rangle = |B_e\rangle + |e\rangle\,, \tag{C.4}$$

with eigenvalues

$$\lambda_1 = -\beta\,, \tag{C.5}$$
$$\lambda_2 = \beta\,, \tag{C.6}$$
$$\lambda_3 = -\Omega\,, \tag{C.7}$$
$$\lambda_4 = \Omega\,, \tag{C.8}$$

Appendix D

Explicit expressions for κ_0 , $1/v_g$ and κ_2

Expressions for κ_0 , $1/v_g$ and κ_2 read

$$\kappa_0 = \eta \frac{S_1}{Q}\,, \tag{D.1}$$

$$\frac{1}{v_g} = \frac{1}{c} + \eta \left(-\frac{g_1}{Q} + \frac{S_1 g_2}{Q^2} \right)\,, \tag{D.2}$$

$$\kappa_2 = \eta \left(-\frac{g_3}{Q} + \frac{1}{Q^2}\left(2g_1 g_2 - S_1 g_4\right) - \frac{S_1 g_2^2}{Q^3} \right)\,, \tag{D.3}$$

with

$$g_1 = t_2^2 + 2t_2 t_3 - \left(|\Omega_3|^2 + |\Omega_4|^2 \right), \tag{D.4}$$

$$g_2 = (t_2 + t_3)\left(|\Omega_1|^2 + |\Omega_2|^2 \right) + (t_1 + t_2)\left(|\Omega_3|^2 + |\Omega_4|^2 \right) - t_1 t_2^2 - t_3 t_2^2 - 2t_1 t_2 t_3, \tag{D.5}$$

$$g_3 = -6\Delta_2 + 2\Delta_3 + 6\Delta_p + i\Gamma_e, \tag{D.6}$$

$$g_4 = -2\left(|\Omega_1|^2 + |\Omega_2|^2 + |\Omega_3|^2 + |\Omega_4|^2 \right) + 2\left(2t_1 t_2 + t_1 t_3 + t_2 t_3\right) + 2t_2^2, \tag{D.7}$$

where t_1, t_2, t_3, S_1 and Q can be obtained by substituting $\omega = 0$ in coefficients $t_1(\omega), t_2(\omega), t_3(\omega)$, $S_1(\omega)$ and $Q(\omega)$, respectively.

Appendix E

Explicit expressions of F_{ba}, F_{ca}, F_{da} and F_{ea}

After some algebraic calculations, the solutions of Eqs. (2.24)–(2.27) can be obtained as ,

$$F_{ba} = \frac{-\Lambda_p S_1(\omega)}{Q(\omega)}, \tag{E.1}$$

$$F_{ca} = \frac{\Lambda_p S_2(\omega)}{Q(\omega)}, \tag{E.2}$$

$$F_{da} = \frac{\Lambda_p S_3(\omega)}{Q(\omega)}, \tag{E.3}$$

$$F_{ea} = \frac{\Lambda_p S_4(\omega)}{Q(\omega)}, \tag{E.4}$$

where

$$S_1(\omega) = t_2^2(\omega)t_3(\omega) - t_2(\omega)\left(|\Omega_3|^2 + |\Omega_4|^2\right), \tag{E.5}$$

$$S_2(\omega) = |\Omega_1||\Omega_4|^2 - |\Omega_2||\Omega_3||\Omega_4|e^{-i\phi} - |\Omega_1|t_2(\omega)t_3(\omega), \tag{E.6}$$

$$S_3(\omega) = |\Omega_2||\Omega_3|^2 - |\Omega_1||\Omega_3||\Omega_4|e^{i\phi} - |\Omega_2|t_2(\omega)t_3(\omega), \tag{E.7}$$

$$S_4(\omega) = t_2(\omega)\left(|\Omega_2||\Omega_4| + |\Omega_1||\Omega_3|e^{i\phi}\right), \tag{E.8}$$

$$\begin{aligned} Q(\omega) =& t_2(\omega)t_3(\omega)\left(|\Omega_1|^2 + |\Omega_2|^2\right) + t_1(\omega)t_2(\omega)\left(|\Omega_3|^2 + |\Omega_4|^2\right) \\ & - t_1(\omega)t_2^2(\omega)t_3(\omega) - |\Omega_2|^2|\Omega_3|^2 - |\Omega_1|^2|\Omega_4|^2 + 2|\Omega_1||\Omega_2||\Omega_3||\Omega_4|\cos(\phi). \end{aligned} \tag{E.9}$$

Appendix F

Kerr nonlinear coefficient

One may write the Maxwell equations under the slowly varying envelope approximation as

$$\frac{\partial \Omega_p}{\partial z} + c^{-1}\frac{\partial \Omega_p}{\partial t} = i\eta \Phi_b \Phi_a^*, \tag{F.1}$$

where $\Phi_b\Phi_a^* = \rho_{ba}$, as well as Φ_a and Φ_b (together with Φ_c, Φ_d and Φ_e) represent the amplitudes of atomic wavefunctions for each atomic state and satisfy the relation

$$|\Phi_a|^2 + |\Phi_b|^2 + |\Phi_c|^2 + |\Phi_d|^2 + |\Phi_e|^2 = 1. \tag{F.2}$$

Initially all atoms are assumed to be in the ground state $|a\rangle$. As the Rabi-frequency of the probe field is much weaker than that of the control fields, one can neglect the depletion of ground level $|a\rangle$, and one has $\Phi_a \approx 1$. Adopting a perturbation treatment of the system response to the first order of probe field, we can take $\Phi_L = \Sigma_L \Phi_L^{(k)}$ $(L = a, b, c, d, e)$. Here $\Phi_L^{(k)}$ is the kth order part of Φ_L in terms of Ω_p, where $\Phi_b^{(0)} = \Phi_c^{(0)} = \Phi_d^{(0)} = \Phi_e^{(0)} = 0$, and $\Phi_a^{(0)} = 1$, while $\Phi_a^{(1)} = 0$. Thus, to the first order in Ω_p we may write

$$\Phi_a = \Phi_a^{(0)}, \tag{F.3}$$
$$\Phi_b\Phi_a^* = \Phi_b^{(1)}\Phi_a^{(0)*} = \Phi_b^{(1)}\Phi_a^{(0)} = \Phi_b^{(1)} = \rho_{ba}^{(1)}, \tag{F.4}$$
$$\Phi_c\Phi_a^* = \Phi_c^{(1)}\Phi_a^{(0)*} = \Phi_c^{(1)}\Phi_a^{(0)} = \Phi_c^{(1)} = \rho_{ca}^{(1)}, \tag{F.5}$$
$$\Phi_d\Phi_a^* = \Phi_d^{(1)}\Phi_a^{(0)*} = \Phi_d^{(1)}\Phi_a^{(0)} = \Phi_d^{(1)} = \rho_{da}^{(1)}, \tag{F.6}$$
$$\Phi_e\Phi_a^* = \Phi_e^{(1)}\Phi_a^{(0)*} = \Phi_e^{(1)}\Phi_a^{(0)} = \Phi_e^{(1)} = \rho_{ea}^{(1)}. \tag{F.7}$$

In this limit Eq. (F.2) reduces to

$$|\Phi_a^{(0)}|^2 + |\Phi_b^{(1)}|^2 + |\Phi_c^{(1)}|^2 + |\Phi_d^{(1)}|^2 + |\Phi_e^{(1)}|^2 = 1. \tag{F.8}$$

Using Eqs. (F.3)–(F.8), the right hand side of wave equation (F.1) can be represented as

$$\begin{aligned} i\eta\Phi_b\Phi_a^* &= i\eta\Phi_b^{(1)}|\Phi_a^{(0)}|^2 \\ &= i\eta\Phi_b^{(1)}\left[1 - (|\Phi_b^{(1)}|^2 + |\Phi_c^{(1)}|^2 + |\Phi_d^{(1)}|^2 + |\Phi_e^{(1)}|^2)\right] \\ &= i\eta\rho_{ba}^{(1)} - i\eta\rho_{ba}^{(1)}(|\rho_{ba}^{(1)}|^2 + |\rho_{ca}^{(1)}|^2 + |\rho_{da}^{(1)}|^2 + |\rho_{ea}^{(1)}|^2)\,. \end{aligned} \tag{F.9}$$

The first term $i\eta\rho_{ba}^{(1)}$ shows the linear part of the right hand side of wave equation (F.1) which was featured in Eq. (6.7). In addition,$-i\eta\mathrm{Kerr} = -i\eta\rho_{ba}^{(1)}(|\rho_{ba}^{(1)}|^2 + |\rho_{ca}^{(1)}|^2 + |\rho_{da}^{(1)}|^2 + |\rho_{ea}^{(1)}|^2)$ represents the nonlinear part of the right hand side of wave equation (F.1). From this expression, the explicit form of the nonlinear coefficient Kerr given in Eq. (2.38) can be readily derived.

Bibliography

[1] L. Jiang, E. R. Nowak, P. E. Scott, J. Johnson, J. M. Slaughter, J. J. Sun, and R. W. Dave. Low-frequency magnetic and resistance noise in magnetic tunnel junctions. *Phys. Rev. B*, 69:054407, Feb 2004.

[2] T. Kawazoe, K. Kobayashi, S. Sangu, and M. Ohtsu. Demonstration of a nanophotonic switching operation by optical near-field energy transfer. *Appl. Phys. Lett*, 82:2957–2959, 2003.

[3] Michael Fleischhauer, Atac Imamoglu, and Jonathan P. Marangos. Electromagnetically induced transparency: Optics in coherent media. *Rev. Mod. Phys.*, 77:633–673, Jul 2005.

[4] S. E. Harris, J. E. Field, and A. Imamoğlu. Nonlinear optical processes using electromagnetically induced transparency. *Phys. Rev. Lett.*, 64:1107–1110, Mar 1990.

[5] M. Fleischhauer, C. H. Keitel, M. O. Scully, Chang Su, B. T. Ulrich, and Shi-Yao Zhu. Resonantly enhanced refractive index without absorption via atomic coherence. *Phys. Rev. A*, 46:1468–1487, Aug 1992.

[6] A. S. Zibrov, M. D. Lukin, D. E. Nikonov, L. Hollberg, M. O. Scully, V. L. Velichansky, and H. G. Robinson. Experimental demonstration of laser oscillation without population inversion via quantum interference in rb. *Phys. Rev. Lett.*, 75:1499–1502, Aug 1995.

[7] Stephen E. Harris. Electromagnetically induced transparency. *Physics Today*, 50:36, 1997.

[8] M. Fleischhauer and M. D. Lukin. Dark-state polaritons in electromagnetically induced transparency. *Phys. Rev. Lett.*, 84:5094–5097, May 2000.

[9] Hai Wang, David Goorskey, and Min Xiao. Enhanced kerr nonlinearity via atomic coherence in a three-level atomic system. *Phys. Rev. Lett.*, 87:073601, Jul 2001.

[10] Mostafa Sahrai, Habib Tajalli, Kishore T. Kapale, and M. Suhail Zubairy. Tunable phase control for subluminal to superluminal light propagation. *Phys. Rev. A*, 70:023813, Aug 2004.

[11] Habib Tajalli and Mostafa Sahrai. Switching from normal to anomalous dispersion via coherent field. *J. Opt. B: Quantum Semiclass. Opt.*, 7:168, 2005.

[12] Rong Yu, Jiahua Li, Pei Huang, Anshou Zheng, and Xiaoxue Yang. Dynamic control of light propagation and optical switching through an rf-driven cascade-type atomic medium. *Physics Letters A*, 373:2992–3000, 2009.

[13] Sajid Qamar, Shi-Yao Zhu, and M. Suhail Zubairy. Atom localization via resonance fluorescence. *Phys. Rev. A*, 61:063806, May 2000.

[14] J. Ruseckas, A. Mekys, and G. Juzeliūnas. Slow polaritons with orbital angular momentum in atomic gases. *Phys. Rev. A*, 83:023812, Feb 2011.

[15] Jiteng Sheng, Xihua Yang, Haibin Wu, and Min Xiao. Modified self-kerr-nonlinearity in a four-level N-type atomic system. *Phys. Rev. A*, 84:053820, Nov 2011.

[16] Hai Wang, David Goorskey, and Min Xiao. Dependence of enhanced kerr nonlinearity on coupling power in a three-level atomic system. *Optics Letters*, 27:258–260, 2002.

[17] Michael Fleischhauer and Gediminas Juzeliūnas. *Slow, Stored and Stationary Light*, pages 359–383. Springer International Publishing, Cham, 2016.

[18] M. O. Scully and M. S. Zubairy. *Quantum Optics*. Cambridge University Press, Cambridge, 1997.

[19] Julius Ruseckas, Gediminas Juzeliūnas, Patrik Öhberg, and Stephen M. Barnett. Polarization rotation of slow light with orbital angular momentum in ultracold atomic gases. *Phys. Rev. A*, 76:053822, Nov 2007.

[20] H. Schmidt and A. Imamoglu. Giant kerr nonlinearities obtained by electromagnetically induced transparency. *Opt. Lett.*, 21:1936Ű1938, 1996.

[21] Chao Hang and Guoxiang Huang. Weak-light ultraslow vector solitons via electromagnetically induced transparency. *Phys. Rev. A*, 77:033830, Mar 2008.

[22] W. Harshawardhan and G. S. Agarwal. Controlling optical bistability using electromagnetic-field-induced transparency and quantum interferences. *Phys. Rev. A*, 53:1812–1817, Mar 1996.

[23] A. Imamoḡlu, H. Schmidt, G. Woods, and M. Deutsch. Strongly interacting photons in a nonlinear cavity. *Phys. Rev. Lett.*, 79:1467–1470, Aug 1997.

[24] Yifu Zhu. Lasing without inversion in a closed three-level system. *Phys. Rev. A*, 45:R6149–R6152, May 1992.

[25] E Paspalakis and P L Knight. Transparency, slow light and enhanced nonlinear optics in a four-levelscheme. *Journal of Optics B: Quantum and Semiclassical Optics*, 4:S372, 2002.

[26] Mostafa Sahrai, Habib Tajalli, Kishore T. Kapale, and M. Suhail Zubairy. Subwavelength atom localization via amplitude and phase control of the absorption spectrum. *Phys. Rev. A*, 72:013820, Jul 2005.

[27] E. A. Korsunsky, N. Leinfellner, A. Huss, S. Baluschev, and L. Windholz. Phase-dependent electromagnetically induced transparency. *Phys. Rev. A*, 59:2302–2305, Mar 1999.

[28] R. G. Unanyan, J. Otterbach, M. Fleischhauer, J. Ruseckas, V. Kudriašov,

and G. Juzeliūnas. Spinor slow-light and dirac particles with variable mass. *Phys. Rev. Lett.*, 105:173603, Oct 2010.

[29] Meng-Jung Lee, Julius Ruseckas, Chin-Yuan Lee, Viaceslav Kudriasov, Kao-Fang Chang, Hung-Wen Cho, Gediminas Juzeliūnas, and Ite A. Yu. Experimental demonstration of spinor slow light. *Nat. Commun.*, 5:5542, 2014.

[30] Amitabh Joshi and Min Xiao. Phase gate with a four-level inverted-y system. *Phys. Rev. A*, 72:062319, Dec 2005.

[31] Luming Li, Hong Guo, Feng Xiao, Xiang Peng, and Xuzong Chen. Control of light in an m-type five-level atomic system. *Journal of the Optical Society of America B*, 22:1309–1313, 2005.

[32] Chunling Ding, Jiahua Li, Zhiming Zhan, and Xiaoxue Yang. Two-dimensional atom localization via spontaneous emission in a coherently driven five-level m-type atomic system. *Phys. Rev. A*, 83:063834, Jun 2011.

[33] S. E. Harris and Lene Vestergaard Hau. Nonlinear optics at low light levels. *Phys. Rev. Lett.*, 82:4611–4614, Jun 1999.

[34] Kouichi Ichimura. Quantum information processing using electromagnetically induced transparency. *The Review of Laser Engineering*, 31:605–611, 2003.

[35] R. G. Beausoleil, W. J. Munro, D. A. Rodrigues, and T. P. Spiller. Applications of electromagnetically induced transparency to quantum information processing. *Journal of Modern Optics*, 51:16–18, 2004.

[36] Dinh Xuan Khoa, Le Van Doai, Doan Hoai Son, and Nguyen Huy Bang. Enhancement of self-kerr nonlinearity via electromagnetically induced transparency in a five-level cascade system: an analytical approach. *Journal of the Optical Society of America B*, 31:1330–1334, 2014.

[37] Yueping Niu, Shangqing Gong, Ruxin Li, Zhizhan Xu, , and Xiaoyan

Liang. Giant kerr nonlinearity induced by interacting dark resonances. *Optics Letters*, 30:3371–3373, 2005.

[38] Yihong Qi, Fengxue Zhou, Ting Huang, Yueping Niu, and Shangqing Gong. Three-dimensional atom localization in a five-level m-type atomic system. *Journal of Modern Optics*, 59:1092–1099, 2012.

[39] Vladimir S. Ivanov, Yuri V. Rozhdestvensky, and Kalle-Antti Suominen. Three-dimensional atom localization by laser fields in a four-level tripod system. *Phys. Rev. A*, 90:063802, Dec 2014.

[40] Zhonghu Zhu, Wen-Xing Yang, Xiao-Tao Xie, Shasha Liu, Shaopeng Liu, and Ray-Kuang Lee. Three-dimensional atom localization from spatial interference in a double two-level atomic system. *Phys. Rev. A*, 94:013826, Jul 2016.

[41] Stefan Beck and Igor E. Mazets. Propagation of coupled dark-state polaritons and storage of light in a tripod medium. *Phys. Rev. A*, 95:013818, Jan 2017.

[42] Julius Ruseckas, Via česlav Kudriašov, Ite A. Yu, and Gediminas Juzeliūnas. Transfer of orbital angular momentum of light using two-component slow light. *Phys. Rev. A*, 87:053840, May 2013.

[43] H. R. Hamedi and G. Juzeliūnas. Phase-sensitive kerr nonlinearity for closed-loop quantum systems. *Phys. Rev. A*, 91:053823, May 2015.

[44] H. R. Hamedi and Gediminas Juzeliūnas. Phase-sensitive atom localization for closed-loop quantum systems. *Phys. Rev. A*, 94:013842, Jul 2016.

[45] H. R. Hamedi and M. R. Mehmannavaz. Phase control of three-dimensional atom localization in a four-level atomic system in lambda configuration. *Journal of the Optical Society of America B*, 33:41–45, 2016.

[46] H. R. Hamedi. Optical switching, bistability and pulse propagation in five-level quantum schemes. *Laser Phys.*, 27:066002, 2017.

[47] H. R. Hamedi, Ali Hamrah Gharamaleki, and Mostafa Sahrai. Colossal kerr nonlinearity based on electromagnetically induced transparency in a five-level double-ladder atomic system. *Appl. Opt.*, 55:5892–5899, 2016.

[48] K.-J. Boller, A. Imamoğlu, and S. E. Harris. Observation of electromagnetically induced transparency. *Phys. Rev. Lett.*, 66:2593–2596, May 1991.

[49] U. Schnorrberger, J. D. Thompson, S. Trotzky, R. Pugatch, N. Davidson, S. Kuhr, and I. Bloch. Electromagnetically induced transparency and light storage in an atomic mott insulator. *Phys. Rev. Lett.*, 103:033003, 2009.

[50] G. Juzeliūnas and H. J. Carmichael. Systematic formulation of slow polaritons in atomic gases. *Phys. Rev. A*, 65:021601, 2002.

[51] J. P. Marangos. Electromagnetically induced transparency. *J. Mod. Opt.*, 45:471– 503, 1998.

[52] A. André, M. D. Eisaman, R. L. Walsworth, A. S. Zibrov, and M. D. Lukin. Quantum control of light using electromagnetically induced transparency. *J. Phys. B: At., Mol. Opt. Phys.*, 38:S589, 2005.

[53] G. Juzeliūnas, M. Mašalas, and M. Fleischhauer. Storing and releasing light in a gas of moving atoms. *Phys. Rev. A*, 67:023809, Feb 2003.

[54] Ying Wu and Lu Deng. Ultraslow bright and dark optical solitons in a cold three-state medium. *Optics Letters*, 29:2064–2066, 2004.

[55] R. Drampyan, S. Pustelny, and W. Gawlik. Electromagnetically induced transparency versus nonlinear faraday effect: Coherent control of light-beam polarization. *Phys. Rev. A*, 80:033815, Sep 2009.

[56] Jia-Hua Li, Xin-You Lü, Jing-Min Luo, and Qiu-Jun Huang. Optical bistability and multistability via atomic coherence in an n-type atomic medium. *Phys. Rev. A*, 74:035801, Sep 2006.

[57] Michael Fleischhauer. Correlation of high-frequency phase fluctuations in

electromagnetically induced transparency. *Phys. Rev. Lett.*, 72:989–992, Feb 1994.

[58] L. V. Hau, S. E. Harris, Z. Dutton, and C. H. Behroozi. Light speed reduction to 17 metres per second in an ultracold atomic gas. *Nature*, 397:594–598, 1999.

[59] Yong Zhao, Hua-Wei Zhao, Xin-Yuan Zhang, Bo Yuan, and Shuo Zhang. New mechanisms of slow light and their applications. *Optics & Laser Technology*, 41:517– 525, 2009.

[60] Robert W. Boyd, Daniel J. Gauthier, and Alexander L. Gaeta. Applications of slow light in telecommunications. *Optics and Photonics News*, 17:18–23, 2006.

[61] M. Bajcsy, S. Hofferberth, V. Balic, T. Peyronel, M. Hafezi, A. S. Zibrov, V. Vuletic, and M. D. Lukin. Efficient all-optical switching using slow light within a hollow fiber. *Phys. Rev. Lett.*, 102:203902, May 2009.

[62] M. D. Eisaman, A. Andre, F. Massou, M. Fleischhauer, A. S. Zibrov, and M. D. Lukin. Electromagnetically induced transparency with tunable single-photon pulses. *Nature*, 438:837–841, 2005.

[63] Pippa Storey, Matthew Collett, and Daniel Walls. Measurement-induced diffraction and interference of atoms. *Phys. Rev. Lett.*, 68:472–475, Jan 1992.

[64] Fam Le Kien, G. Rempe, W. P. Schleich, and M. S. Zubairy. Atom localization via ramsey interferometry: A coherent cavity field provides a better resolution. *Phys. Rev. A*, 56:2972–2977, Oct 1997.

[65] Maksim Yu Gordeev, Ekaterina A Efremova, and Yuri V Rozhdestvensky. Atom localization with double-cascade configuration. *J. Phys. B: At. Mol. Opt. Phys*, 49:065001, 2016.

[66] Mostafa Sahrai and Habib Tajalli. Sub-half-wavelength atom localization of a v-type three-level atom via relative phase. *Journal of the Optical Society of America B*, 30:512–517, 2013.

[67] W. Heisenberg. Uber den anschaulichen inhalt der quantentheoretischen kinematik und mechanik ,. *Zeitschrift für Physik*, 43:172, 1927.

[68] Alexey V. Gorshkov, Liang Jiang, Markus Greiner, Peter Zoller, and Mikhail D. Lukin. Coherent quantum optical control with subwavelength resolution. *Phys. Rev. Lett.*, 100:093005, Mar 2008.

[69] Hebin Li, Vladimir A. Sautenkov, Michael M. Kash Kash, Alexei V. Sokolov, George R. Welch, Yuri. V. Rostovtsev, M. S. ZubairyZubairy, and Marlan O. Scully. Optical imaging beyond the diffraction limit via dark states. *Phys. Rev. A*, 78:013803, Jul 2008.

[70] J. A. Miles, Z. J. Simmons, and D. D. Yavuz. Subwavelength localization of atomic excitation using electromagnetically induced transparency. *Phys. Rev. X*, 3:031014, Sep 2013.

[71] J. R. Gardner, K. L. Marable, G. R. Welch, and J. E. Thomas. Suboptical wavelength position measurement of moving atoms using optical fields. *Phys. Rev. Lett*, 70:3404–3407, 1993.

[72] Kishore T. Kapale, Shahid Qamar, and M. Suhail Zubairy. Spectroscopic measurement of an atomic wave function. *Phys. Rev. A*, 67:023805, 2003.

[73] J. Mompart, V. Ahufinger, and G. Birkl. Coherent patterning of matter waves with subwavelength localization. *Phys. Rev. A*, 79:053638, May 2009.

[74] M. Holland, S. Marksteiner, P. Marte, and P. Zoller. Measurement induced localization from spontaneous decay. *Phys. Rev. Lett.*, 76:3683–3686, May 1996.

[75] Fazal Ghafoor, Sajid Qamar, and M. Suhail Zubairy. Atom localization via phase and amplitude control of the driving field. *Phys. Rev. A*, 65:043819, Apr 2002.

[76] Sajid Qamar, Shi-Yao Zhu, and M.Suhail Zubairy. Precision localization of single atom using autlerŰtownes microscopy. *Optics Communications*, 176:409Ű416, 2000.

[77] E. Paspalakis and P. L. Knight. Localizing an atom via quantum interference. *Phys. Rev. A*, 63:065802, May 2001.

[78] N. A. Proite, Z. J. Simmons, and D. D. Yavuz. Observation of atomic localization using electromagnetically induced transparency. *Phys. Rev. A*, 83:041803, Apr 2011.

[79] J. A. Miles, Diptaranjan Das, Z. J. Simmons, and D. D. Yavuz. Localization of atomic excitation beyond the diffraction limit using electromagnetically induced transparency. *Phys. Rev. A*, 92:033838, Sep 2015.

[80] Murray Sargent III Pierre Meystre. *Elements of Quantum Optics*. Springer, 1999.

[81] R. W. Boyd. *Nonlinear Optics (Academic, San Diego, 1992)*. Academic Press, 1992.

[82] S. E. Harris and Y. Yamamoto. Photon switching by quantum interference. *Phys. Rev. Lett.*, 81:3611–3614, Oct 1998.

[83] Zeng-Bin Wang, Karl-Peter Marzlin, and Barry C. Sanders. Large cross-phase modulation between slow copropagating weak pulses in ^{87}Rb. *Phys. Rev. Lett.*, 97:063901, Aug 2006.

[84] Bor-Wen Shiau, Meng-Chang Wu, Chi-Ching Lin, and Ying-Cheng Chen. Low-light-level cross-phase modulation with double slow light pulses. *Phys. Rev. Lett.*, 106:193006, May 2011.

[85] Yi-Hsin Chen, Meng-Jung Lee, Weilun Hung, Ying-Cheng Chen, Yong-Fan Chen, and Ite A. Yu. Demonstration of the interaction between two stopped light pulses. *Phys. Rev. Lett.*, 108:173603, Apr 2012.

[86] Vivek Venkataraman, Kasturi Saha, and Alexander L. Gaeta. Phase modulation at the few-photon level for weak-nonlinearity-based quantum computing. *Nature Photonics*, 7:138Ű141, 2013.

[87] D. Maxwell, D. J. Szwer, D. Paredes-Barato, H. Busche, J. D. Pritchard, A. Gauguet, K. J. Weatherill, M. P. A. Jones, and C. S. Adams. Storage

and control of optical photons using rydberg polaritons. *Phys. Rev. Lett.*, 110:103001, Mar 2013.

[88] Simon Baur, Daniel Tiarks, Gerhard Rempe, and Stephan Dürr. Single-photon switch based on rydberg blockade. *Phys. Rev. Lett.*, 112:073901, Feb 2014.

[89] K. Hakuta, L. Marmet, and B. P. Stoicheff. Electric-field-induced second-harmonic generation with reduced absorption in atomic hydrogen. *Phys. Rev. Lett.*, 66:596–599, Feb 1991.

[90] Andrew J. Merriam, S. J. Sharpe, M. Shverdin, D. Manuszak, G. Y. Yin, and S. E. Harris. Efficient nonlinear frequency conversion in an all-resonant double- Λ system. *Phys. Rev. Lett.*, 84:5308–5311, Jun 2000.

[91] Richard R. Moseley, Sara Shepherd, David J. Fulton, Bruce D. Sinclair, and Malcolm H. Dunn. Spatial consequences of electromagnetically induced transparency: Observation of electromagnetically induced focusing. *Phys. Rev. Lett.*, 74:670–673, Jan 1995.

[92] Yanxu Han, Jintao Xiao, Yonghong Liu, Chunhong Zhang, Hai Wang, Min Xiao, and Kunchi Peng. Interacting dark states with enhanced nonlinearity in an ideal four-level tripod atomic system. *Phys. Rev. A*, 77:023824, Feb 2008.

[93] Yueping Niu and Shangqing Gong. Enhancing kerr nonlinearity via spontaneously generated coherence. *Phys. Rev. A*, 73:053811, May 2006.

[94] David Petrosyan and Yuri P. Malakyan. Magneto-optical rotation and cross-phase modulation via coherently driven four-level atoms in a tripod configuration. *Phys. Rev. A*, 70:023822, Aug 2004.

[95] A. B. Matsko, I. Novikova, G. R. Welch, and M. S. Zubairy. Enhancement of kerr nonlinearity by multiphoton coherence. *Opt. Lett.*, 28:96, 2003.

[96] Hoonsoo Kang and Yifu Zhu. Observation of large kerr nonlinearity at low light intensities. *Phys. Rev. Lett.*, 91:093601, Aug 2003.

[97] Ying Wu, Joseph Saldana, and Yifu Zhu. Large enhancement of four-wave mixing by suppression of photon absorption from electromagnetically induced transparency. *Phys. Rev. A*, 67:013811, Jan 2003.

[98] S. E. Harris and Lene Vestergaard Hau. Nonlinear optics at low light levels. *Phys. Rev. Lett.*, 82:4611–4614, Jun 1999.

[99] G. P. Agrawal. *Nonlinear Fiber Optics*. Academic, New York, 2001.

[100] Ying Wu and L. Deng. Ultraslow optical solitons in a cold four-state medium. *Phys. Rev. Lett.*, 93:143904, Sep 2004.

[101] Yanpeng Zhang, Blake Anderson, and Min Xiao. Efficient energy transfer between four-wave-mixing and six-wave-mixing processes via atomic coherence. *Phys. Rev. A*, 77:061801, Jun 2008.

[102] Amitabh Joshi, Andy Brown, Hai Wang, and Min Xiao. Controlling optical bistability in a three-level atomic system. *Phys. Rev. A*, 67:041801, Apr 2003.

[103] Si-Cong Tian, Ren-Gang Wan, Cun-Zhu Tong, and Yong-Qiang Ning. Controlling optical bistability via interacting double dark resonances in linear quantum dot molecules. *Journal of the Optical Society of America B*, 31:2681–2688, 2014.

[104] Zhen Wang, Ai-Xi Chen, Yanfeng Bai, Wen-Xing Yang, and Ray-Kuang Lee. Coherent control of optical bistability in an open lambda-type three-level atomic system. *Journal of the Optical Society of America B*, 29:2891–2896, 2012.

[105] Mario I. Molina Rodrigo A. Vicencio and Yuri S. Kivshar. Controlled switching of discrete solitons in waveguide arrays. *Optics Letters*, 28:1942–1944, 2003.

[106] John E. Heebner, Robert W. Boyd, and Q-Han Park. Slow light, induced dispersion, enhanced nonlinearity, and optical solitons in a resonator-array waveguide. *Phys. Rev. E*, 65:036619, Mar 2002.

[107] Francesco Morichetti Andrea Melloni and Mario Martinelli. Optical slow wave structures. *Optics and Photonics News*, 14:44–48, 2003.

[108] Xiong-Jun Liu, Hui Jing, and Mo-Lin Ge. Solitons formed by dark-state polaritons in an electromagnetic induced transparency. *Phys. Rev. A*, 70:055802, Nov 2004.

[109] Y. S. Kivshar and B. Luther-Davies. Dark optical solitons: physics and applications. *Phys. Rep.*, 298:81, 1998.

[110] S. Burger, K. Bongs, S. Dettmer, W. Ertmer, K. Sengstock, A. Sanpera, G. V. Shlyapnikov, and M. Lewenstein. Dark solitons in bose-einstein condensates. *Phys. Rev. Lett.*, 83:5198–5201, Dec 1999.

[111] J. Denschlag, J. E. Simsarian, D. L. Feder, Charles W. Clark, L. A. Collins, J. Cubizolles, L. Deng and. W. Hagley, K. Helmerson, W. P. Reinhardt, S. L. Rolston, B. I. Schneider, and W. D. Phillips. Generating solitons by phase engineering of a bose-einstein condensate. *Science*, 287:97, 2000.

[112] A. Hasegawa and M. Matsumoto. *Optical Solitons in Fibers*. Springer, 2003.

[113] Dingan Han, Yaguang Zeng, Yanfeng Bai, and Chunqing Huang. Superluminal optical solitons in a four-level tripod atomic system. *J. Phys. B: At. Mol. Opt. Phys.*, 39:3029, 2006.

[114] Wen-Xing Yang, Jing-Min Hou, YuanYao Lin, and Ray-Kuang Lee. Detuning management of optical solitons in coupled quantum wells. *Phys. Rev. A*, 79:033825, Mar 2009.

[115] Chao Hang, Guoxiang Huang, and L. Deng. Stable high-dimensional spatial weak-light solitons in a resonant three-state atomic system. *Phys. Rev. E*, 74:046601, Oct 2006.

[116] Liu-Gang Si, Wen-Xing Yang, Ji-Bing Liu, Jin Li, and Xiaoxue Yang. Slow vector optical solitons in a cold five-level hyper v-type atomic system. *Optics Express*, 17:7771, 2009.

[117] Liu-Gang Si, Wen-Xing Yang, Xin-You Lü, Xiangying Hao, and Xiaoxue Yang. Formation and propagation of ultraslow three-wave-vector optical solitons in a cold seven-level triple-Λ atomic system under raman excitation. *Phys. Rev. A*, 82:013836, Jul 2010.

[118] Liang Li and Guoxiang Huang. Linear and nonlinear light propagations in a doppler-broadened medium via electromagnetically induced transparency. *Phys. Rev. A*, 82:023809, Aug 2010.

[119] Yang Chen, Zhiming Chen, and Guoxiang Huang. Storage and retrieval of vector optical solitons via double electromagnetically induced transparency. *Phys. Rev. A*, 91:023820, Feb 2015.

[120] Yang Chen, Zhengyang Bai, and Guoxiang Huang. Ultraslow optical solitons and their storage and retrieval in an ultracold ladder-type atomic system. *Phys. Rev. A*, 89:023835, Feb 2014.

[121] Guoxiang Huang, L. Deng, and M. G. Payne. Dynamics of ultraslow optical solitons in a cold three-state atomic system. *Phys. Rev. E*, 72:016617, Jul 2005.

[122] Ji-Bing Liu, Na Liu, Chuan-Jia Shan, Tang-Kun Liu, and Yan-Xia Huang. Slow optical soliton pairs via electron spin coherence in a quantum well waveguide. *Phys. Rev. E*, 81:036607, Mar 2010.

[123] Michael M. Kash, Vladimir A. Sautenkov, Alexander S. Zibrov, L. Hollberg, George R. Welch, Mikhail D. Lukin, Yuri Rostovtsev, Edward S. Fry, and Marlan O. Scully. Ultraslow group velocity and enhanced nonlinear optical effects in a coherently driven hot atomic gas. *Phys. Rev. Lett.*, 82:5229–5232, Jun 1999.

[124] Ying Wu and Xiaoxue Yang. Electromagnetically induced transparency in *v*-, Λ-, and cascade-type schemes beyond steady-state analysis. *Phys. Rev. A*, 71:053806, May 2005.

[125] Nobuyuki Matsuda, Ryosuke Shimizu, Yasuyoshi Mitsumori, Hideo Kosaka, and Keiichi Edamatsu. Observation of optical-fibre kerr nonlinearity at the single-photon level. *Nature Photonics*, 3:95 – 98, 2009.

[126] Mark N. Kobrak and Stuart A. Rice. Selective photochemistry via adiabatic passage: An extension of stimulated raman adiabatic passage for degenerate final states. *Phys. Rev. A*, 57:2885–2894, Apr 1998.

[127] K. Bergmann, H. Theuer, and B. W. Shore. Coherent population transfer among quantum states of atoms and molecules. *Rev. Mod. Phys.*, 70:1003–1025, Jul 1998.

[128] Frank Vewinger, Bruce W. Shoreb, and Klaas Bergmann. Chapter 3 Ű superpositions of degenerate quantum states:preparation and detection in atomic beams. *Adv. At., Mol., Opt. Phys.*, 58:113–172, 2010.

[129] J. Gong and S. A. Rice. Measurement-assisted coherent control. *J. Chem. Phys*, 120:9984, 2004.

[130] M. Sugawara. Measurement-assisted quantum dynamics control of 5-level system using intense cw-laser fields. *Chem. Phys. Lett.*, 428:457–460, 2006.

[131] M. Mahmoudi, M. Sahrai, and M. A. Allahyari. Amplitude and phase control of absorption and dispersion in a kobrak-rice 5-level quantum system. *Prog. Electromagn. Res. B*, 24:333, 2010.

[132] L. Ebrahimi Zohravi, R. Doostkam, S. M. Mousavi, and M. Mahmoudi. Controlling the optical bistability in a kobrak-rice 5-level quantum system. *Prog. Electromagn. Res. B*, 25:1–11, 2012.

[133] D. L. Campbell, G. Juzeliūnas, and I. B. Spielman. Realistic rashba and dresselhaus spin-orbit coupling for neutral atoms. *Phys. Rev. A*, 84:025602, 2011.

[134] Andrew M. C. Dawes, Lucas Illing, Susan M. Clark, and Daniel J. Gauthier. All-optical switching in rubidium vapor. *Scienceă*, 308:672–674, 2005.

[135] G. S. Agarwal and Tarak Nath Dey. Slow light in doppler-broadened two-level systems. *Phys. Rev. A*, 68:063816, Dec 2003.

[136] Kishore T. Kapale and M. Suhail Zubairy. Subwavelength atom localiza-

tion via amplitude and phase control of the absorption spectrum. ii. *Phys. Rev. A*, 73:023813, Feb 2006.

[137] G. S. Agarwal and K. K. T. Kapale. Subwavelength atom localization via coherent population trapping. *J. Phys. B: At. Mol. Opt. Phys.*, 39:3437, 2006.

[138] Sajid Qamar, Shi-Yao Zhu, and M. Suhail Zubairy. Atom localization via resonance fluorescence. *Phys. Rev. A*, 61:063806, May 2000.

[139] Xiao-Bing Xu, Shu-Long Gu, and Zhi-Ping Wang. 1d atom localization via probe absorption spectrum in a four-level cascade-type atomic system. *Optical and Quantum Electronics*, 45:1157–1165, 2013.

[140] Jun Xu, Qian Li, Wen chao Yan, Xiang dong Chen, and Xiang ming Hu. Sub-half-wavelength localization of a two-level atom via trichromatic phase manipulation. *Physics Letters A*, 372:6032–6036, 2008.

[141] Vladimir Ivanov and Yuri Rozhdestvensky. Two-dimensional atom localization in a four-level tripod system in laser fields. *Phys. Rev. A*, 81:033809, Mar 2010.

[142] Chunling Ding, Jiahua Li, Xiaoxue Yang, Duo Zhang, and Hao Xiong. Proposal for efficient two-dimensional atom localization using probe absorption in a microwave-driven four-level atomic system. *Phys. Rev. A*, 84:043840, Oct 2011.

[143] Ren-Gang Wan, Tong-Yi Zhang, and Jun Kou. Two-dimensional sub-half-wavelength atom localization via phase control of absorption and gain. *Phys. Rev. A*, 87:043816, Apr 2013.

[144] Zhiping Wang and Benli Yu. High-precision two-dimensional atom localization via quantum interference in a tripod-type system. *Laser Phys. Lett.*, 11:035201, 2014.

[145] Ali Raheli, iM. Sahrai, and H. R. Hamedi. Atom position measurement in a four-level lambda-shaped scheme with twofold lower-levels. *Optical and Quantum Electronics*, 47:3221Ű3236, 2015.

[146] Matthew S. Bigelow, Nick N. Lepeshkin, and Robert W. Boyd. Observation of ultraslow light propagation in a ruby crystal at room temperature. *Phys. Rev. Lett.*, 90:113903, Mar 2003.

[147] K. S. Choi, H. Deng, J. Laurat, and H. J. Kimble. Mapping photonic entanglement into and out of a quantum memory. *Nature*, 452:67–71, 2008.

[148] Seong-Min Ma, Hua Xu, and Byoung Seung Ham. Electromagnetically-induced transparency and slow light in gaas/algaas multiple quantum wells in a transient regime. *Optics Express*, 17:14902–14908, 2009.

[149] M. G. Payne and L. Deng. Consequences of induced transparency in a double-Λ scheme: Destructive interference in four-wave mixing. *Phys. Rev. A*, 65:063806, Jun 2002.

[150] E. A. Korsunsky and D. V. Kosachiov. Phase-dependent nonlinear optics with double-Λ atoms. *Phys. Rev. A*, 60:4996–5009, Dec 1999.

[151] H. Shpaisman, A. D. Wilson-Gordon, and H. Friedmann. Electromagnetically induced waveguiding in double-Λ systems. *Phys. Rev. A*, 71:043812, Apr 2005.

[152] Robert Fleischhaker and Jörg Evers. Nonlinear effects in pulse propagation through doppler-broadened closed-loop atomic media. *Phys. Rev. A*, 77:043805, Apr 2008.

[153] T. J. Gramila, J. P. Eisenstein, A. H. MacDonald, L. N. Pfeiffer, and K. W. West. Mutual friction between parallel two-dimensional electron systems. *Phys. Rev. Lett.*, 66:1216–1219, Mar 1991.

[154] L. Allen, M. W. Beijersbergen, R. J. C. Spreeuw, and J. P. Woerdman. Orbital angular momentum of light and the transformation of laguerre-gaussian laser modes. *Phys. Rev. A*, 45:8185–8189, Jun 1992.

[155] Miles Padgett, Graeme Whyte, John Girkin, Amanda Wright, Les Allen, Patrik Ohberg, and Stephen M. Barnett. Polarization and image rota-

tion induced by a rotating dielectric rod: an optical angular momentum interpretation. *Optics Letters*, 31:2205–2207, 2006.

[156] L. Allen, Stephen M. Barnett, and Miles J. Padgett. *Optical Angular Momentum*. Taylor and Francis, 2003.

[157] Zhi-Yuan Zhou, Shi-Long Liu, Yan Li, Dong-Sheng Ding, Wei Zhang, Shuai Shi, Ming-Xin Dong, Bao-Sen Shi, and Guang-Can Guo. Orbital angular momentum-entanglement frequency transducer. *Phys. Rev. Lett.*, 117:103601, Aug 2016.

[158] R. Pugatch, M. Shuker, O. Firstenberg, A. Ron, and N. Davidson. Topological stability of stored optical vortices. *Phys. Rev. Lett.*, 98:203601, May 2007.

[159] Zachary Dutton and Janne Ruostekoski. Transfer and storage of vortex states in light and matter waves. *Phys. Rev. Lett.*, 93:193602, Nov 2004.

[160] G. A. Swartzlander and C. T. Law. Optical vortex solitons observed in kerr nonlinear media. *Phys. Rev. Lett.*, 69:2503–2506, Oct 1992.

[161] Galen Duree, Matthew Morin, Gregory Salamo, Mordechai Segev, Bruno Crosignani, Paolo Di Porto, Edward Sharp, and Amnon Yariv. Dark photorefractive spatial solitons and photorefractive vortex solitons. *Phys. Rev. Lett.*, 74:1978–1981, Mar 1995.

[162] Zhigang Chen, Mordechai Segev, Daniel W. Wilson, Richard E. Muller, and Paul D. Maker. Self-trapping of an optical vortex by use of the bulk photovoltaic effect. *Phys. Rev. Lett.*, 78:2948–2951, Apr 1997.